IJAE

Italian Journal of Anatomy and Embryology

Official Organ of the Italian Society
of Anatomy and Histology

Vol. 129
N. 2
2025
ISSN 1122-6714

FIRENZE
UNIVERSITY
PRESS

IJAE
Italian Journal of Anatomy and Embryology
Official Organ of the Italian Society of Anatomy and Histology

Founded by Giulio Chiarugi in 1901

Journal e-mail: ijae@unifi.it – Web site: https://www.fupress.com/ijae

Firenze University Press
via Cittadella, 7
I-50144 Firenze, Italy
E-mail: journals@fupress.com
Available online at
https://www.fupress.com/ijae

Italian Journal of Anatomy and Embryology

IJAE

Vol. 129, n. 2 – 2025

Firenze University Press

Italian Journal of Anatomy and Embryology
https://www.fupress.com/ijae
ISSN 1122-6714 (print) | ISSN 2038-5129 (online)

Direttore responsabile: **Ferdinando Paternostro, University of Firenze, Italy**
Direttore scientifico: **Domenico Ribatti, University of Bari, Italy**

Published by Firenze University Press

Firenze University Press
Università degli Studi di Firenze
via Cittadella, 7, 50144 Firenze, Italy
www.fupress.com

IJAE
ITALIAN JOURNAL OF ANATOMY AND EMBRYOLOGY

Firenze University Press
www.fupress.com/ijae

OPEN ACCESS

Citation: Nziyane, P. N., Mpholwane, M. L., & Xhakaza, N. K. (2025). Effects of streptozocin-induced diabetes on the histomorphometry of the small and large intestines of male Sprague Dawley rats. *Italian Journal of Anatomy and Embryology* 129(2): 3-12. doi: 10.36253/ijae-15973

Data Availability Statement: All relevant data are within the paper and its Supporting Information files.

Competing Interests: The Author(s) declare(s) no conflict of interest.

Effects of streptozocin-induced diabetes on the histomorphometry of the small and large intestines of male Sprague Dawley rats

Nziyane PN[1], Mpholwane ML[2], Xhakaza NK[1]

[1] *Department of Anatomy, School of Medicine, Sefako Makgatho Health Sciences University, Ga-Rankuwa, Pretoria, South Africa*
[2] *Department of Physiology and Environmental Health, University of Limpopo, Sovenga, 0727, South Africa*
*Corresponding author. Email: patiencenziyane@gmail.com

Abstract. Gastrointestinal tract (GIT) disorders affecting intestinal tissues are common among diabetes mellitus (DM) patients. GIT side effects of antidiabetic medication are a reason for an increase in use of antidiabetic herbal medicine, prompting research that uses 50mg/kg of streptozocin (STZ) to induce DM in animal experiments prior to testing safety and efficacy of the herbs over 21 days in most experiments. As DM is a progressive disease, it is not clear whether 21 days of DM is enough to induce intestinal tissue changes. We investigated effects of 50mg/kg STZ induced DM in intestines of male Sprague Dawley rats observed over 21 days. Intestinal tissues of 16 (control, n=8, STZ diabetic=8) rats stained with Masson's Trichrome, hematoxylin and eosin were used. Villi height, width, number of goblet cells (GC), mucosa, submucosal collagen fibre (SCF) and muscularis externa (ME) were measured using ImageJ software in photomicrographs taken from slides with a microscope camera. Means were analysed using SPSS software. In DM animals, there was a significant increase in width of ileal villi ($p < 0.001$), reduction in number of GC in jejunum ($p = 0.033$) and ileum ($p < 0.001$). SCF thickness increased in duodenum ($p < 0.001$), jejunum ($p = 0.003$), ileum ($p = 0.005$), and colon ($p = 0.004$). ME only increased in ileum ($p = 0.004$). 50mg/kg STZ DM induces significant changes across the intestines over 21 days, suggesting that this duration is effective for experimental modelling for future DM studies on the intestines.

Keywords: gastrointestinal tract, diabetes mellitus, Sprague Dawley rats, streptozocin (STZ), antidiabetic herbal medication.

INTRODUCTION

Diabetes Mellitus (DM) is a group of metabolic disorders characterized by increased blood glucose levels commonly known as hyperglycemia (Cho et al., 2018; Lovic et al., 2020). It develops as a result of a deficiency in insulin secretion by pancreatic beta cells or insulin action (Cho et al., 2018). It is predicted that by 2040, 693 million people aged 18-99 years old will have

diabetes, a number accounting for 9.9% of the world's population (Lovic et al., 2020). The gastrointestinal tract (GIT) disorders are common among DM patients and have recently been identified as one of the most common DM complications (Zhao et al., 2017). Animal and human studies have shown that DM has negative effects on intestinal health, including impaired healing and cellular damage to the intestinal mucosa (Gotfried et al., 2017). The above could be partly due to the fact that hyperglycemia causes an overproduction and accumulation of advanced glycation end products (AGEs) in tissues which affect the structure and function of proteins and other intestinal wall components like collagen fibres (Zhao et al., 2017).

Metformin is a commonly used antidiabetic medication, but it has been shown to slow gastric emptying, reduce pyruvate dehydrogenase activity, and cause lactic acidosis in typer 2 diabetes mellitus patients (Borg et al., 2020). It can also cause abdominal pain, vomiting, diarrhoea, agitation, confusion, tachypnoea, and hypotension (Kalsi et al., 2017). Due to the above side effects of conventional medication, several diabetic patients are increasingly using antidiabetic herbal medication which is perceived to be safe (Atinga et al., 2018; Mekuria et al., 2018). However, the safety and efficacy of herbal medication lacks scientific validation in most cases (Mukherjee et al., 2022). Consequently, there is an increase in studies investigating the safety and efficacy of the antidiabetic herbal medication. These studies use streptozocin (STZ) to induce diabetes in experimental animals followed by treatment intervention (Eleazu et al., 2013; Goyal yet al., 2017). The dosage and duration of STZ used to induce diabetes is inconsistent across different experiments, with those that are interested in physiological changes employing shorter duration of between 7 to 21 days, while the dosage of STZ used to induce diabetes ranges from 20mg/kg to as high as 200mg/kg (Kooti et al., 2016). The short duration of diabetes may induce physiological changes but not necessarily tissue changes as diabetes is a progressive disease (Zhao et al., 2017). A dose of 50mg/kg of STZ with animals kept for 21 days either with or without treatment intervention is one of the most common experimental designs.

There is currently a lack of information on the pathologic profile of STZ-induced diabetes in the small intestines and the colon. While some studies have examined specific regions of the intestines after 21 days period of STZ induced diabetes, a more comprehensive investigation of the complete intestinal pathologic profile is lacking to fully comprehend the effects of STZ induced diabetes in the intestinal tissues. The current study has been designed against this backdrop to investigate the effects of 50mg/kg STZ induced diabetes on the histomorphometry of the small and large intestines of the male Sprague Dawley rats observed over 21 days after induction of diabetes. Such a study is important for accurate interpretation of the results in studies that use this experimental design in drug testing.

MATERIALS AND METHODS

Animals

Sixteen three months old male Sprague Dawley rats weighing 220–300 g that were purchased from Northwest University, Potchefstroom were used in the current study. Ethics approval (SMUAEC 03/2021) was obtained from the animal ethics committee at Sefako Makgatho Health Sciences University prior to conducting the study. The animals were kept in the Department of Physiology's Laboratory Animal Center at Sefako Makgatho Health Sciences University. Each animal was kept in a separate cage in a temperature-controlled environment with a 12-hour light/12-hour dark cycle with free access to rat chow and water.

Diabetes induction

After a week of acclimation, animals were fasted for 18 hours before receiving a once-off intraperitoneal injection of 50mg/kg bodyweight of pancreatic-cell toxin STZ, 1ml/kg dissolved in 0.1M sodium citrate buffer (pH = 4.5) to induce type 1 DM. To avoid hypoglycemia, the STZ injected animals received a 5% glucose solution in their drinking water overnight. After 72 hours, blood glucose levels were measured in both normal control and STZ injected animals using blood samples obtained from the tail vein and analyzed with the accu-chek active glucometer (Roche Diabetes Care South Africa) to confirm diabetic status. For STZ injected animals, fasting blood glucose values exceeding 10.0 mM were considered indicative of hyperglycemia. All animals with the above blood glucose levels were included in the study and those animals that had glucose levels below 10mM were excluded from the study. The measurement of blood glucose levels in the normal control group was done for control purposes. After confirmation of diabetic status, both the normal control and STZ diabetic animals were put on unlimited food and water and observed for 21 days with glucose levels measured in days 14 and 21 of the experimental period and body weights measured on a daily basis.

Experimental design

Animals were randomly assigned to one of two experimental groups at random as follows: Group 1 (n=8) were normal rats that were not exposed to any treatment and used as a control, while Group 2 (n=8) were 50mg/kg STZ-induced diabetic rats. After induction of diabetes, the animals were kept for 21 days with no intervention. At the end of the 21 days (day 22) all animals were euthanised with an intraperitoneal injection of a mixture (1.4 ml/kg.bw) of Anaket V (Ketamine) 40-80mg/kg and Rompun 2% (Xylazine) 5-10mg/kg. The intestinal tissues were collected and preserved in 10% buffered formalin before processing and staining.

Specimen processing and staining

Four 1cm segments were harvested from the duodenum, jejunum, ileum and the colon. A segment of the duodenum was taken in its second part, 1cm from the pylorus. Jejunum was sampled 5cm below the ligament of Treitz, the ileum sampled 5cm proximally to the ileocecal valve and the colon sampled 5cm distal to the ileocecal valve as per the sampling method adopted by Zhao et al., (2017). The blocks of the intestinal tissues were processed, embedded, and serially sectioned at 5µm thickness with a rotary microtome, and one in two sections were mounted on glass slides for Masson's Trichrome (MT) and Hematoxylin and Eosin (H&E) staining (Bancroft and Gamble, 2008). Hematoxylin and Eosin stains were used for tissue architecture to evaluate thickness of the layers and quantifying goblet cells, while the MT stain was used for connective tissue assessment of submucosal collagen fiber bundles. Photomicrographs of stained and mounted sections were taken with Leica software (Version 3.0), a Leica ICC50 HD camera, and a Leica microscope DM500 at 4X, 10X, and 40X.

Histomorphometric measurements

Villi height, width, and goblet cells

Twenty serial sections of the duodenum, jejunum and ileum were used in the current study to measure the height and width of the small intestines for each animal at 4X (duodenum) and 10X (jejunum and ileum) magnification. The length of the villi was measured from the tip of the villi to the base at the junction with the intestinal crypts, whereas the width was measured halfway between the tip and base of the villi. These measurements were randomly taken from the longitudinal sections of 5 well-oriented villi per tissue section in 20 sections adding up to 100 villi measured for each segment of the small intestine per animal (Lerkdumnernkit et al., 2022). Goblet cells characterised by visible wine glass shape cells with clear cytoplasm and round or oval shaped nucleus at the base were also counted in the above villi. The measurements and counts were done using the line and multi-point feature tools of the ImageJ software (Schneider et al., 2012) and the means were recorded for statistical analyses.

Thickness of the mucosa, muscularis externa and submucosal collagen fibre bundles

Twenty serial sections of the colon were used to measure the mean thickness of the mucosa, muscularis externa and in H&E-stained sections at 4X, and collagen fibres in MT-stained sections at 10X magnification using the line tool of the ImageJ software. Measurements of the mucosa were taken at two random points that were three mucosal glands apart in each of the twenty sections per animal from the tips of the mucosa to the muscularis mucosae, making it a total of forty points measured per animal in the colon. The muscularis externa of the colon was measured at two points in line with the mucosa measurement described above. For the small intestines, the muscularis externa was measured at two points that were two villi apart, while the submucosal collagen fibre thickness was measured at 40X (MT) magnification from the point where the muscularis mucosae ends to where the muscularis externa begins at two random points two intestinal crypts apart.

Data analysis

A student t-test was used to compare the means of villi parameters, thickness of intestinal layers and counts of goblet cells for normal control and STZ diabetic group in a Statistical Package for the Social Sciences (SPSS) software (Version 28). Data was normally distributed in Shapiro Wilk test. All variables were expressed as mean ± standard deviation and a p-value of ≤ 0.05 was considered significant.

RESULTS

Induction of diabetes, weights and glucose level changes

Prior to the induction of diabetes with STZ injection, all animals had normal blood glucose levels ranging from 4.8 to 5.8 mmol/L. After 72 hours of diabetic

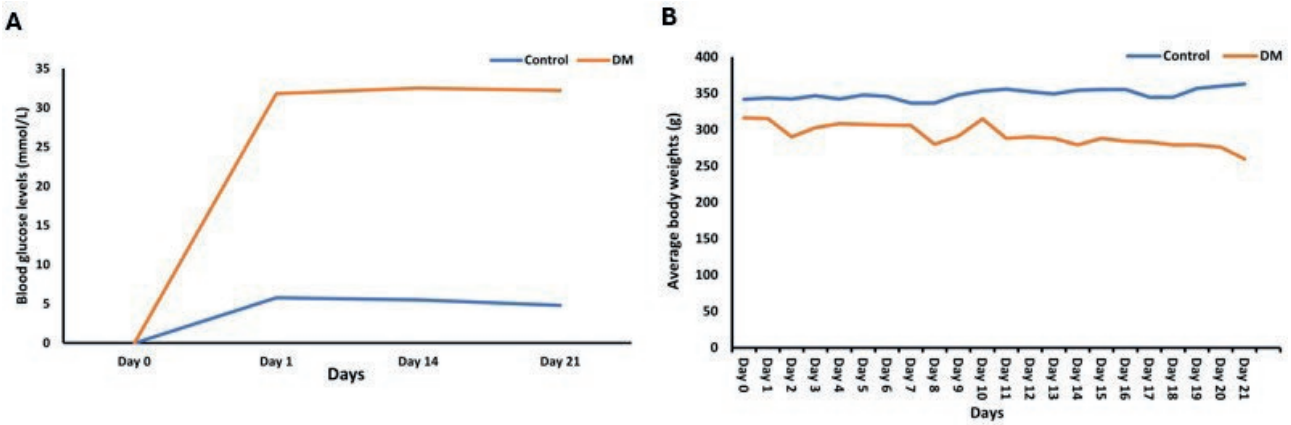

Figure 1. A changes of glucose levels of STZ induced diabetic and control animals from day 0 to day 21. B: Graphic representation of the weight changes of the animals throughout the 21 days period of the experiment.

induction, there STZ diabetic induced animals (DM) had a drastic increase of blood glucose levels to an average of 31.83 mmol/L to 33.20 mmol/L, which persisted throughout the 21 days of the experiment while the control group maintained normal blood glucose levels ranging from 4.8-5.5 mmol/L (Figure 1A).

In this current study, animals with approximately the same body weights were used with an average weight of 310 g for the DM group, and an average weight of 338 g for control. The body weight of the control group significantly increased when comparing the initial and terminal body weights (28.00 ± 17.23; p = 0.003). The diabetic group had a significant weight loss by the end of 21 days when comparing the initial and terminal body weights (65.00 ± 38.60; p = 0.002; Figure 1B). The small and large intestine's mean weight of the diabetic group (60.59 ± 9.25 g) was significantly higher than that of the control group (23.81 ± 2.51 g) (p <0.001; Table 1).

Table 1. Body weights, GIT weight and blood glucose levels.

	Control	DM P-values
Initial BW (g)	338.71 ± 7.57	310.71 ± 14.78 0.003
Terminal BW(g)	364.00 ± 15.28	299.00 ± 36.82 0.002
Weight of small & large intestines (g)	23.81 ± 2.51	60.59 ± 9.25 <0.001
Glucose levels (mmol/L)	5.26 ± 0.48	31.83 ± 0.59 <0.001

Data of all variables expressed as mean ± standard deviation. P <0.05.

Histological findings

Morphological changes in the villi of the duodenum

The duodenum of the control group showed intact villi, and the Paneth cells (PC) had densely packed eosinophilic secretory granules (Figure 2A). In the DM group, the villi appeared to be short and mildly deformed (Figure 2B). The duodenal villi height of the DM group was slightly lower (1216.272 ± 274.59 μm) than that of the control group (1244.558 ± 04 μm; p = 0.425; Figure 2C) in the t-test. Similarly, the duodenal villi width of the DM group (182.155 ± 28.10 μm) was slightly lower than that of the control group (190.819 ± 26.11 μm; p = 0.311; Figure 2D). The number of goblet cells in the villi of the duodenum of the DM group was significantly lower (7.883 ± 2.16) than that of the control group (13.667 ± 1.85; p < 0.001; Figure 2E).

There were no statistically significant differences in the thickness of the muscularis externa (ME) of the duodenum of the DM group (214.809 ± 39.04 μm) compared to the control group (175.116 ± 36.60 μm, p = 0.090). However, the ME of the DM group was slightly thicker than that of the control group (Figure 2F).

In MT-stained sections, the control group had moderate amount of submucosal collagen fibre bundles (Figure 2G), and the DM group had a large amount of submucosal collagen fibre bundles (Figure 2H). The submucosal collagen fibre thickness of the duodenum of the DM group was significantly thicker (57.865 ± 6.69 μm) when compared to that of the control group (40.542 ± 2.06 μm; p < 0.001; Figure 2I).

Morphological changes in the Jejunum

Normal histological structures were observed in the jejunum of the control group such as finger-like villi and normal shaped intestinal crypts (Figure 3A). The jejunum of the DM group however showed distortion of

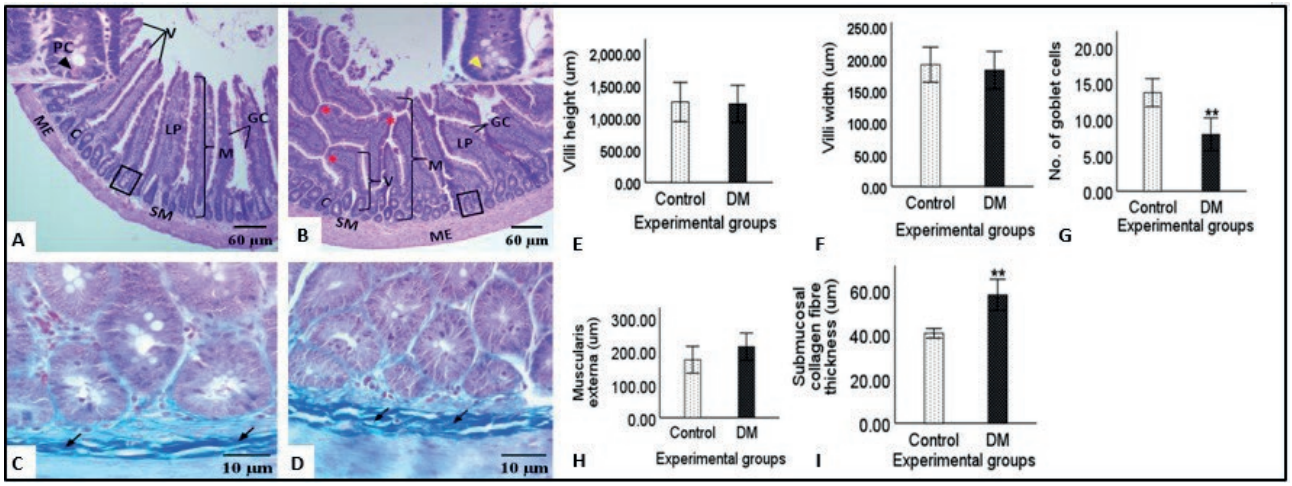

Figure 2. Hematoxylin and Eosin photomicrographs (4X) showing changes in the histological structure of the duodenum in the control (A) and Diabetes Mellitus (B) groups. Masson's Trichrome stained micrographs (40X) of control (C) and DM (D) groups showing changes in the submucosal collagen fibre bundle thickness (black arrows) in the duodenum. E to I) Bar graphs representing changes in villi, number of goblet cells and thicknesses of muscularis externa and submucosal collagen fibre bundles in the duodenum. The standard error of the mean is represented by the error bars. ** represents significant changes. Mucosa= M; submucosa= SM; muscularis externa= ME; villi= V; crypt= C; lamina propria= LP; red asterisks= short and deformed villi.

the villi, cell infiltration in the lamina propria as well as disrupted crypts (Figure 3B). The jejunal villi height of the DM group (615.623 ± 184.644 µm) was slightly lower than that of the control group (655.603 ± 58.99 µm; p = 0.321; Figure 3C), while the jejunal villi width of the DM group (177.547 ± 26.14 µm) was slightly higher than that of the control group (147.594 ± 32.91 µm; p = 0.090; Figure 3D). The number of goblet cells in the villi of the jejunum of the DM group (8.033 ± 2.35 µm) was significantly lower compared to that of the control group (13.217 ± 4.03 µm; p = 0.033; Figure 3E).

The t-test further showed that the thickness of the muscularis externa of the jejunum (ME) of the DM group (127.914 ± 41.63 µm) was not significantly different from that of the control group (152.991 ± 20.78 µm; p = 0.117; Figure 3F). However, the thickness of the ME of the DM group was slightly lower than that of the control group.

The MT-stained sections of the control group (Figure 3G) showed moderate amounts of collagen fibre bundles while the DM group had a large amount of submucosal collagen fibre bundles (Figure 3H). The submucosal collagen fibre thickness of the DM group was significantly higher (43.975 ± 2.69 µm) than that of the control group (34.101 ± 4.911 µm, p = 0.003; Figure 3I).

Morphological changes in the ileum

The ileum of the control group showed the normal histological structure with intact villi and epithelial lining (Figure 4A). In the DM group, the villi of the ileum appeared to be blunt and distorted (Figure 4B). The t-test showed that the ileal villi height of the DM group (6548.225 ± 38.44 µm) was not statistically significant when compared to that of the control group (536.481 ± 66.92 µm; p = 0.354). However, the villi height of the DM group was slightly higher than that of the control group (Figure 4C). Additionally, the ileal villi width of the DM group (183.283 ± 15.51 µm) was significantly higher compared to that of the control group (114.905 ± 8.03 µm; p < 0.001; Figure 4D). There were no significant differences in the number of goblet cells of the ileal villi of the DM (13.000 ± 1.25) and control groups (12.850 ± 1.34) in the t-test (p = 0.384). However, the number of goblet cells of the DM group was slightly higher than that of the control group (Figure 4E). The t-test also showed that the thickness of the muscularis externa of the DM group (178.227 ± 21.85 µm) was significantly higher when compared to that of the control group (142.501 ± 18.36 µm; p = 0.004; Figure 4F).

In MT-stained sections, the collagen fibre bundles showed a continuous layer around the epithelial cells in the control group, indicating an intact basement membrane (Figure 4G). In the DM group, collagen fibre bundles were spars around the epithelial cells, indicating the destruction of the basement membrane (Figure 4H). The submucosal collagen fibre thickness of the DM group (42.467 ± 4.06 µm) was significantly thicker when compared to that of the control group (35.331 ± 3.79 µm; p = 0.005; Figure 4I).

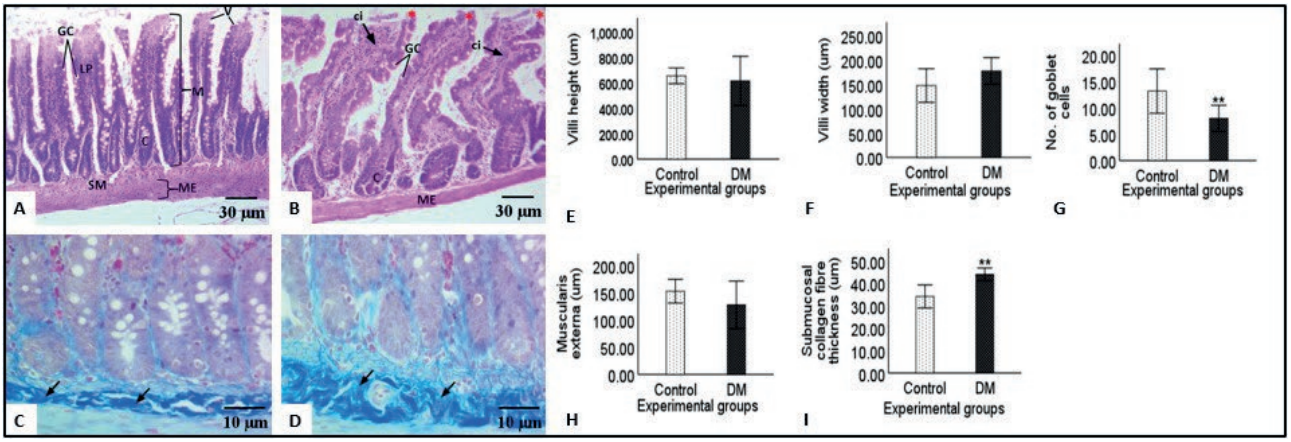

Figure 3. Hematoxylin and eosin micrographic (10X) showing changes in the histological structure of the walls of the jejunum in the control (A) and Diabetic mellitus (B) groups. Masson's Trichrome stained micrographs (40X) of control (C) and DM (D) groups showing changes in the submucosal collagen fibre bundle thickness (black arrows) in the jejunum. E to I) Bar graphs representing changes in villi, number of goblet cells and thicknesses of muscularis externa and submucosal collagen fibre bundles in the jejunum. The standard error of the mean is represented by the error bars. ** represents significant changes. Mucosa= M; villi= V; lamina propria= LP; submucosa= SM; crypts= C; muscularis externa= ME; red asterisks at the tip of the villi= distorted villi; cell infiltration= ci.

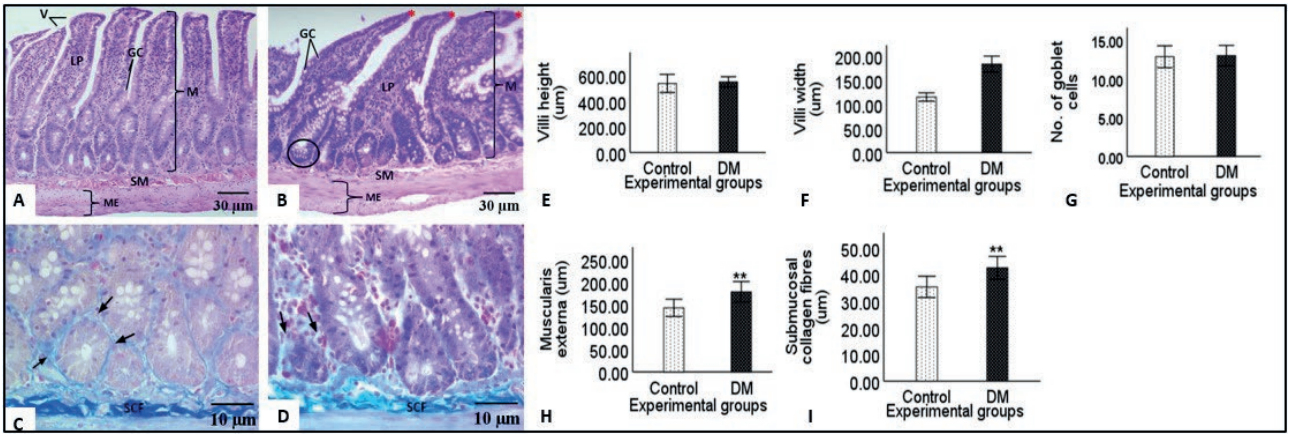

Figure 4. Hematoxylin and eosin micrographic (10X) showing changes in histological structure of the walls of the ileum in the control (A) and Diabetic mellitus (B) groups. Masson's Trichrome stained micrographs (40X) of control (C) and DM (D) groups showing changes in the submucosal collagen fibre bundle thickness (black arrows) in the ileum. E to I) Bar graphic representing changes in villi, number of goblet cells and thicknesses of muscularis externa and submucosal collagen fibre bundles in the ileum. The standard error of the mean is represented by the error bars. ** represents significant changes. Villi= V; lamina propria= LP; goblet cells= GC; mucosa= M; submucosa= SM; muscularis externa= ME.

Morphological changes in the Colon

The colon of the group showed normal shaped mucosal crypts with intact epithelial lining on the luminal surface and narrow lumens (Figure 5A). In the DM group, some crypts had mildly distorted shape and the ME appeared thicker (Figure 5B). The colonic mucosal layer of the DM group (446.264 ± 81.97 µm) was significantly higher than that of the control group (318.528 ± 34.39 µm; p = 0.008; Figure 5C). The t-test also showed that the thickness of the colonic muscularis externa (ME) of the DM group (172.546 ± 79.22 µm) was not significantly different from that of the control group (152.434 ± 15.70 µm; p = 0.291; Figure 5D). However, the thickness of the ME of the DM group was higher than that of the control group (Figure 5D).

The MT-stained tissue sections of the control group showed moderate amount of submucosal collagen fibre bundles (Figure 5E) while the DM group (Figure 5F) had abundant submucosal collagen fibre bundles when

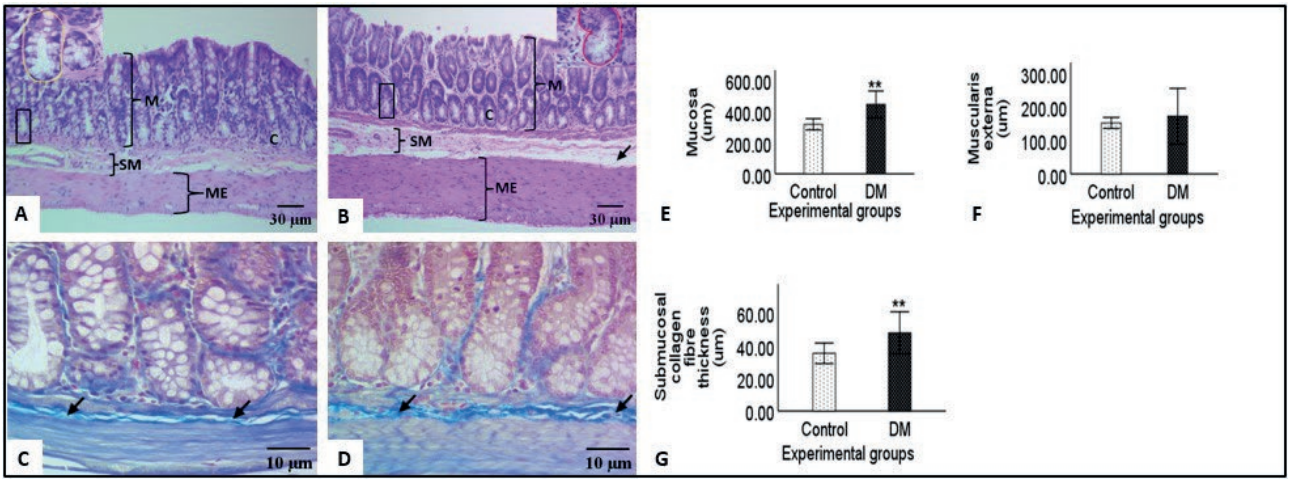

Figure 5. Hematoxylin and eosin micrographic (10X) showing changes in histological structure of the walls of the colon in the control (A) and Diabetic mellitus (B) groups. Masson's Trichrome stained micrographs (40X) of control (C) and DM (D) groups showing changes in the submucosal collagen fibre bundle thickness (black arrows) in the colon. E to G: Bar graphs representing changes in the mucosa and thickness of muscularis externa of the colon. The standard error of the mean is represented by the error bars. ** represents significant changes. Mucosa= M; crypts= C; submucosa= SM; muscularis externa= ME; black arrow= separation of layers in figure 4B; black square= crypts in 100X magnification to show their shape; distorted crypt encircled in red, normal crypt encircled in yellow.

compared to the control group. The colonic submucosal collagen fibre thickness of the DM group (47.87 ± 12.27 µm) was significantly higher than that of the control group (35.348 ± 6.00 µm; p = 0.004; Figure 5G).

DISCUSSION

The diabetic group exhibited mildly distorted and blunt villi in the small intestines compared to the normal control group. This observation may be attributed to an increased enterocyte proliferation rate reported in the diabetic animals (Boudry et al.,2007). The migration of immature cells to the villus surface is a possible explanation for the observed blunting and distortion of the villi (Boudry et al., 2007).

The present study revealed a decrease in villi height in the duodenum and jejunum of the diabetic group, consistent with the findings of previous authors (Mesgari-Abbasi et al., 2019). This reduction is likely attributed to chronic inflammation associated with diabetes, as previously suggested (Garci et al., 2010). In the ileum, an increase in villi height was observed in the diabetic group compared to the normal group, in line with the previous studies (Chen et al., 2012; Hvid et al., 2016). Diabetes has been shown to significantly affect the terminal intestinal segment of the small intestine, potentially increasing villi height (Chen et al., 2012).

It must be noted that conflicting findings have been reported regarding the effect of diabetes on specific intestinal segments. One study found an increase in the villi height of the duodenum (Lerkdumnernkit et al., 2022), while another study reported an increase in the villi height of the jejunum (Hvid et al., 2016), both of which contradicts the findings of the current study. In the studies mentioned above, animals were kept for 28 days with dosages of 60mg/kg and 54mg/kg respectively, contrary to the 21 days and 50mg/kg of STZ of the current study. It is known that longer durations of diabetes are associated with more severe effects on the tissues (American Diabetes Association, 2014). Therefore, differences in the duration of the experiments can be a reason for conflicting findings.

In the present study, a decrease in villi width was observed in the duodenum of the DM group compared to the control group as previously reported (Mesgari-Abbasi et al., 2019), while in the jejunum and ileum, the villi width increased in DM group. The reduction in villi width can be attributed to alterations in the production of growth factors, particularly insulin-like growth factor-1 and 2 (IGF-1 and IGF-2), which play a crucial role in the growth and maintenance of the villi (Dube et al., 2006). The observed increase in villi width in the jejunum and ileum of diabetic rats can be attributed to villous hypertrophy (Zhao et al., 2003; Zhao et al., 2017).

The number of goblet cells significantly decreased in the duodenum and jejunum of the diabetic group compared to the control group, in agreement with previous reports (Mesgari-Abbasi et al., 2019; Lerkdumnernkit et al., 2022). The reduction in the number of goblet cells is

Table 2. Summary of findings from previous authors in comparison with the current study.

Author(s)	Dosage	Duration	Duodenum					Jejunum					Ileum					Colon			
			VH	VW	GC	ME	SCFT	VH	VW	GC	ME	SCFT	VH	VW	GC	ME	SCFT	M	ME	SCFT
Lerkdumnernkit *et al.*, (2022)	60mg/kg	28 days	↑		↓		↑													
Hvid *et al.*, (2016)	54mg/kg	28 days	↑						↑				↑							
Zhao *et al.*, (2017)	-	56 days				↑	↑				↑	↑				↑	↑	↑	↑	↑
Mesgari-Abbasi *et al.*, (2019)	55mg/kg	21 days						↓	↑	↓										
Akinola *et al.*, (2009)	70mg/kg	50 days													↓					
Chen *et al.*, (2012)	-	-											↑							
Current study	50mg/kg	21 days	↓	↓	↓	↑	↑**	↓	↑	↓**	↓	↑**	↑	↑**	↑	↑**	↑**	↑**	↑	↑**

Villi height (VH), villi width (VW), goblet cells (GC), muscularis externa (ME), submucosal collagen fibre thickness (SCFT), mucosa (M). ↑: increase, ↓: decrease/reduction. ** represents significant changes.

due to increase in tumor necrosis factor alpha (TNF-α) secretion by intestinal macrophages in the diabetic intestines, which ultimately cause production of active caspase-8 which activates caspase-3, resulting in apoptosis of goblet cells (Lau et al., 2012).

In the ileum of diabetic rats, the number of goblet cells increased consistent with the view that the terminal portion of the intestinal tract is less affected by diabetes (Chen et al., 2012). Contrary to these findings, Akinola et al., (2009) reported a decrease in the number of goblet cells in the ileum of diabetic rats, probably due to longer period of 50 days and the STZ dosage of 70mg/kg in their experiment.

In the current study, an increase in the thickness of the muscularis externa was recorded in the duodenum and ileum of the diabetic group compared to the control group in line with previous reports (Chen et al., 2012; Zhao et al., 2017). The increase may be due to hyperplasia, a condition in which the number of cells in the muscularis externa increases, contributing to a rise in overall thickness (Zhao et al., 2003; Zhao et al., 2017). The current study also reported a reduction in the ME of the jejunum in the diabetic group compared to the control group. The decrease of ME noted in the jejunum could be due to the sensitivity of smooth muscle to oxidative stress which increase cell death (Kashyap and Farrugia, 2011). A significant increase in the thickness of the submucosal collagen fibre bundles of the diabetic group was recorded in the duodenum, jejunum and ileum compared to the control group in agreement with previous reports (Zhao et al., 2017; Lerkdumnernkit et al., 2022). The above could be indicative of fibrosis caused by inflammation and tissue damage in diabetic animals (Lenti and Di Sabatino, 2019).

The current study recorded a significant increase in the thickness of the mucosa, muscularis externa and submucosal collagen fibre bundles compared to the control group as previously reported (Zhao et al., 2017; D'arpino et al., 2018). The increase in thickness of the layers of the colon is due to inflammation (Kashyap and Farrugia, len2011). Chronic inflammation can lead to fibrosis, muscular hypertrophy and smooth muscle hyperplasia leading to increased muscle thickness and reduced flexibility (Gromova et al., 2021). Table 2 summarises the comparisons of the findings of the effects of STZ diabetes by different authors. It is apparent from the table that the current study is the first to report on the effects of STZ diabetes on the entire intestinal tissue and that the longer duration the diabetic animals are kept in experiments is a contributing factor in the contradiction in the results by different authors

CONCLUSION

In this study, we conclude that a dosage of 50mg/kg of streptozocin (STZ) administered over a period of 21 days is sufficient to induce diabetes and produce observable tissue changes in various parts of the intestines. This timeframe is deemed appropriate for future research focused on analysing the effects of diabetes mellitus on intestinal health. The findings also provide a solid foundation for subsequent studies exploring the therapeutic effects of antidiabetic treatments on intestinal tissue.

AUTHOR CONTRIBUTIONS

Conceptualization: ML Mpholwane, PN Nziyane and NK Xhakaza. Manuscript drafting: PN Nziyane. Critical review of the manuscript: ML Mpholwane and NK Xhakaza. Final manuscript approval: Both authors.

ACKNOWLEDGEMENTS

The authors of current study declare no conflict of interests. Data used in the current study may be shared by the corresponding author upon reasonable request. The authors would like to thank Dr Du Plessis for valuable advises. Authors would also like to acknowledge Ms Thuso Valencia Mudau for her contribution in handling of the live animals during the experiment and Ms Phindi Matsebane for her technical assistance.

FUNDING

This work was supported by the National Research Foundation (NRF) grant number 14159.

REFERENCES

AKINOLA, O.B., ZATTA, L., DOSUMU, O.O., AKINOLA, O.S., ADELAJA, A.A., DINI, L., CAXTON-MARTINS, E.A., 2009. Intestinal lesions of streptozotocin-induced diabetes and the effects of Azadirachta indica treatment. *Pharmacology*, 3:872-881.

AMERICAN DIABETES ASSOCIATION, 2014. Diagnosis and classification of diabetes mellitus. *Diabetes care*, 37(Suppl. 1): S81-S90, https://doi.org/10.2337/dc14-S081.

ATINGA, R.A., YARNEY, L., GAVU, N.M., 2018. Factors influencing long-term medication non-adherence among diabetes and hypertensive patients in Ghana: a qualitative investigation. *PloS one*,13(3): e0193995, https://doi.org/10.1371/journal.pone.0193995.

BANCROFT, J.D., GAMBLE, M., 2008. Theory and practice of histological techniques. Elsevier health sciences.

BORG, M.J., RAYNER, C.K., JONES, K.L., HOROWITZ, M., XIE, C., WU, T., 2020. Gastrointestinal mechanisms underlying the cardiovascular effect of metformin. *Pharmaceuticals*, 13(11):410, https://doi.org/10.3390/ph13110410.

BOUDRY, G., JURY, J., YANG, P.C., PERDUE, M.H., 2007. Chronic psychological stress alters epithelial cell turn-over in rat ileum. *American Journal of Physiology-Gastrointestinal and Liver Physiology*, 292(5): 1228-1232, https://doi.org/10.1152/ajpgi.00358.2006.

CHEN, P., ZHAO, J., GREGERSEN, H., 2012. Up-regulated expression of advanced glycation end-products and their receptor in the small intestine and colon of diabetic rats. *Digestive diseases and sciences*, 57:48-57, https://doi.org/10.1007/s10620-011-1951-0.

CHO, N.H., SHAW, J.E., KARURANGA, S., HUANG, Y., DA ROCHA FERNANDES, J.D., OHLROGGE, A.W., MALANDA, B.I., 2018. IDF Diabetes Atlas: Global estimates of diabetes prevalence for 2017 and projections for 2045. *Diabetes research and clinical practice*, 138:271-281, https://doi.org/10.1016/j.diabres.2018.02.023.

D'ARPINO, M.C., FUCHS, A.G., SÁNCHEZ, S.S., HONORÉ, S.M., 2018. Extracellular matrix remodelling and TGF-β1/Smad signalling in diabetic colon mucosa. *Cell biology international*, 42(4):443-456, https://doi.org/10.1002/cbin.10916.

DUBÉ, P.E., FORSE, C.L., BAHRAMI, J., BRUBAKER, P.L., 2006. The essential role of insulin-like growth factor-1 in the intestinal tropic effects of glucagon-like peptide-2 in mice. *Gastroenterology*, 131(2):589-605, https://doi.org/10.1053/j.gastro.2006.05.055.

ELEAZU, C.O., ELEAZU, K.C., CHUKWUMA, S., ESSIEN, U.N., 2013. Review of the mechanism of cell death resulting from streptozotocin challenge in experimental animals, its practical use and potential risk to humans. *Journal of diabetes & metabolic disorders*, 12(60):1-7, https://doi.org/10.1186/2251-6581-12-60.

GARCIA, C., FEVE, B., FERRE, P., HALIMI, S., BAIZRI, H., BORDIER, L., GUIU, G., DUPUY, O., BAUDUCEAU, B., MAYAUDON, H., 2010. Diabetes and inflammation: fundamental aspects and clinical implications. *Diabetes & metabolism*, 36(5):327-338, https://doi.org/10.1016/j.diabet.2010.07.001.

GOTFRIED, J., PRIEST, S., SCHEY, R., 2017. Diabetes and the small intestine. *Current treatment options in*

gastroenterology, 15:490-507, https://doi.org/10.1007/s11938-017-0155-x.

GOYAL, S.N., REDDY, N.M., PATIL, K.R., NAKHATE, K.T., OJHA, S., PATIL, C.R., AGRAWAL, Y.O., 2016. Challenges and issues with streptozotocin-induced diabetes–a clinically relevant animal model to understand the diabetes pathogenesis and evaluate therapeutics. *Chemico-biological interactions*, 244:49-63, https://doi.org/10.1016/j.cbi.2015.11.032.

GROMOVA, L.V., FETISSOV, S.O., GRUZDKOV, A.A., 2021.Mechanisms of glucose absorption in the small intestine in health and metabolic diseases and their role in appetite regulation. *Nutrients*,13(7):2474, https://doi.org/10.3390/nu13072474.

HVID, H., JENSEN, S.R, WITGEN, B.M., FLEDELIUS, C., DAMGAARD, J., Pyke, C., RASMUSSEN, T.B., 2016. Diabetic phenotype in the small intestine of Zucker diabetic fatty rats. *Digestion*, 94(4):199-214, https://doi.org/10.1159/000453107.

KALSI, A., SINGH, S., TANEJA, N., KUKAL, S., MANI, S., 2017. Current treatments for Type 2 diabetes, their side effects and possible complementary treatments. *International Journal*, 10(3):13-18.

KASHYAP, P., FARRUGIA, G., 2011. Oxidative stress: key player in gastrointestinal complications of diabetes. *Neuro-gastroenterology & Motility*, 23(2):111-114, https://doi.org/10.1111/j.1365-2982.2010.01659.x.

KOOTI, W., FAROKHIPOUR, M., ASADZADEH, Z., ASHTARY-LARKY, D., ASADI-SAMANI, M., 2016. The role of medicinal plants in the treatment of diabetes: a systematic review. *Electronic physician*, 8(1):1832-1842, https://doi.org/10.19082/1832.

LAU, K.S, CORTEZ-RETAMOZO, V., PHILIPS, S.R, PITTET, M.J., LAUFFENBURGER, D.A., HAIGIS, K.M., 2012. Multi-scale in vivo systems analysis reveals the influence of immune cells on TNF-α-induced apoptosis in the intestinal epithelium. *PLOS Biology*, 10(9): e1001393, https://doi.org/10.1371/journal.pbio.1001393.

LENTI, M.V, DI SABATINO, A., 2019. Intestinal fibrosis. *Molecular aspects of medicine*, 65:100-109, https://doi.org/10.1016/j.mam.2018.10.003.

LERKDUMNERNKIT, N., SRICHAROENVEJ, S., LANLUA, P., NIYOMCHAN, A., BAIMAI, S., CHOOKLIANG, A., PLAENGRIT, K., PIANRUMLUK, S., MANOONPOL, C., 2022. The Effects of Early Diabetes on Duodenal Alterations in the Rats. *International Journal of Morphology*, 40(2):389-395, doi:10.4067/S0717-95022022000200389.

LOVIC, D., PIPERIDOU, A., ZOGRAFOU, I., GRASSOS, H., PITTARAS, A., MANOLIS, A., 2020. The growing epidemic of diabetes mellitus. Current vascular *Pharmacology*, 18(2):104-109, https://doi.org/10.2174/1570161117666190405165911.

MEKURIA, AB., BELACHEW, S.A., TEGEGN, HG., ALI, DS., NETERE, AK., LEMLEMU, E., ERKU, D.A., 2018. Prevalence and correlates of herbal medicine use among type 2 diabetic patients in Teaching Hospital in Ethiopia: a cross-sectional study. *BMC complementary and alternative medicine*,18(article 85):1-8, https://doi.org/10.1186/s12906-018-2147-3.

MESGARI-ABBASI, M., GHADERI, S., KHORDADMEHR, M., NOFOUZI, K., TAYEFI-NASRABADI, H., MCINTYRE, G., 2019. Enteroprotective effect of Tsukamurella inchonensis on streptozotocin induced type 1 diabetic rats. *Turkish Journal of Biochemistry*, 44(5):683-91, https://doi.org/10.1515/tjb-2018-0309.

MUKHERJEE, P.K., BANERJEE, S., GUPTA, B.D., KAR, A., 2022. Evidence-based validation of herbal medicine: Translational approach. In Evidence-Based Validation of Herbal Medicine, (pp. 1-41). Elsevier, doi:10.1016/B978-0-323-85542-6.00025-1.

SCHNEIDER, C.A., W.S. RASBAND, & ELICIERI K.W., 2012. NIH Image to ImageJ: 25 years of image analysis. *Nature Methods*, 9(7): 671.

ZHAO, J., YANG, J., GREGERSEN, H., 2003. Biomechanical and morphometric intestinal remodelling during experimental diabetes in rats. *Diabetologia*, 46:1688-1697, https://doi.org/10.1007/s00125-003-1233-2.

ZHAO, M., LIAO, D., ZHAO, J., 2017. Diabetes-induced mechano-physiological. changes in the small intestine and colon. *World journal of diabetes*, 8(6):249-269, https://doi.org/10.4239/wjd.v8.i6.249.

IJAE
ITALIAN JOURNAL OF ANATOMY AND EMBRYOLOGY

Firenze University Press
www.fupress.com/ijae

OPEN ACCESS

Citation: Kaya, G., Yazici, G. N., Alavanda, C., & Küçük, Ö. S. (2025). Embryologic layers in dermatology: Developmental checkpoint disorders, diagnostic insight, and regenerative futures. *Italian Journal of Anatomy and Embryology* 129(2): 13-28. doi: 10.36253/ijae-16696

Data Availability Statement: All relevant data are within the paper and its Supporting Information files.

Competing Interests: The Author(s) declare(s) no conflict of interest.

Embryologic layers in dermatology: Developmental checkpoint disorders, diagnostic insight, and regenerative futures

Gökhan Kaya[1,*], Gülce Naz Yazici[2], Ceren Alavanda[3], Özlem Su Küçük[4]

[1] *Department of Dermatology, Sivas Medicana Hospital, Sivas, Türkiye*
[2] *Department of Histology and Embryology, Faculty of Medicine, Erzincan Binali Yıldırım University, Erzincan, Türkiye*
[3] *Department of Medical Genetics, Istanbul Faculty of Medicine, Istanbul University, Istanbul, Türkiye*
[4] *Department of Dermatology, Faculty of Medicine, Bezmiâlem Vakıf University, Istanbul, Türkiye*
*Corresponding Author. E-mail: gkhnkya@gmail.com

Abstract. Objectives: This review aims to present a developmental framework linking embryonic lineage with non-heritable cutaneous anomalies to improve diagnostic precision and educational approaches in dermatology. **Materials and Methods:** A narrative literature review was conducted using PubMed, Scopus, and Web of Science databases covering the years 2000–2025. Keywords included "skin development," "embryology," "developmental checkpoint disorders," and "non-genetic congenital disorders." Data on morphogenesis, embryologic signaling pathways, and representative disorders were synthesized into a layer-based model. **Results:** Disorders such as self-healing collodion baby (periderm retention anomaly), pigmentary mosaicism (postzygotic melanocyte patterning defect), and focal dermal hypoplasia (connective tissue maldevelopment) reflect disruptions at specific morphogenetic checkpoints. Mapping these conditions to their embryonic origins revealed layer-specific vulnerability windows and facilitated differential diagnosis from inherited disorders. Understanding these embryologic principles supports earlier diagnosis, informed prenatal counseling, and structured integration into dermatology curricula. Advances in regenerative medicine, particularly stem cell–based strategies, highlight the translational potential of dermatoembryology in developing targeted therapies. **Conclusion:** A layer-oriented dermatoembryological perspective enhances recognition of developmental skin disorders, especially when genetic analyses are inconclusive. Incorporating embryologic concepts into clinical reasoning not only improves diagnostic accuracy but also fosters regenerative therapeutic innovations and enriches dermatology education.

Keywords: embryonic development, skin abnormalities, congenital disorders, dermatology, regenerative medicine.

1. INTRODUCTION

Human skin is a complex, multilayered organ essential for homeostasis, immune defense, and environmental interaction. Structurally, it comprises three principal layers: epidermis, dermis, and hypodermis. Each derives from distinct embryonic sources – surface ectoderm gives rise to the epidermis, mesoderm to the dermis and hypodermis, and neural crest cells to melanocytes, vascular elements, and select sensory structures (1–3). While epidermal and dermal development has been extensively characterized, the hypodermis remains comparatively underexplored, despite its key functions in mechanical cushioning, endocrine signaling, and immune regulation. Recent advances in tri-layered skin modeling demonstrate that inclusion of adipose tissue enhances both structural fidelity and physiological relevance in engineered constructs (4).

Skin morphogenesis begins in the third gestational week, encompassing sequential processes such as epidermal stratification, melanoblast migration, adnexal morphogenesis, and maturation of the dermoepidermal junction (2). Single-cell transcriptomic and spatial analyses have revealed dynamic interactions between immune and nonimmune populations during this period; notably, macrophages actively shape angiogenesis, neurogenesis, and hair follicle formation beyond their classical immunologic roles (5). Keratinocyte differentiation proceeds from basal progenitors upward through spinous and granular layers, with lineage specification orchestrated by conserved signaling pathways – Wnt, Notch, Hedgehog, FGF, and MAPK/ERK – operating in precise spatiotemporal patterns (6–8). Although epithelial cells are embryologically committed, regenerative studies highlight latent plasticity that links embryogenesis with postnatal repair, bridging developmental and regenerative dermatology (9).

Errors in these morphogenetic checkpoints may result in clinically significant anomalies, some without defined genetic etiologies. Conditions such as self-healing collodion membrane, pigmentary mosaicism, and focal dermal hypoplasia illustrate how disruption of critical embryonic stages can yield cutaneous phenotypes resembling monogenic disorders (2,10). For instance, incomplete periderm desquamation beyond 21 weeks or impaired melanoblast migration before week 12 exemplify layer-specific vulnerability windows that manifest independently of identifiable mutations. Figure 1 schematically correlates germ-layer origins with clinical phenotypes, underscoring the diagnostic utility of developmental timing in dermatology.

Despite its relevance, dermatoembryology remains underrepresented in dermatology training and diagnostic practice (11). A developmentally informed, layer-specific perspective could strengthen early recognition of congenital anomalies, refine prenatal assessments, and foster integration between developmental biology and clinical dermatology (12). Accordingly, this review delineates the embryologic origins of major skin components, analyzes how disruptions in developmental checkpoints produce genetically undetermined disorders, and situates these insights within diagnostic reasoning, medical education, and regenerative medicine. Unlike traditional Mendelian paradigms, our framework emphasizes embryologic timing and layer-specific vulnerability as central to understanding dermatologic phenotypes.

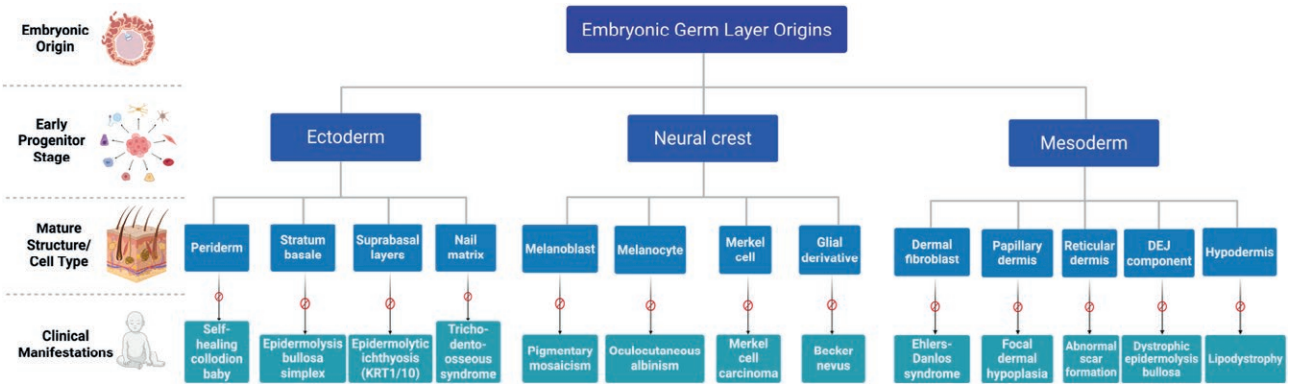

Figure 1. Embryology-Based Classification of Non-Genetic Skin Disorders. Schematic diagram showing the embryonic origins of skin structures from ectoderm, neural crest, and mesoderm. Germ-layer derivatives are linked to their progenitor stages, mature structures, and representative disorders arising from morphogenetic checkpoint disruptions. The model highlights the importance of developmental timing and lineage specificity in shaping dermatologic phenotypes beyond Mendelian inheritance.

2. OVERVIEW OF SKIN DEVELOPMENT

2.1. Embryological timeline

Skin development begins in the third week of embryogenesis, involving coordinated morphogenetic events derived from the ectoderm, mesoderm, and neural crest. The surface ectoderm generates the epidermis, the mesoderm forms the dermis and hypodermis, and neural crest cells contribute melanocytes and mechanosensory structures (1–3). By week 4, the ectoderm appears as a single-cell layer that thickens between weeks 4 and 6 into a bilayer of proliferative basal cells and superficial periderm (13). The periderm serves as a transient barrier and is normally shed into the amniotic fluid by week 21 (14). Simultaneously, mesenchymal cells differentiate into early dermis, and neural crest–derived melanoblasts begin migrating toward the basal epidermis around embryonic day 50 (approximately week 7), continuing through weeks 8–12 under the influence of transcription factors such as SOX10, PAX3, and MITF (15).

During the second trimester, epidermal stratification accelerates, adnexal structures begin to form, and the dermoepidermal junction matures. By the third trimester, the epidermis and dermis are structurally mature, adnexal appendages such as hair follicles, glands, and nails are largely developed, and vascularization, innervation, and immune cell colonization provide barrier and sensory functions at birth (16). Figure 2 summarizes these developmental milestones and highlights the temporal coordination of epidermal, dermal, adnexal, and immune maturation across gestation.

2.2. Epidermal and dermal layer formation

Between weeks 4 and 6, the surface ectoderm and mesoderm initiate the formation of the epidermis and dermis. The ectoderm gives rise to basal keratinocytes and the transient periderm, which expands without division and is shed by week 21 (13,14). Stratification begins around week 11 with the appearance of an intermediate layer, and by week 24 the epidermis is composed of spinous, granular, and cornified layers (13,17). Basal cells express keratins K5 and K14 from week 8, while suprabasal cells begin producing differentiation markers such as filaggrin, involucrin, and loricrin. Together with SPRs, envoplakin, and periplakin, these proteins are cross-linked by transglutaminases to form the cornified envelope.

The dermis, derived from mesenchymal precursors, produces collagens I, III, V, and VI between weeks 8 and 12, and by week 14 it organizes into papillary and reticular layers (18). The dermoepidermal junction matures in parallel, with hemidesmosomes and type VII collagen fibrils providing stable adhesion between epidermis and dermis (17,18).

2.3. Melanocyte migration

Melanocytes originate from neural crest cells, which undergo epithelial-to-mesenchymal transition before migrating dorsolaterally toward the epidermis. Their migration is regulated by transcription factors including SOX10, PAX3, and MITF (19). During this process, melanoblasts alter adhesion profiles, downregulating E-cadherin and adopting a P-cadherin phenotype to facilitate epidermal integration (19,20). Chemotactic cues, most notably SDF-1α/CXCL12 acting through CXCR4, direct migration, while α-MSH enhances responsiveness (21). These developmental mechanisms not only establish pigmentation during embryogenesis but also underpin postnatal processes such as wound healing.

2.4. Adnexal structure formation

The formation of adnexal structures, including hair follicles, sebaceous glands, sweat glands, and nails, occurs through reciprocal epithelial–mesenchymal interactions beginning around weeks 9–20. Hair follicles develop from epidermal placodes and interact with dermal papillae to guide follicular differentiation and shaft formation. Sebaceous glands arise from follicular epithelium and release sebum by holocrine secretion. Eccrine sweat glands develop independently from epidermal downgrowths, forming coiled secretory units within the deep dermis, whereas apocrine glands originate from follicular structures in the axillary and anogenital regions, releasing secretions via decapitation (22). These developmental events are regulated by signaling pathways including WNT, EDA/EDAR, SHH, and BMP, and disruption of these cascades results in ectodermal dysplasias (22,23).

2.5. Molecular signaling pathways

Skin morphogenesis is orchestrated by a network of evolutionarily conserved signaling pathways. Wnt signaling initiates placode formation and appendage patterning, with Dkk1 acting as a major inhibitor. Notch signaling regulates cell fate specification through lateral inhibition, whereas FGF signaling promotes epithelial–mesenchymal crosstalk critical for tissue morphogenesis.

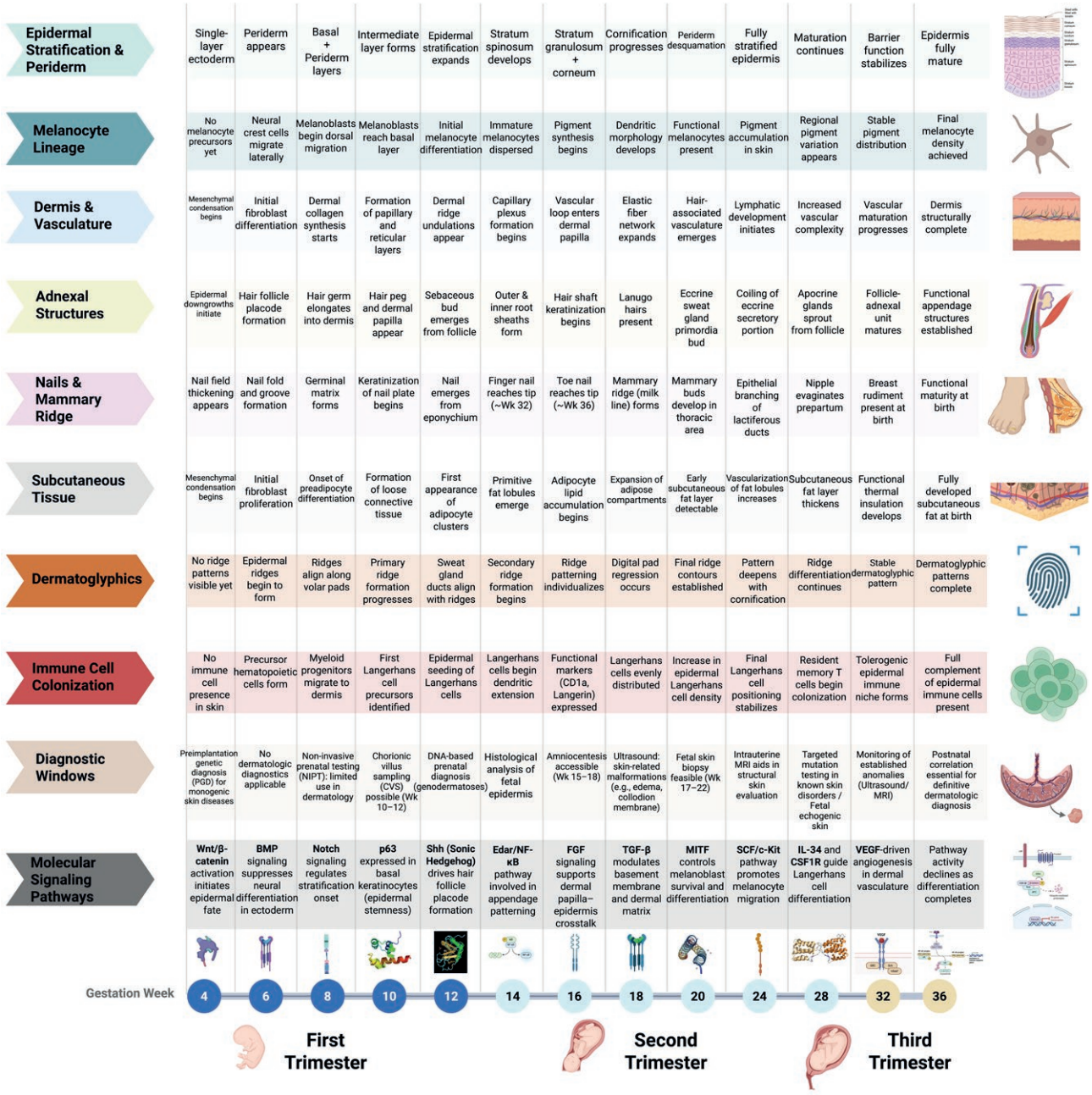

Figure 2. Developmental Timeline of Human Skin. Schematic overview of key embryonic and fetal milestones between gestational weeks 4–36. The timeline highlights epidermal stratification, melanocyte differentiation and migration, dermal and adnexal morphogenesis, nail and mammary ridge development, immune cell colonization, and major molecular signaling events that coordinate skin maturation.

BMP signaling drives epidermal differentiation while suppressing appendage formation in the interfollicular epidermis (8,24). MAPK/ERK signaling integrates proliferative and differentiative cues, contributing both to morphogenesis and to regenerative capacity (24). The precise temporal coordination of these pathways ensures normal skin development, while their dysregulation produces congenital dermatologic disorders and offers potential therapeutic targets for regenerative strategies. Figure 3 illustrates the sequential progression of epidermal stratification, melanocyte differentiation, dermal remodeling, adnexal development, and hypodermal maturation throughout gestation.

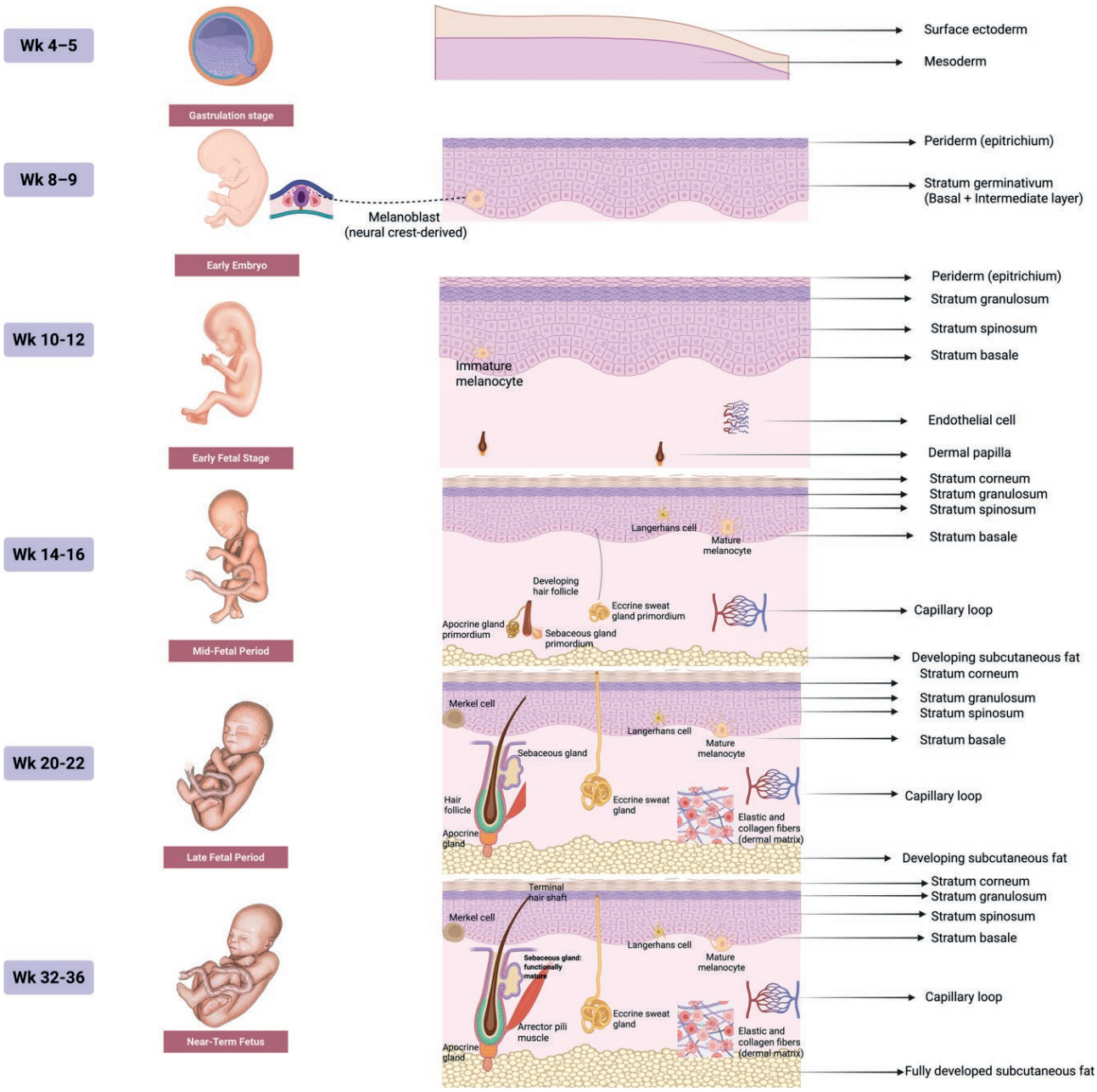

Figure 3. Temporal Differentiation of Skin Layers and Adnexal Structures. Schematic overview of human skin development from gestational weeks 4–36, showing epidermal stratification, melanocyte differentiation, dermal remodeling, adnexal formation (hair follicles, glands), and maturation of subcutaneous adipose tissue leading to a fully functional integument at term.

3. DEVELOPMENTAL DEFECTS AND RELATED NON-GENETIC DISORDERS

3.1. Periderm defects

The periderm, a transient embryonic layer, protects the developing epidermis and contributes to epithelial integrity and amniotic exchange. Failure of timely shedding produces the collodion baby phenotype, often linked to TGM1 mutations in autosomal recessive ichthyoses (25,26). In some cases, spontaneous resolution occurs as self-healing collodion baby (27). Persistent periderm caused by IRF6, IKKα, or SFN mutations underlies syndromes such as popliteal pterygium and

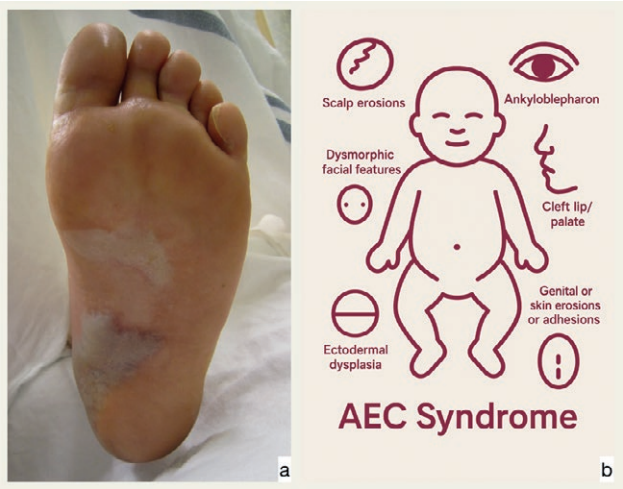

Figure 4. Basal layer and stratification defects in epidermal development. (a) Epidermolysis bullosa simplex with plantar erosions due to KRT5/KRT14 mutations impairing keratin filament stability. (b) Schematic of AEC (ankyloblepharon–ectodermal dysplasia–clefting) syndrome from TP63 mutations, showing scalp erosions, ankyloblepharon, clefting, nail and hair abnormalities, and impaired adnexal development.

Bartsocas-Papas (28). Harlequin-like collodion due to ABCA12 variants represents a milder defect with potential for improvement under supportive care (29). Vernix caseosa, composed of periderm remnants and sebaceous secretions, supports maturation and thermoregulation; its absence predisposes premature infants to dehydration and infection, reflecting a clinically relevant model of incomplete skin maturation (30).

3.2. Basal Layer and stratification defects

Abnormal keratinocyte proliferation and stratification in the basal layer result in distinct disorders. Mutations in KRT5 or KRT14 cause epidermolysis bullosa simplex (EBS), characterized by intraepidermal blistering of variable severity (31). PLEC mutations lead to syndromic EBS with muscular dystrophy, while TP63 mutations disrupt stratification and adnexal development, producing AEC (Hay-Wells) syndrome with erosions, ankyloblepharon, clefting, and nail anomalies (32) (Figure 4).

3.3. Granular layer and cornification abnormalities

Cornification defects include epidermolytic ichthyosis, caused by dominant KRT1 or KRT10 mutations, presenting with neonatal blistering that progresses to diffuse hyperkeratosis with suprabasal cytolysis and clumped keratohyalin granules (33). Lamellar ichthyosis, classically recessive, has also been linked to dominant NKPD1 mutations, producing milder congenital scaling (34) (Figure 5).

Figure 5. Epidermolytic ichthyosis: clinical manifestation. Clinical photograph of a child with dominant KRT1/KRT10 mutations, showing neonatal blistering evolving into diffuse hyperkeratosis with verrucous plaques, erosions, and secondary infection. Histology demonstrates suprabasal cytolysis, clumped keratohyalin granules, and perinuclear vacuolization.

3.4. Embryological pigment patterning defects

Defects in melanocyte function and patterning create pigmentary anomalies. Oculocutaneous albinism type 1 (OCA1), due to TYR mutations, manifests as generalized hypopigmentation despite normal migration (35,36). Segmental pigmentary disorders, including hypomelanosis of Ito and nevus depigmentosus, result from postzygotic mosaicism (37,38). Becker nevus, associated with ACTB mutations, presents with unilateral hyperpigmentation and hypertrichosis, whereas nevus spilus exhibits scattered dark macules over lighter patches (39,40) (Figure 6).

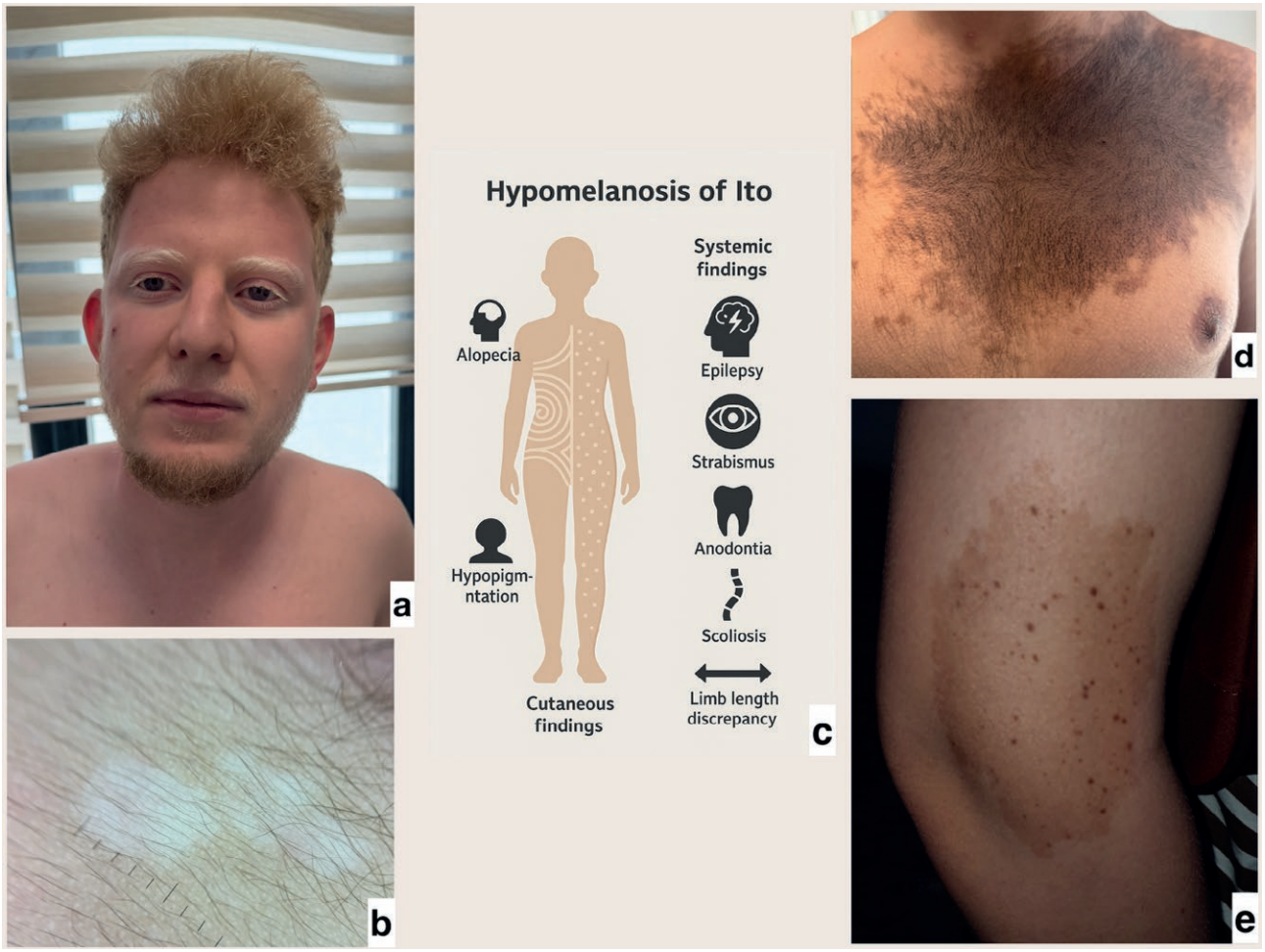

Figure 6. Clinical spectrum of embryological pigment patterning defects. (a) Oculocutaneous albinism (TYR mutation) with generalized hypopigmentation and nystagmus. (b) Nevus depigmentosus: stable, segmental hypopigmented macule. (c) Hypomelanosis of Ito: mosaic hypopigmentation along Blaschko's lines with extracutaneous anomalies. (d) Becker nevus: unilateral hyperpigmentation with hypertrichosis, linked to ACTB mutations. (e) Nevus spilus: benign mosaic disorder with dark macules on a lighter background.

3.5. Dermal formation defects

Dermal development depends on positional identity maintained by HOX gene expression (40). Mutations in collagen genes (COL1A1, COL3A1, COL5A1) cause Ehlers-Danlos syndromes, with skin hyperextensibility, fragility, and vascular complications (41,42). In contrast, focal dermal hypoplasia (Goltz syndrome), caused by PORCN mutations, produces linear dermal atrophy, fat herniation, and skeletal anomalies (43) (Figure 7).

3.6. Dermal–epidermal junction defects

Defects at the dermoepidermal junction manifest as different subtypes of epidermolysis bullosa. Mutations in KRT5, KRT14, or PLEC produce EBS with basal keratinocyte cleavage; LAMA3, LAMB3, LAMC2, COL17A1, or ITGB4 mutations cause junctional EB (JEB) with lamina lucida blistering (44,45); and COL7A1 mutations lead to dystrophic EB (DEB) with sublamina densa cleavage, scarring, and SCC risk (46). Kindler syndrome (FERMT1) features mixed-level cleavage, poikiloderma, photosensitivity, and cancer predisposition (47) (Figure 8).

3.7. Adnexal development defects

Defective appendage development produces diverse phenotypes. Hypohidrotic ectodermal dysplasia (EDA, EDAR, EDARADD) presents with hypotrichosis, hypodontia, and hypohidrosis (48). FOXN1 mutations cause

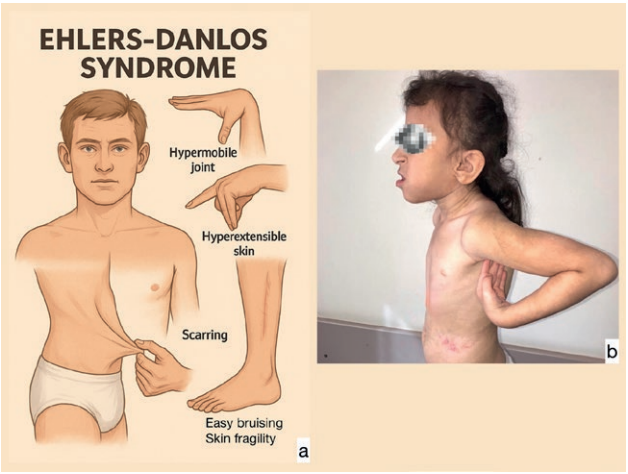

Figure 7. Comparative features of connective tissue disorders: Ehlers-Danlos syndrome and Goltz-Gorlin syndrome. (a) Ehlers-Danlos syndrome (EDS): schematic showing hypermobile joints, hyperextensible skin, atrophic scars, and tissue fragility due to collagen gene mutations (COL5A1, COL5A2, COL3A1). (b) Goltz-Gorlin syndrome (focal dermal hypoplasia): clinical image with patchy dermal atrophy along Blaschko's lines, fat herniation, skeletal asymmetry, and linear hypo-/hyperpigmented streaks.

alopecia, nail dystrophy, and severe T-cell immunodeficiency (49). Monilethrix (KRT81/83/86) is characterized by fragile, beaded hairs and keratosis pilaris (50). Tricho-dento-osseous syndrome involves curly hair, enamel hypoplasia, and skeletal sclerosis (51). Nevus sebaceous of Jadassohn is a congenital hamartoma with risk of secondary BCC, while Gorlin syndrome (PTCH1 mutations) links follicular morphogenesis defects to multiple BCCs and systemic anomalies (19,52,53) (Figure 9).

3.8. Embryological patterning lines

Cutaneous mosaic disorders often follow Blaschko's lines due to postzygotic mutations (54). Incontinentia pigmenti (IKBKG) progresses through vesiculobullous, verrucous, hyperpigmented, and atrophic stages, often with dental, ocular, and neurological abnormalities (56). Epidermal nevi, either isolated or syndromic, similarly trace embryonic patterning lines (55,57) (Figure 10).

3.9. Externally induced developmental defects

Exogenous factors may disrupt embryonic skin development. Amniotic band sequence causes constrictions and limb defects (58). Valproic acid exposure induces neural tube and craniofacial anomalies via epigenetic and folate metabolism interference (59).

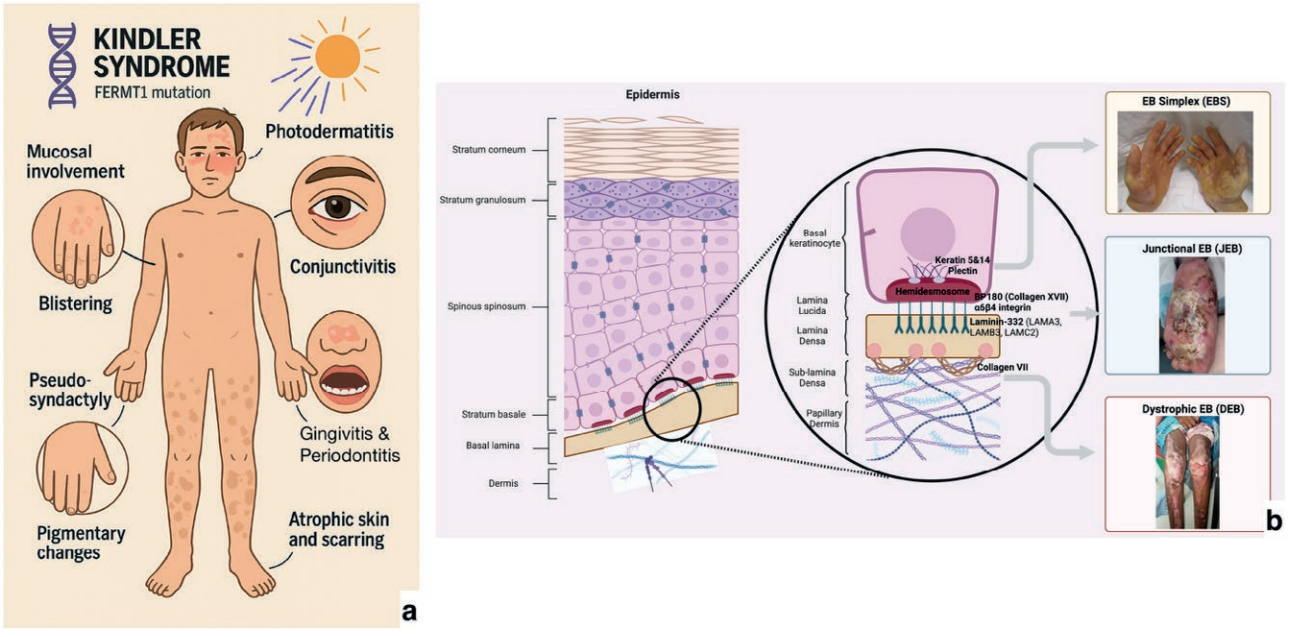

Figure 8. Structural and clinical features of dermal–epidermal junction disorders. (a) Kindler syndrome (FERMT1 mutation) showing trauma-induced blistering, poikiloderma, photosensitivity, mucosal involvement, and increased SCC risk. (b) Schematic of the epidermal–dermal junction (EDJ) highlighting adhesion structures. Disruption causes distinct epidermolysis bullosa (EB) subtypes: EBS (KRT5, KRT14, PLEC; basal keratinocyte cleavage), JEB (COL17A1, LAMA3, LAMB3, LAMC2, ITGB4; lamina lucida blistering), and DEB (COL7A1; sublamina densa cleavage with scarring).

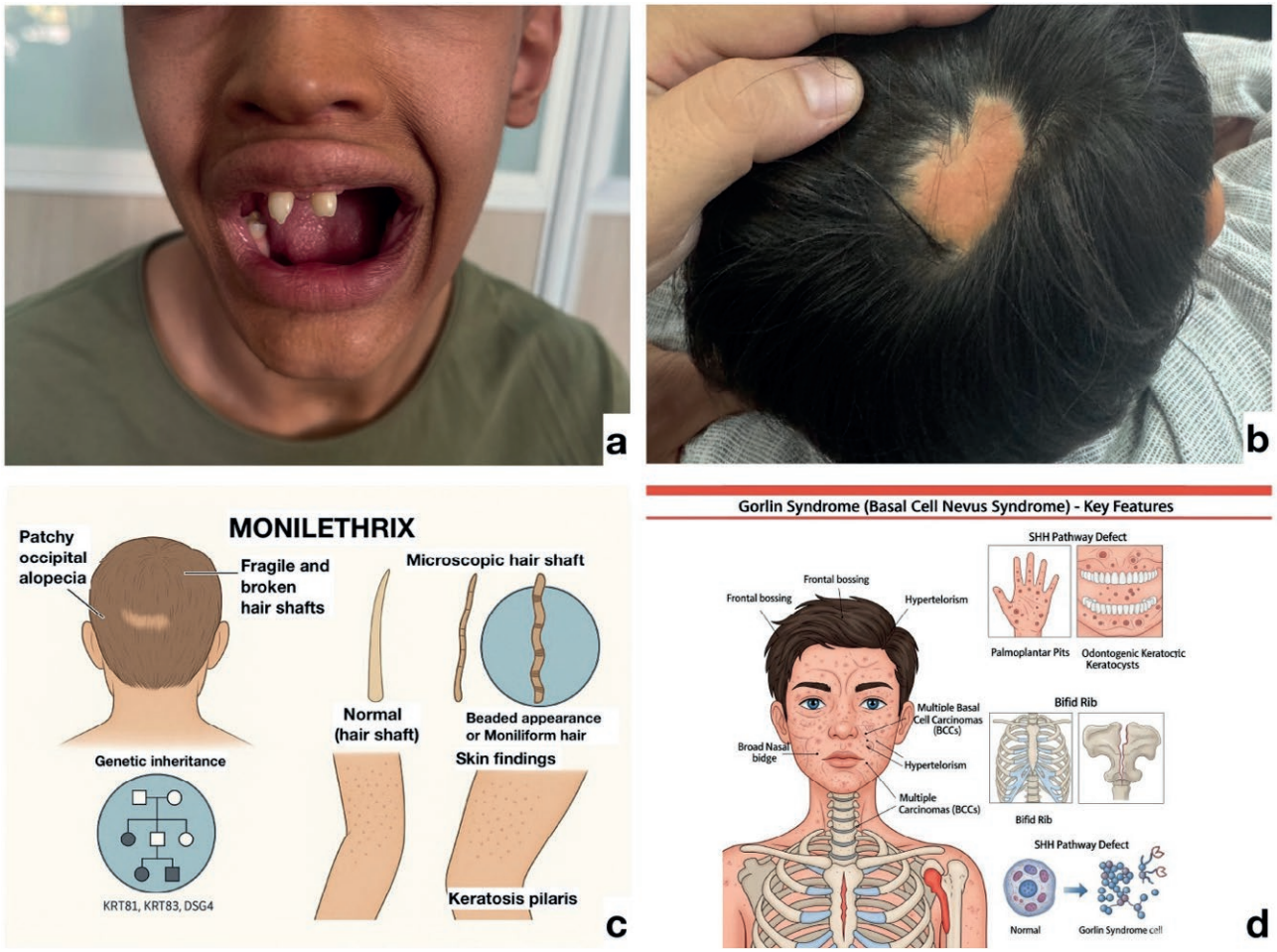

Figure 9. Clinical presentation of adnexal development disorders. (a) Hypohidrotic ectodermal dysplasia (EDA/EDAR/EDARADD mutations): sparse hair, hypodontia with conical teeth, and perioral wrinkling. (b) Nevus sebaceous of Jadassohn: congenital yellowish alopecic scalp plaque with risk of secondary BCC. (c) Monilethrix (KRT81/83/86 mutations): patchy occipital alopecia with fragile beaded hair shafts and associated keratosis pilaris. (d) Gorlin syndrome (PTCH1 mutation): multiple basal cell carcinomas, odontogenic cysts, palmar/plantar pits, skeletal anomalies, and craniofacial features.

Excess retinoic acid produces craniofacial malformations through retinoid receptor activation (60). Infections such as congenital cytomegalovirus and Zika virus impair growth and neurodevelopment, particularly with early gestational exposure (61,62). Figure 11 presents an embryology-based diagnostic framework that integrates lesion timing, morphology, and layer attribution for congenital skin anomalies.

4. DISCUSSION

4.1. Diagnostic utility of dermatoembryology

Dermatoembryology provides a valuable interpretive framework for prenatal dermatologic diagnosis, particularly for congenital anomalies of developmental rather than strictly genetic origin. Cutaneous structures derive from distinct embryological layers: ectoderm produces the epidermis and periderm, mesoderm forms dermal and vascular components, and neural crest cells give rise to melanocytes and some dermal elements. Each follows a defined developmental timeline: periderm forms by week 5 and regresses by week 21, while melanocyte migration occurs between weeks 8 and 12 (63). Recognizing these sequences is critical when interpreting fetal biopsies or ultrasonography.

Persistence of the periderm beyond week 22 may indicate delayed epidermal maturation, clinically manifesting as a transient collodion membrane. Likewise, impaired melanocyte migration or differentiation may explain segmental hypopigmentation patterns that are

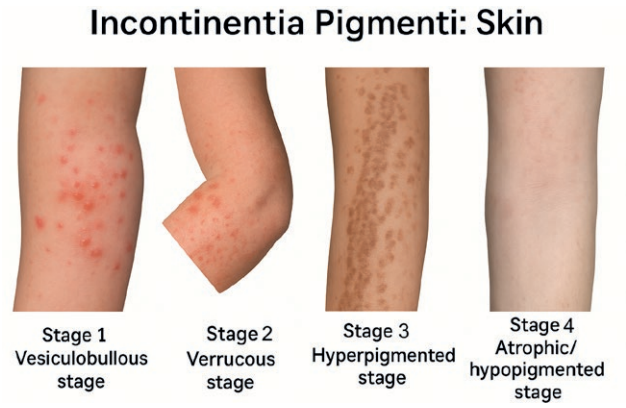

Figure 10. Cutaneous stages of Incontinentia Pigmenti. Incontinentia pigmenti is an X-linked dominant genodermatosis caused by mutations in the *IKBKG* (NEMO) gene, primarily affecting females. The disease progresses through four characteristic cutaneous stages, often following Blaschko's lines: Stage 1 (Vesiculobullous stage): Linear or grouped vesicles and bullae appearing shortly after birth. Stage 2 (Verrucous stage): Hyperkeratotic, wart-like papules typically seen in the first few weeks of life. Stage 3 (Hyperpigmented stage): Swirling or streaked hyperpigmented macules appearing during infancy or early childhood. Stage 4 (Atrophic/hypopigmented stage): Residual hypopigmented or atrophic streaks in adolescence or adulthood, often persistent. These stages may overlap or vary in duration and intensity between individuals. In addition to skin findings, the condition may involve dental, ocular, neurological, and hair anomalies.

evident at birth but not attributable to known genodermatoses. Such findings, particularly when genetic testing is inconclusive, underscore the role of developmental landmarks in prenatal diagnosis, as also supported by recent whole-exome sequencing (WES) studies (64). Thus, dermatoembryology bridges morphology with prenatal diagnostics, offering a layer-specific perspective that enhances both invasive and non-invasive assessments. Figure 11 illustrates this integrated diagnostic approach.

4.2. Educational integration: teaching dermatologic development

Despite its relevance, dermatologic embryology remains underrepresented in medical curricula, leading to fragmented knowledge (11). A layer-based teaching model that links ectodermal, mesodermal, and neural crest derivatives to common dermatologic conditions could strengthen both basic science education and clinical reasoning. Fakoya et al. (12) highlighted the need for an internationally standardized embryology syllabus emphasizing clinical translation, while Moraes et al. (65) showed that case-based and multimedia-enhanced teaching improves student engagement. Incorporating such approaches into dermatology education – particularly in pediatrics and prenatal dermatology – may foster early pattern recognition, diagnostic accuracy, and appreciation of developmental timing in cutaneous pathology.

4.3. Future directions: a stem cell perspective

Recent advances in stem cell biology have expanded the translational potential of dermatoembryology. Skin-derived stem cells, including epidermal stem cells (EpSCs), mesenchymal stromal cells (MSCs), and neural crest–derived melanocyte precursors, are central to both development and regeneration (66). These cells, residing in niches such as the basal epidermis, hair follicle bulge, and dermis, are regulated by pathways including Wnt/β-catenin, Notch, and p63 (67). Their plasticity is evident during wound healing, where follicular stem cells contribute to interfollicular repair, recapitulating developmental programs (68).

Stem cell–based therapies have shown promise in chronic wounds, autoimmune dermatoses, and hereditary blistering disorders. Adipose- and bone marrow–derived MSCs enhance re-epithelialization, angiogenesis, and immunomodulation in both experimental and clinical settings (69,70). Induced pluripotent stem cells (iPSCs) from dermal fibroblasts offer opportunities for gene-corrected autografts in conditions such as epidermolysis bullosa (66). Emerging human skin explant (HSE) models further demonstrate that ex vivo tissue maintains architecture, immune competence, and multipotent stem cell reservoirs (SKPs, MSCs), enabling studies on neuro-immune-cutaneous interactions relevant to both regenerative medicine and drug development (71).

5. CONCLUSION

Human skin develops through tightly coordinated interactions among ectodermal, mesodermal, and neural crest–derived lineages, each contributing to its structural and functional integrity. While dermatology research often emphasizes genetic causes, many congenital disorders arise instead from developmental disruptions at critical morphogenetic checkpoints. Examples include anomalies in periderm shedding, melanoblast migration, dermal extracellular matrix formation, and adnexal morphogenesis, all of which can be traced to layer-specific vulnerabilities during embryogenesis.

A dermatoembryological, layer-oriented framework improves diagnostic accuracy, particularly when genetic testing is inconclusive, and supports prenatal counseling,

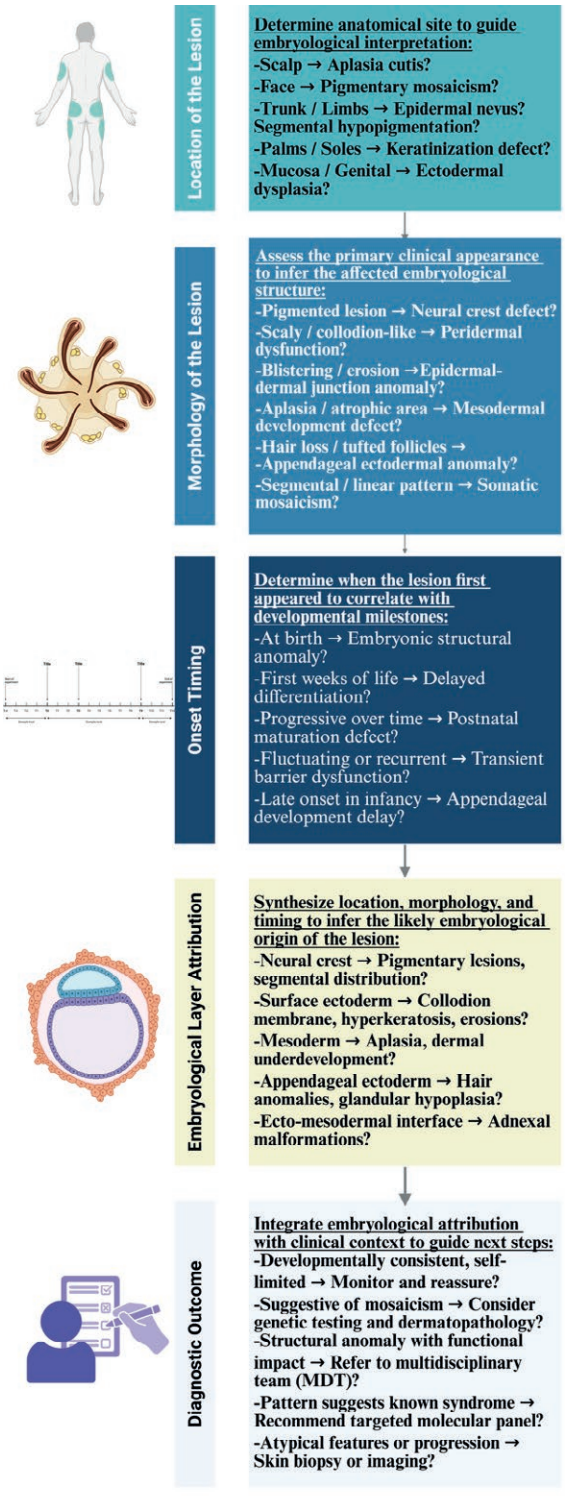

Figure 11. Embryology-Guided Diagnostic Framework for Congenital Skin Lesions with Clinical Case Applications. (a) Diagnostic algorithm presenting a structured, five-step approach integrating lesion anatomical localization, morphology, timing of onset, embryological layer attribution, and clinical decision pathways for congenital dermatologic anomalies. (b) Illustrative application of this diagnostic framework to three representative clinical scenarios: Mongolian spot (neural crest–derived pigmentary delay), aplasia cutis congenita of the scalp (mesodermal fusion defect), and self-healing collodion baby (ectodermal periderm retention anomaly). This model facilitates targeted diagnostic evaluation and clinical management based on embryological insights.

Table 1. Embryological Origins of Cutaneous Stem Cells and Their Therapeutic Potential. This table summarizes major stem cell types involved in skin development and regeneration, categorized by their embryological origins. It highlights their differentiated outcomes and potential clinical or research applications in dermatology.

Embryological Layer	Stem Cell Type(s)	Differentiated Outcomes	Clinical/Research Applications
Ectoderm	Epidermal Stem Cells (EpSCs)	Keratinocytes, epidermis layers	Epidermolysis bullosa, skin grafting, wound healing
Neural Crest	Melanocyte SCs, EPI-NCSC	Melanocytes, neural/glial lineages	Pigment disorders, vitiligo, melanoma modeling
Mesoderm	Mesenchymal Stromal Cells (MSCs)	Fibroblasts, adipocytes, endothelial, myocytes	Wound healing, fibrosis modulation, immunotherapy
iPSC-derived (Exogenous)	iPSC-derived keratinocytes/fibroblasts	Any germ-layer lineage (pluripotent)	Gene-corrected autografts, in vitro disease modeling

early biopsy decisions, and interdisciplinary management. Incorporating these principles into medical curricula also enriches dermatology education by deepening understanding of congenital anomalies and their developmental origins.

Finally, the same principles carry translational value: regenerative dermatology increasingly leverages stem cell biology and developmental pathways to restore tissue architecture. Together, these insights emphasize the diagnostic, educational, and therapeutic importance of embryology in contemporary dermatologic practice.

ABBREVIATIONS

ABCA12: ATP-binding cassette sub-family A member 12
ABS: Amniotic band sequence
ACTB: Actin beta
ADHD: Attention deficit hyperactivity disorder
AEC: Ankyloblepharon-ectodermal defects-cleft lip/palate (Hay-Wells) syndrome
ASD: Autism spectrum disorder
BMP: Bone morphogenetic protein
CXCL12: C-X-C motif chemokine ligand 12
CXCR4: C-X-C chemokine receptor type 4
DEB: Dystrophic epidermolysis bullosa
DEJ: Dermoepidermal junction
EBS: Epidermolysis bullosa simplex
E-cadherin: Epithelial cadherin
EDAR: Ectodysplasin A receptor
EDARADD: EDAR-associated death domain
EDA: Ectodysplasin A
EpSCs: Epidermal stem cells
FGF: Fibroblast growth factor
FOXN1: Forkhead box N1
HED: Hypohidrotic ectodermal dysplasia
HSE: Human skin explants
iPSCs: Induced pluripotent stem cells
IRF6: Interferon regulatory factor 6
IKKα: IκB kinase alpha
JEB: Junctional epidermolysis bullosa
KRT: Keratin
LAMA3, LAMB3, LAMC2: Laminin subunits α3, β3, γ2
MAPK/ERK: Mitogen-activated protein kinase/extracellular signal-regulated kinase
MITF: Microphthalmia-associated transcription factor
MSCs: Mesenchymal stromal cells
NKPD1: NTPase KAP family P-loop domain-containing protein 1
OCA1: Oculocutaneous albinism type 1
PAX3: Paired box gene 3
P-cadherin: Placental cadherin
PLEC: Plectin
SAM: Sterile alpha motif
SCs: Stem cells
SDF-1α: Stromal cell-derived factor 1 alpha
SFN: Stratifin
SHH: Sonic hedgehog
SKPs: Skin-derived precursors
SOX10: SRY-box transcription factor 10
TDO: Tricho-dento-osseous syndrome
TGM1: Transglutaminase 1
TP63: Tumor protein p63
TYR: Tyrosinase
VPA: Valproic acid
WES: Whole-exome sequencing

AUTHORS' CONTRIBUTIONS

G.K. conceived the study, conducted the literature review, drafted, and critically revised the manuscript. **G.N.Y.** handled the ethical approval process, critically appraised the manuscript content, and contributed to

the evaluation of the study's scope and structure. **C.A.** provided clinical images and case data, participated in the interpretation of clinical findings, and critically revised the manuscript for important intellectual content. **Ö.S.K.** contributed substantially to the conception and design of the study, supervised manuscript development, and performed critical revisions for important intellectual content. All authors read and approved the final version of the manuscript and agreed to be accountable for all aspects of the work.

ACKNOWLEDGMENTS

Throughout the course of this study, we adhered strictly to the World Medical Association Declaration of Helsinki and the Good Clinical and Laboratory Practice standards.

The schematic illustrations included in this article were created using BioRender.com under an academic license intended for scientific research and publication purposes. These include Figures 4b, 6c, 7a, 8b, 9a–c, and 11a–b.

All other clinical images, including patient photographs and case examples, originate from the personal archive of the authors and are used with written informed consent from the patients and/or their legal guardians, in accordance with ethical publishing standards.

ETHICS STATEMENT

The study was conducted in accordance with the principles of the Declaration of Helsinki. The study protocol was approved by the Erzincan Binali Yıldırım University Clinical Research Ethics Committee on June 13, 2025, with the decision number 456343.

REFERENCES

1. Sadler TW. Langman's medical embryology. 12th ed. Philadelphia: Lippincott Williams & Wilkins; 2012. Available from: https://integratedsciences.lwwhealthlibrary.com/book.aspx?bookid=770
2. Schoenwolf GC, Bleyl SB, Brauer PR, Francis-West PH. Larsen's human embryology. 5th ed. Philadelphia: Elsevier; 2014.
3. Fitzpatrick TB, Kang S, Goldsmith LA, Gilchrest BA, Paller AS, Leffell DJ, Wolff K, editors. Structure and function of skin. In: Fitzpatrick's dermatology in general medicine. 10th ed. New York: McGraw-Hill; 2024. Chapter 7.
4. Workman VL, Giblin AV, Green NH, et al. Development of a tissue-engineered skin model with epidermal, dermal and hypodermal components. In Vitro Models. 2023;2:297-306. https://doi.org/10.1007/s44164-023-00058-9.
5. Gopee NH, Winheim E, Olabi B, et al. A prenatal skin atlas reveals immune regulation of human skin morphogenesis. Nature. 2024;635:679-689. https://doi.org/10.1038/s41586-024-08002-x.
6. Park S. Building vs. rebuilding epidermis: Comparison embryonic development and adult wound repair. Front Cell Dev Biol. 2022;9:796080. https://doi.org/10.3389/fcell.2021.796080.
7. Fuchs E. Scratching the surface of skin development. Nature. 2007;445(7130):834-842. https://doi.org/10.1038/nature05659.
8. Sonnen KF, Janda CY. Signalling dynamics in embryonic development. Biochem J. 2021;478(23):4045-4070. https://doi.org/10.1042/BCJ20210043.
9. Fu X, editor. Regenerative medicine in China. Singapore: Springer; 2021. https://doi.org/10.1007/978-981-16-1182-7.
10. De Falco M, Pisano MM, De Luca A. Embryology and anatomy of the skin. In: Brash UT, Maitland ML, editors. Skin cancer. New York: Springer; 2014. p.3-17. https://doi.org/10.1007/978-1-4614-7357-2_1.
11. Tumiene B, Peters H, Melegh B, et al. Rare disease education in Europe and beyond: time to act. Orphanet J Rare Dis. 2022;17:441. https://doi.org/10.1186/s13023-022-02527-y.
12. Fakoya FA, Emmanouil-Nikoloussi E, Sharma D, Moxham BJ. A core syllabus for the teaching of embryology and teratology to medical students. Clin Anat. 2017;30(2):159-167. https://doi.org/10.1002/ca.22802.
13. Cochard LR, Netter FH. Netter's atlas of human embryology. Updated ed. Philadelphia: Saunders Elsevier; 2012.
14. Chetty R. Pathology of vascular skin lesions: Clinicopathological correlations: Sangueza OP, Requena L. J Clin Pathol. 2003;56(7):559-560.
15. Schlessinger DI, Patino SC, Belgam Syed SY, et al. Embryology, epidermis. [Updated 2022 Oct 10]. In: StatPearls [Internet]. Treasure Island (FL): StatPearls Publishing; 2025 Jan-. Available from: https://www.ncbi.nlm.nih.gov/books/NBK441867/
16. Voiță-Mekereș F. Assessment of the embryological origin, anatomical and histological structure of the

skin. Arch Pharm Pract. 2024;15(2):69-74. https://doi.org/10.51847/SWViK4kyKx.
17. Hoeger PH, Kinsler V, Yan AC, Harper J, Oranje AP, Bodemer C, et al., editors. Harper's textbook of pediatric dermatology. 4th ed. Oxford: Wiley-Blackwell; 2019.
18. Singh V. Textbook of clinical embryology. New Delhi: Elsevier India; 2012.
19. Griffiths CEM, Barker J, Bleiker TO, Hussain W, Simpson RC, editors. Rook's textbook of dermatology. 10th ed. Oxford: Wiley-Blackwell; 2024.
20. Mort RL, Jackson IJ, Patton EE. The melanocyte lineage in development and disease. Development. 2015;142(4):620-632. https://doi.org/10.1242/dev.106567.
21. Keswell D, Kidson SH, Davids LM. Melanocyte migration is influenced by E-cadherin-dependent adhesion of keratinocytes in both two- and three-dimensional in vitro wound models. Cell Biol Int. 2015;39(2):169-176. https://doi.org/10.1002/cbin.10350.
22. Yamauchi A, Hadjur C, Takahashi T, Suzuki I, Hirose K, Mahe YF. Human skin melanocyte migration towards stromal cell-derived factor-1α demonstrated by optical real-time cell mobility assay: modulation of their chemotactic ability by α-melanocyte-stimulating hormone. Exp Dermatol. 2013;22(10):664-667. https://doi.org/10.1111/exd.12232.
23. Alsaad KO, Obaidat NA, Ghazarian D. Skin adnexal neoplasms--part 1: an approach to tumours of the pilosebaceous unit. J Clin Pathol. 2007;60(2):129-144. https://doi.org/10.1136/jcp.2006.040337.
24. Sanz-Ezquerro JJ, Münsterberg AE, Stricker S. Signaling pathways in embryonic development. Front Cell Dev Biol. 2017;5:76. https://doi.org/10.3389/fcell.2017.00076.
25. Tüzün Y, İşçimen A, Pehlivan Ö. Collodion baby. J Turk Acad Dermatol. 2008;2(2):Article 82201r. Available from: http://www.jtad.org/2008/2/jtad82201r.pdf
26. Simalti AK, Sethi H. Collodion baby. Med J Armed Forces India. 2017;73(2):197-199. https://doi.org/10.1016/j.mjafi.2015.10.007.
27. Nguyen MA, Gelman A, Norton SA. Practical events in the management of a collodion baby. JAMA Dermatol. 2015;151(9):1031-1032. https://doi.org/10.1001/jamadermatol.2015.0694.
28. Richardson RJ, Hammond NL, Coulombe PA, et al. Periderm prevents pathological epithelial adhesions during embryogenesis. J Clin Invest. 2014;124(9):3891-3900. https://doi.org/10.1172/JCI71946.
29. Chen H. Collodion baby. In: Puri RD, Agarwal S, editors. Atlas of genetic diagnosis and counseling. New York: Springer; 2016. p. 1-10. https://doi.org/10.1007/978-1-4614-6430-3_47-2.
30. Bamalan OA, Moore MJ, Menezes RG. Vernix caseosa. [Updated 2023 Jul 4]. In: StatPearls [Internet]. Treasure Island (FL): StatPearls Publishing; 2025 Jan-. Available from: https://www.ncbi.nlm.nih.gov/books/NBK559238/
31. So JY, Teng J. Epidermolysis bullosa simplex. 1998 Oct 7 [Updated 2022 Aug 4]. In: Adam MP, Feldman J, Mirzaa GM, et al., editors. GeneReviews® [Internet]. Seattle (WA): University of Washington, Seattle; 1993-2025. Available from: https://www.ncbi.nlm.nih.gov/books/NBK1369/
32. Smith LD, Masood M, Bajaj GS, Couser NL. Genetic abnormalities of the anterior segment, eyelids, and external ocular adnexa. In: Singh AD, Damato BE, Pe'er J, Murphree AL, Perry JD, editors. Ophthalmic genetic diseases: A quick reference guide to the eye and external ocular adnexa abnormalities. Amsterdam: Elsevier; 2019. p. 15-39. https://doi.org/10.1016/B978-0-323-65414-2.00002-7.
33. Rice AS, Crane JS. Epidermolytic hyperkeratosis. [Updated 2023 Jul 31]. In: StatPearls [Internet]. Treasure Island (FL): StatPearls Publishing; 2025 Jan-. Available from: https://www.ncbi.nlm.nih.gov/books/NBK544323/
34. Komlosi K, Glocker C, Hsu-Rehder HH, Alter S, Kopp J, Hotz A, et al. Autosomal dominant lamellar ichthyosis due to a missense variant in the gene NKPD1. J Invest Dermatol. 2024;144(12):2754-2763.e6. https://doi.org/10.1016/j.jid.2024.03.041.
35. Summers CG. Albinism: classification, clinical characteristics, and recent findings. Optom Vis Sci. 2009;86(6):659-662. https://doi.org/10.1097/OPX.0b013e3181a5254c.
36. Federico JR, Krishnamurthy K. Albinism. In: StatPearls [Internet]. Treasure Island (FL): StatPearls Publishing; 2025 Jan-.
37. Kromann AB, et al. Pigmentary mosaicism. Orphanet J Rare Dis. 2018;13:39. https://doi.org/10.1186/s13023-018-0778-6.
38. Schaffer JV. Pigmentary mosaicism. Clin Dermatol. 2022;40(4):322-338. https://doi.org/10.1016/j.clindermatol.2022.02.005.
39. Zhou YJ, et al. Becker's nevus. Dermatol Ther. 2022;35(7):e15548. https://doi.org/10.1111/dth.15548.
40. Brownell I, Loomis CA, Koss T. Skin development and maintenance. In: Bolognia JL, Schaffer JV, Cerroni L, editors. Dermatology. 5th ed. Amsterdam: Elsevier; 2024.

41. Malfait F, Castori M, Francomano CA, et al. The Ehlers–Danlos syndromes. Nat Rev Dis Primers. 2020;6:64. https://doi.org/10.1038/s41572-020-0194-9.
42. Miklovic T, Sieg VC. Ehlers-Danlos syndrome. In: StatPearls [Internet]. Treasure Island (FL): StatPearls Publishing; 2025 Jan-. PMID: 31747221.
43. Ghosh SK, Dutta A, Sarkar S, Nag SS, Biswas SK, Mandal P. Focal dermal hypoplasia (Goltz syndrome): A cross-sectional study from eastern India. Indian J Dermatol. 2017;62(5):498-504. https://doi.org/10.4103/ijd.IJD_317_17.
44. Pfendner EG, Lucky AW. Junctional epidermolysis bullosa. 2008 Feb 22 [Updated 2018 Dec 20]. In: Adam MP, Feldman J, Mirzaa GM, et al., editors. GeneReviews® [Internet]. Seattle (WA): University of Washington, Seattle; 1993–2025. Available from: https://www.ncbi.nlm.nih.gov/books/NBK1125/
45. Khanna D, Bardhan A. Epidermolysis bullosa. [Updated 2024 Jan 11]. In: StatPearls [Internet]. Treasure Island (FL): StatPearls Publishing; 2025 Jan–. Available from: https://www.ncbi.nlm.nih.gov/books/NBK599531/
46. Lucky AW, Pope E, Crawford S. Dystrophic epidermolysis bullosa. 2006 Aug 21 [Updated 2025 May 8]. In: Adam MP, Feldman J, Mirzaa GM, et al., editors. GeneReviews® [Internet]. Seattle (WA): University of Washington, Seattle; 1993–2025. Available from: https://www.ncbi.nlm.nih.gov/books/NBK1304/
47. Youssefian L, Vahidnezhad H, Uitto J. Kindler syndrome. 2016 Mar 3 [Updated 2022 Jan 6]. In: Adam MP, Feldman J, Mirzaa GM, et al., editors. GeneReviews® [Internet]. Seattle (WA): University of Washington, Seattle; 1993–2025. Available from: https://www.ncbi.nlm.nih.gov/books/NBK349072/
48. Shamim H, Hanif S. Hypohidrotic ectodermal dysplasia: A case report. Cureus. 2023;15(10):e46530. https://doi.org/10.7759/cureus.46530.
49. Pignata C, Fusco A, Amorosi S. Human clinical phenotype associated with FOXN1 mutations. In: Maiese K, editor. Forkhead transcription factors. Advances in experimental medicine and biology. Vol. 665. New York: Springer; 2009. p. 195–206. https://doi.org/10.1007/978-1-4419-1599-3_15.
50. Chabchoub I, Souissi A. Monilethrix. [Updated 2023 Jun 12]. In: StatPearls [Internet]. Treasure Island (FL): StatPearls Publishing; 2025 Jan–. Available from: https://www.ncbi.nlm.nih.gov/books/NBK539813/
51. Al-Batayneh OB. Tricho-dento-osseous syndrome: Diagnosis and dental management. Int J Dent. 2012;2012:514692. https://doi.org/10.1155/2012/514692.
52. Moody MN, Landau JM, Goldberg LH. Nevus sebaceous revisited. Pediatr Dermatol. 2012;29(1):15–23. https://doi.org/10.1111/j.1525-1470.2011.01562.x.
53. Idriss MH, Elston DM. Secondary neoplasms associated with nevus sebaceus of Jadassohn: A study of 707 cases. J Am Acad Dermatol. 2014;70(2):332–337. https://doi.org/10.1016/j.jaad.2013.10.004.
54. Moss C. Cytogenetic and molecular evidence for cutaneous mosaicism: The ectodermal origin of Blaschko lines. Am J Med Genet. 1999;85(4):330–333. https://doi.org/10.1002/(sici)1096-8628(19990806)85:4<330::aid-ajmg3>3.0.co;2-m.
55. Brar BK, Mahajan BB, Puri N. Linear and whorled nevoid hypermelanosis. Indian J Dermatol Venereol Leprol. 2008;74(5):512–513. https://doi.org/10.4103/0378-6323.44325.
56. Yadlapati S, Tripathy K. Incontinentia pigmenti (Bloch-Sulzberger syndrome). In: StatPearls [Internet]. Treasure Island (FL): StatPearls Publishing; 2025 Jan–. PMID: 35201722.
57. Nicholson CL, Daveluy S. Epidermal nevus syndromes. [Updated 2023 Jun 12]. In: StatPearls [Internet]. Treasure Island (FL): StatPearls Publishing; 2025 Jan–. Available from: https://www.ncbi.nlm.nih.gov/books/NBK559003/.
58. Singh AP, Gorla SR. Amniotic band syndrome. [Updated 2022 Dec 11]. In: StatPearls [Internet]. Treasure Island (FL): StatPearls Publishing; 2025 Jan–. Available from: https://www.ncbi.nlm.nih.gov/books/NBK545283/
59. Ornoy A, Echefu B, Becker M. Valproic acid in pregnancy revisited: Neurobehavioral, biochemical and molecular changes affecting the embryo and fetus in humans and in animals: A narrative review. Int J Mol Sci. 2023;25(1):390. https://doi.org/10.3390/ijms25010390.
60. Matt N, Ghyselinck NB, Wendling O, Chambon P, Mark M. Retinoic acid-induced developmental defects are mediated by RARbeta/RXR heterodimers in the pharyngeal endoderm. Development. 2003;130(10):2083–2093. https://doi.org/10.1242/dev.00428.
61. Akpan US, Pillarisetty LS. Congenital cytomegalovirus infection. [Updated 2023 Aug 8]. In: StatPearls [Internet]. Treasure Island (FL): StatPearls Publishing; 2025 Jan–. Available from: https://www.ncbi.nlm.nih.gov/books/NBK541003/.
62. Dos Santos ALS, Rosolen BB, Ferreira FC, Chiancone IS, Pereira SS, Pontes KFM, et al. Intrauterine Zika virus infection: An overview of the current findings. J Pers Med. 2025;15(3):98. https://doi.org/10.3390/jpm15030098.

63. Dermitzakis I, Chatzi D, Kyriakoudi SA, Evangelidis N, Vakirlis E, Meditskou S, et al. Skin development and disease: A molecular perspective. Curr Issues Mol Biol. 2024;46(8):8239–8267. https://doi.org/10.3390/cimb46080487.
64. Zhu X, Petrovski S, Xie P, Ruzzo EK, Lu YF, McSweeney KM, et al. Whole-exome sequencing in undiagnosed genetic diseases: Interpreting 119 trios. Genet Med. 2015;17(10):774–781. https://doi.org/10.1038/gim.2014.191.
65. Moraes SG, Pereira LA. A multimedia approach for teaching human embryology: Development and evaluation of a methodology. Ann Anat. 2010;192(6):388–395. https://doi.org/10.1016/j.aanat.2010.05.005.
66. Prodinger CM, Reichelt J, Bauer JW, Laimer M. Current and future perspectives of stem cell therapy in dermatology. Ann Dermatol. 2017;29(6):667–687. https://doi.org/10.5021/ad.2017.29.6.667.
67. Taub AF, Pham K. Stem cells in dermatology and anti-aging care of the skin. Facial Plast Surg Clin North Am. 2018;26(4):425–437. https://doi.org/10.1016/j.fsc.2018.06.004.
68. Farabi B, Roster K, Hirani R, Tepper K, Atak MF, Safai B. The efficacy of stem cells in wound healing: A systematic review. Int J Mol Sci. 2024;25(5):3006. https://doi.org/10.3390/ijms25053006.
69. Nakamuta A, Yoshido K, Naoki H. Stem cell homeostasis regulated by hierarchy and neutral competition. Commun Biol. 2022;5:1268. https://doi.org/10.1038/s42003-022-04218-7.
70. Ogliari KS, Marinowic D, Brum DE, Loth F. Stem cells in dermatology. An Bras Dermatol. 2014;89(2):286–291. https://doi.org/10.1590/abd1806-4841.20142530.
71. Cousin I, Misery L, de Vries P, Lebonvallet N. Emergence of new concepts in skin physiopathology through the use of in vitro human skin explants models. Dermatology. 2023;239(6):849–859. https://doi.org/10.1159/000533261.

IJAE
ITALIAN JOURNAL OF ANATOMY AND EMBRYOLOGY

Firenze University Press
www.fupress.com/ijae

Citation: Zucchini, E., Ribatti, D., Paternostro, F., Belviso, I., & Lippi, D. (2025). An anatomical interpretation of Pesellino's *Miracle of St. Anthony of Padua*. *Italian Journal of Anatomy and Embryology* 129(2): 29-31. doi: 10.36253/ijae-16623

Data Availability Statement: All relevant data are within the paper and its Supporting Information files.

Competing Interests: The Author(s) declare(s) no conflict of interest.

An anatomical interpretation of Pesellino's *Miracle of St. Anthony of Padua*

Elisa Zucchini[1], Domenico Ribatti[2], Ferdinando Paternostro[3,*], Immacolata Belviso[4], Donatella Lippi[3]

[1] *Department of History, Archaeology, Geography, Fine and Performing Art, University of Florence, Florence, Italy*
[2] *Department of Translational Biomedicine and Neuroscience, University of Bari Medical School, Bari, Ital.*
[3] *Department of Experimental and Clinical Medicine, University of Florence, Florence, Italy*
[4] *Department of Psychology and Health Sciences, Telematic University Pegaso, Naples, Italy*
*Corresponding author. E-mail: ferdinando.paternostro@unifi.it

Abstract. Background: The research takes inspiration from field trips at the Uffizi Gallery organized by the Department of Medicine of the University of Florence, in which professors encourage students to discuss medical aspects of artworks, and the participation of an art historian fosters interdisciplinary dialogue. **Methods:** The research started with the historical contextualisation and stylistic and iconographic analysis of the painting. Then, it dealt with the evaluation of Renaissance medical sources and the bibliography about the painting. Lastly, it compared the painting with contemporary texts and images. **Results:** The research evidenced that Pesellino meant to represent an anatomy lesson as it used to be carried out in Medieval universities, under the guise of a miracle of saint Anthony of Padua. **Conclusions:** The paper could contribute to the investigation of anatomical knowledge of artists and iconographic documentation of medical practice in the fifteenth century.

Keywords: art and medicine, history of anatomy, anatomical dissection, Uffizi, Vesalius.

INTRODUCTION

The *predella* of the *Madonna and Child Enthroned with Saints Francis of Assisi, Cosmas and Damian, Anthony of Padua* (*Novitiate Altarpiece*) by Fra Filippo Lippi is the only painting by Francesco di Stefano, known as Pesellino, cited by Vasari in his *Lives of the Artists*. [1]

Lippi's altarpiece was commissioned by Cosimo de' Medici for the Novitiate Chapel in S. Croce in Florence, and it is dated between 1442 and 1450, as Pesellino, born in 1422, could not have painted the *predella* before that date. Furthermore, the Novitiate Chapel, designed by Michelozzo at the behest of Cosimo de' Medici, was completed in 1445. [2] [3]

The *predella* was probably painted in conjunction with the altarpiece. In 1813, it was removed from the Accademia Gallery in Florence; subsequently, it was taken to France and divided into two parts. The left one, with the *Stigmata of St. Francis* and the *Miracle of Saints Cosmas and Damian*, remained at the Louvre, but it was copied. The copies are now at the Uffizi with the rest of the *predella*, depicting the *Nativity*, the *Martyrdom of Saints Cosmas and Damian*, the *Miracle of the Miser's Heart of St. Anthony of Padua*. [4]

Pesellino's biography seems to confirm his collaboration with Filippo Lippi approximately between 1445 and 1450; in fact, Pesellino's works in this period are similar to Lippi's, while maintaining echoes of Fra Angelico, his probable teacher. [5]

The panel representing the *Miracle of the Miser's Heart,* one of the best-known miracles of Saint Anthony of Padua, is an important testimony to the diffusion of anatomical dissection [Figure 1].

Figure 1. Francesco di Stefano called Pesellino, *The Miracle of the Miser's Heart of St. Anthony of Padua,* detail of the *predella* of the *Novitiate Altarpiece* by Filippo Lippi, 1442-50, tempera on panel, 35 x 144 x 12 cm, Florence, Galleria degli Uffizi (© Gabinetto Fotografico delle Gallerie degli Uffizi)

DESCRIPTION

Arnaldo da Serrano drew the subject of chapter fifty-two of the *Liber Miraculorum* (written circa 1370) from the biography of Saint Anthony of Padua written at the beginning of the fourteenth century by the Franciscan Giovanni Rigaldi, who had heard it from Brother Pietro di Raimondo, the author of an anthology of miracles attributed to the intercession of Saint Anthony. [6] According to the hagiographies dedicated to the saint (especially *Sancti Antonii Vita* by Sicco Polentone), during the funeral of a very rich and greedy man in Tuscany Saint Anthony shouted that the deceased should not be buried in consecrated ground, because his soul was damned to hell and his body heartless, according to the saying of Jesus: "For where your treasure is, there also will your heart be" (Luke 12, 34). The shocked bystanders called some doctors, who opened the deceased's chest and did not find the heart, which was found in the safe, among the money that the miser had loved above everything else, instead. [7]

Pesellino – perhaps to extol the art of medicine, consequently the Medici family, patron of the Novitiate Chapel – focused the scene on the physician performing the dissection, who inspects the visibly empty opening of the ribcage, to the amazement of his colleagues, while three women listen to the saint speaking from a wooden pulpit. In another room, on the left, a young man opens the strongbox of the deceased to look for the heart.

Some critics see Cosimo's imprint in the choice of the story, which can be interpreted both as a model of Franciscan preaching virtue for novices and as a warning against avarice, since, according to Vespasiano da Bisticci, Cosimo tried to atone for his sin of usury through religious patronage. [8]

DISCUSSION

The scene depicts a 'testimonial' autopsy, almost an expert opinion. [9]

The man wearing a red *lucco* (a long hooded surcoat) can be identified with the physician intent on dissecting the miser's body.

Details such as the coins in the strongbox, the physician's robe, and the hat are painted accurately; everything converges everything converges toward the vanishing point, located at the anatomist's position, in order to give credibility to the miraculous, visibly significant event.

The central figure of the young doctor, assisted by an older male figure with a red cap, fits in the typical Renaissance iconography of doctors, the only ones able to wear a *lucco* as a symbol of their rank, according to Florentine sumptuary laws. [10]

In fact, the physician saints Cosmas and Damian are usually represented with this clothing.

In Pesellino's painting, St. Anthony encourages the opening of the body, documenting a practice that had already partially established itself but was still far from the High Renaissance revolution, which would be spearheaded by Jacopo Berengario da Carpi and Andreas Vesalius in the sixteenth century. [11]

Dissection of the human body as a teaching tool to show its anatomy to medical students began to be prac-

ticed in the Christian West between the late thirteenth and early fourteenth centuries. Mondino de' Liuzzi performed the first public autopsy in Bologna in 1315: he opened the corpses of two women fifteen years after the promulgation of Boniface VIII's bull *Detestandae feritatis*, published in 1299. [12] This bull has often been interpreted as an explicit ban by the Church on the dismemberment of corpses and, therefore, on dissection. Actually, it was directed against the custom of separating the bones from the soft parts of corpses to bring back the remains of people who had died abroad to their homeland.

Anatomical dissection represented a sector in which different attitudes clashed, from prohibition to regulation and institutional control of anatomical practice, from rhetorical procedures to the norms with which the manipulation and opening of cadavers was progressively authorized. [13] Only thanks to the decision of Pope Sixtus IV, who authorized anatomical practice in 1472 because it was useful for medicine and art, it was possible to begin the systematic study of the human body.

In the late Middle Ages, dissection involved three people: the reader (*lector*), a custodian of knowledge, who read Galen's texts; the anathomist (*dissector*) who cut the corpse; and the commentator (*ostensor*) who indicated the bodily parts as the reader mentioned them.

The reader, however, was far from the corpse and restricted himself to explaining what Galen had written without verifying the truthfulness of Galen's words.

In fact, Galen had conducted animal anatomies, managing to build a system that brought medicine and religion together, remaining valid until well into the Renaissance. [14]

In this scene, St. Anthony represents the *lector*, who preaches from the height of his role and his seat.

The opening of the corpse of the miser painted by Pesellino is far from the dramatic depiction of the same subject by Donatello by Donatello in the altar of the Basilica del Santo in Padua, but it looks like the 'unbuttoning of a doublet'. [9]

The precision and specificity of the gesture leave no doubt about the fact that the painter wanted to represent an anatomical dissection, according to a well-known compositional scheme, with the aligned and foreshortened disposition of the bystanders and the chest with the miser's heart above the pile of coins on the left, almost modestly preserved in another room.

The exploration is exclusively aimed at identifying the heart *in situ* and avoids the first part of the canonical dissection, which, in this period, would have started from the abdominal cavity, which contained less noble and more easily deteriorated organs, and was dissected first, followed by the thorax, head, and extremities.

A true revolution only took place thanks to Vesalius, because Vesalius came down from the *lector*'s throne and no longer needed a *dissector* and an *ostensor*, as he carried out all the three functions himself. At that point, he saw Galen's mistakes and he was able to correct them.

But by now, times had changed.

REFERENCES

1. G, Vasari, Le Vite de' Più Eccellenti Architetti, Pittori e Scultori Italiani, da Cimabue insino a' Tempi Nostri. Nell' Edizione per i Tipi di Lorenzo Torrentino, eds. L. Bellosi, A. Rossi, Turin, Einaudi, 1991, p. 400.
2. M. Pittaluga, Filippo Lippi, Florence, Del Turco, 1949) 176.
3. G. Marchini, Filippo Lippi, Milan, Electa, 1975, p. 204 No. 21.
4. A. Uguccioni, Francesco di Stefano, detto Pesellino, in: Dizionario Biografico degli Italiani, Vol. 50, 1998. https://www.treccani.it/enciclopedia/francesco-di-stefano-detto-pesellino_(Dizionario-Biografico)/ (accessed 27 February 2025).
5. A, Tartuferi, Omaggio a Filippo Lippi, Florence, Centro Di, 2010.
6. Vite Raymundina e Rigaldina, ed. V. Gamboso, Padua, Edizioni Messaggero, 1992.
7. Libro dei Miracoli di Sant'Antonio, ed. V. Gamboso, Padua, Edizioni Messaggero, 2012.
8. M. Holmes, Fra Filippo Lippi the Carmelite Painter, New Haven – London, Yale University Press, 1999, pp. 191-204.
9. G. Weber, Mal d'Arte. Patologo fra gli Artisti, Florence, Pagliai, 2012.
10. A. Corsini, Il Costume del Medico nelle Pitture Fiorentine del Rinascimento, Florence, Istituto Micrografico Italiano, 1912.
11. O. Habbal, The Science of Anatomy: A Historical Timeline, Sultan Qaboos Univ. Med. J. 17(2017), 18-22. https://doi.org/10.18295/squmj.2016.17.01.004
12. P. Charlier, I. Huynh-Charlier, J. Poupon, E. Lancelot, P. F. Campos, D. Favier et al., A Glimpse into the Early Origins of Medieval Anatomy through the Oldest Conserved Human Dissection (Western Europe, 13th c. A. D.), Arch. Med. Sci. 10 (2014), 366-73. https://doi.org/10.5114/aoms.2013.33331
13. K. Park, The Life of the Corpse: Division and Dissection in Late Medieval Europe, *J. Hist. Med. Allied Sci.,* 50(1995), 111-32. https://doi.org/10.1093/jhmas/50.1.111
14. K. Park, The Criminal and the Saintly Body: Autopsy and Dissection in Renaissance Italy, *Renaiss. Q.,* 47 (1994), 1-33. https://doi.org/10.2307/2863109

IJAE
ITALIAN JOURNAL OF ANATOMY AND EMBRYOLOGY

Firenze University Press
www.fupress.com/ijae

OPEN ACCESS

Citation: Mancinelli, R., Vivacqua, G., Leone, S., Arciprete, F., Vaccaro, R., Garro, L., Caturano, C., Tagliafierro, M., Bellomi, F. E., Bassi, F. M., Velardi, V., Bocci, E., Ceci, L., Vitali, S., Bassi, A., Franchitto, A., Onori, P., Gaudio, E., & Casini, A. (2025). Overview of the gut-liver-brain axis with particular emphasis on ferroptosis. *Italian Journal of Anatomy and Embryology* 129(2): 33-53. doi: 10.36253/ijae-16577

Data Availability Statement: All relevant data are within the paper and its Supporting Information files.

Competing Interests: The Author(s) declare(s) no conflict of interest.

Overview of the gut-liver-brain axis with particular emphasis on ferroptosis

Romina Mancinelli[1], Giorgio Vivacqua[3,*], Stefano Leone[1], Francesca Arciprete[3], Rosa Vaccaro[1], Ludovica Garro[1], Claudia Caturano[3], Marco Tagliafierro[1], Francesco Emanuele Bellomi[3], Filippo Maria Bassi[1], Viola Velardi[3], Emanuele Bocci[1], Ludovica Ceci[5], Sara Vitali[1], Andrea Bassi[4], Antonio Franchitto[2], Paolo Onori[1], Eugenio Gaudio[1], Arianna Casini[1]

[1] *Department of Anatomical, Histological, Forensic Medicine and Orthopaedics Sciences, Sapienza University of Rome, Italy*
[2] *Division of Health Sciences, Department of Movement, Human and Health Sciences, University of Rome Foro Italico, Italy*
[3] *Integrated Research Center (PRAAB), Campus Biomedico University of Rome, Italy*
[4] *Department of Life Science, Health and Health Professions, Link Campus University, Rome, Italy*
[5] *Interdisciplinary Department of Well-Being, Health and Environment Sustainability (BESSA), Sapienza University, Rieti, Italy*
*Corresponding author. E-mail: g.vivacqua@unicampus.it

Abstract. Ferroptosis is a form of cellular death involved in the origin, progression, but also regulation of several human diseases. Its regulatory role in the gut-liver-brain axis (GLBA) has not been clarified. Therefore, we sought to summarize the possible correlations between ferroptosis and the GLBA. In this review, we first introduce the phenotype and the main mechanisms of this relatively newly described form of regulated cell death. Then, we analyse the anatomy of the GLBA, describing the connections between the gut and the liver, followed by the anatomical pathways from the gut to the brain and from the liver to the brain. After the morphological aspects, we summarize the main biological modulators of the GLBA, highlighting their physiological and pathological roles. In the end, we discuss in detail the regulatory role of ferroptosis on neuroinflammation and oxidative stress along GLBA, highlighting the key aspects that could be of significant clinical importance as future diagnostic and therapeutic targets.

Keywords: ferroptosis, gut-brain axis, neuroinflammation.

1. FERROPTOSIS: A NEW FORM OF NON-APOPTOTIC CELL DEATH

Ferroptosis is an iron-dependent, lipid peroxidation-driven form of regulated cell death (RCD). First discovered by Brent R. Stockwell et al. (2012), it was described as erastin-induced cell death characterized by a peculiar phenotype.[1] Morphological (such as loss of membrane integrity, swollen of the cytoplasm and smaller mitochondria), biochemical and genetic features distinguish ferroptosis from the other types of RCD described to date[2]. The

regulation of this unique process of cell death is closely linked to the interplay between iron, lipid and amino acid metabolism resulting in oxidative perturbations of the intracellular microenvironment and loss of redox homeostasis. Recent advances in the discovery of ferroptosis markers revealed how ferroptosis is the main feature of a series of physiological processes, including tumor suppression pathways and adequate immunological response.[3] The relevance of ferroptosis is further highlighted by its role in the development of pathological conditions, spanning from kidney injuries and endocrine imbalances to neurodegenerative disorders[4], including Alzheimer's Disease (AD) and Parkinson's Disease (PD) along with synucleinopathy.[5]

1.1. Molecular and morphological phenotypes

The buildup of peroxidized lipids, resulting in the unrepaired damage of cell membranes, is the ultimate driver of ferroptosis.[6,7] The contribution of different organelles in the biochemical evolution of ferroptosis explains the main morphological changes affecting these subcellular compartments. Mitochondria can add up to cysteine-starvation mediated GSH-depletion-induced damage by means of electrons leakage from the cellular respiration machinery, which would facilitate the initiation of a Fenton reaction by producing hydrogen peroxide. The endoplasmic reticulum, being the critical site of lipid peroxidation, is fundamental for clustering of oxidized Poly-Unsaturated Fatty Acids (PUFA) and phospholipids (PLs) leading to progression of ferroptosis.[7] Overall, the modifications at the cellular and subcellular levels include: mitochondria shrinkage and cristae reduction or disappearance, increased endoplasmic reticulum viscosity and ER membrane stiffness, loss of plasma membrane structural and functional integrity, and possible formation of pores that can promote membrane rupture.[8–11]

1.2. Mechanism

The molecular mechanism of ferroptosis is driven by the increase of intracellular ferrous iron (Fe^{2+}), capable of subsequently promoting both non-enzymatic and enzymatic lipid peroxidation by initiating a Fenton reaction or by exploiting its role as a critical cofactor of lipoxygenases.[12] The detrimental effects of lipid peroxidation fall into two, possibly overlapping, categories:[13] direct dampening of cellular membranes stability and formation of lipid pores, with consequent increase the permeability of the membranes, or the activation of downstream signaling pathways that result in membrane perforation.[14,15]

Iron homeostasis, primarily controlled by the hepatic secretion of hepcidin,[16] is met by a tightly balanced exchange of iron between extracellular and intracellular compartments, in which the transition metal is found as ferric (Fe^{3+}) and ferrous (Fe^{2+}) iron, respectively.[17] The expansion of the cellular labile iron pool (LIP), reaching more than 5% of total cell iron,[18] promotes reactive oxygen species (ROS) formation through the reaction of ferrous iron with hydrogen peroxide, according to Fenton chemistry.[19] The rise in intracellular Fe^{2+} could be secondary to a variety of conditions, which include: (i) an increase of transferrin receptor (TFR1) expression, (ii) RAS mutations or NCOA4-mediated ferritinophagy, which induces a decrease in ferritin levels,[20,21] and (iii) excessive degradation of heme by heme oxygenase 1 (HO-1)[22] (Figure 1). Lipid peroxidation can occur through both non-enzymatic and enzymatic pathways.

Non-enzymatic lipid peroxidation

Non-enzymatic lipid peroxidation consists of free radical driven reactions. Initiation requires a Fenton reaction to take place: the abundant ferrous iron moieties react with hydrogen peroxide derived from oxidoreductase activity, such as that of cytochromes P450 oxidoreductase (POR) and P450 reductase (CPR) localized on the smooth endoplasmic reticulum, producing ROS. [23] The hydroxyl radicals then extract hydrogen from the bis-allylic position of poly-unsaturated fatty acids (PUFAs) to form lipid radicals, which further react with molecular oxygen (O_2) to produce lipid peroxy-radicals. More hydrogen moieties are removed from PUFAs to form lipid hydroperoxides and new lipid peroxy-radicals, the latter providing a way of amplification of the oxidation reaction[24,25] (Figure 2).

Enzymatic peroxidation

Enzymatic lipid peroxidation, as the name implies, consists of a series of enzymatically driven reactions. In the endoplasmic-reticulum-associated subcellular compartments, selective oxidation of phosphatidylethanolamines (PEs) followed by lipids oxygenation takes place.[26] Firstly acyl-CoA synthetases, such as ACSL4 (especially acting on arachidonic acid), activate free fatty acids (FFAs) by adding to them a coenzyme A moiety. Then, lysophospholipid acyltransferases, such as LPCAT3, catalyze the transfer of the fatty acyl chain from fatty acyl-CoA and incorporate into PEs to form various classes of phospholipids. Finally, lipoxygenases familiy (LOXs) generate doubly and triply oxygenated (15-hydroperoxy)-diacylated PE compounds[26,27] (Figure 3).

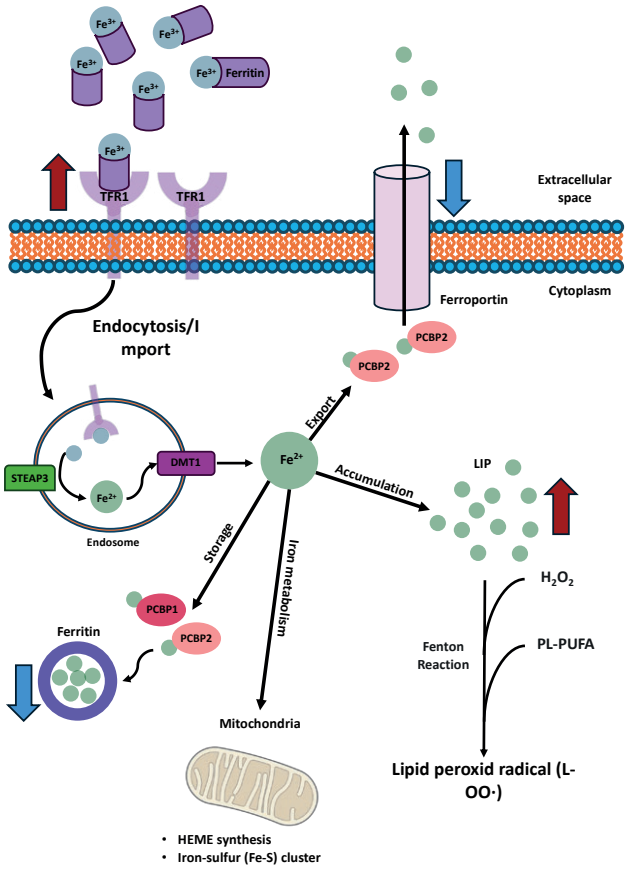

Figure 1. The regulatory mechanisms of ferroptosis. The extracellular domain of transferrin receptors (TFR1) binds Trasferrin-Fe3+ on the cell surface, triggering the receptor-mediated endocytosis. In the endosome, STEAP3 reduced the Fe3+ into Fe2+, which is transported in the cytosol by the DMT1. Elevated levels of ferrous ions (Fe2+) were found in the cytoplasm due to: (i) reduction of the ferroportin activity, (ii) increase accumulation of Fe2+ as cellular Labile Iron Poll (LIP) in the cytosol, and (iii) increase of iron-mediated mitochondrial homeostasis. At last, reduced expression of ferritin due to ferritinophagy could increase Fe2+ in the cytoplasm. Imbalance between iron uptake, storage and export may increase the susceptibility of cells to ferroptosis.

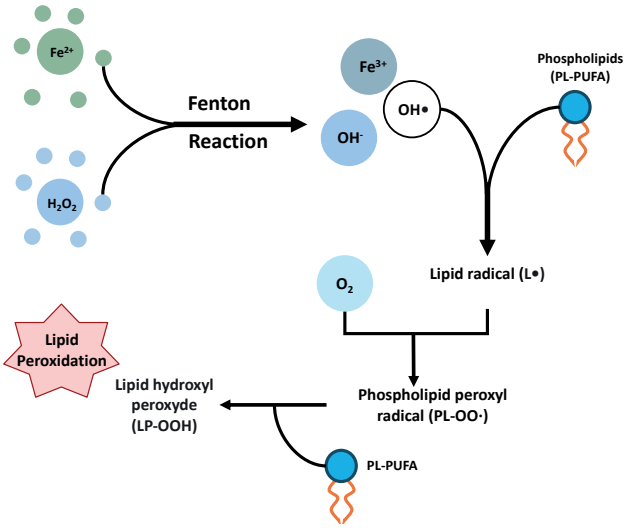

Figure 2. Non-enzymatic lipid peroxidation (autoxidation) requires a Fenton reaction, but the precise role of iron in the process of lipid peroxidation is still being debated whether this peroxidation occurs in an enzymatic or non-enzymatic way.

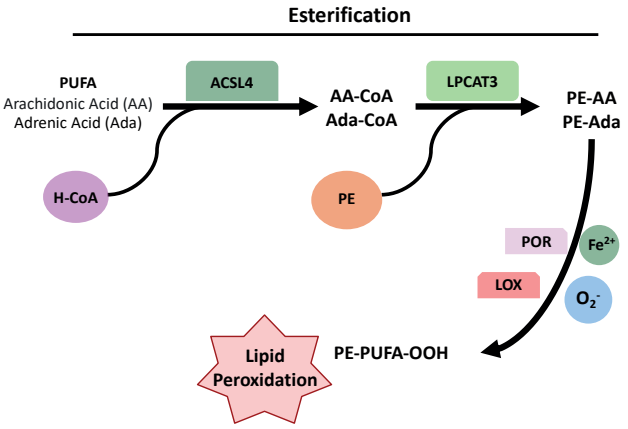

Figure 3. Enzymatic lipid peroxidation requires numerous enzymatically reactions. Although the effectors leading to ferroptosis in physiological conditions are not well known, but lipid peroxidation and GPX4 enzymology are critical for this process. When the homeostatic control of the steady state between LOOH formation and reduction is lost, lipid peroxidation is activated and ferroptosis is executed.

2. THE ANATOMY OF THE GUT-LIVER-BRAIN AXIS

2.1. The gut-liver axis

The gut-liver axis (GLA) concept was first introduced by Marshall in 1998 and refers to the connection between the gastrointestinal (GI) tract and the liver. This axis is characterized by a complex network of bidirectional anatomical and functional interactions between the GI tract and the liver. Over the years, the GLA has gained increasing attention due to its implications in various pathologies. Key components of this axis include portal circulation, gut microbiota, intestinal tight junctions, bile acids, and mucosal hormones.[28–30]

Portal circulation

Most of the venous blood from the GI tract, primarily from the small and large intestines, drains into the portal vein. This vein transports nutrient-rich blood, along with signalling molecules produced by the gut

microbiota, neuroendocrine and immune cells of the gut, directly to the liver. Moreover, the portal circulation carries to the liver the products of hemocatheresis occurring in the spleen, including globins, heme and iron produced by the catabolism of haemoglobin.

Gut microbiota

The gut hosts diverse microbial communities that play essential roles in maintaining intestinal integrity and producing signalling molecules. A balanced microbiota is critical to produce various metabolites, particularly short-chain fatty acids (SCFAs), such as acetate, propionate, and butyrate.[31] Acetate, absorbed in the proximal colon, is rapidly transported to the liver, where it contributes to cholesterol biosynthesis.[32] Propionate, a substrate for lipogenesis, gluconeogenesis and protein synthesis in the liver,[33] was observed to inhibit hepatic cholesterol synthesis.[34] Butyrate was demonstrated to be central for the health of colon enterocytes by providing energy to colonic epithelial cells.[35] However, recent studies suggest that excessive accumulation of butyrate induces cholestasis, hepatocyte death, and neutrophil-driven inflammation in the liver, potentially leading to icteric hepatocellular carcinoma.[36] Additionally, SCFAs, especially butyrate, stimulate the release of fasting-induced adipocyte factor (FIAF) from L cells in the gut;[37] FIAF subsequently inhibits lipoprotein lipase (LPL) activity, preventing triglyceride accumulation in both adipose tissue and liver. [7,38] Therefore, the microbiota plays a central role in the GLA and dysbiosis can lead to an imbalance of signalling molecules, contributing to liver damage. Not surprisingly, an imbalanced gut microbiota can result in increased intestinal ethanol production, contributing to the development of non-alcoholic steatohepatitis (NASH) and non-alcoholic fatty liver disease (NAFLD), today included in metabolic dysfunction-associated steatotic liver disease (MASLD).[39,40]

Tight Junctions (TJs)

Tight junctions (TJs) are components of the gut mucosal barrier, a multifaceted system of physical, chemical, microbial, and immunological defences that limit the spread of intestinal antigens.[41] TJs are composed of proteins such as claudins, TJ-associated marvel proteins (TAMPs), junctional adhesion molecules (JAMs), and zona occludens-1 (ZO-1).[42–44] In the context of the GLA, the loss of barrier integrity, for example due to inflammation, can increase portal leakage of lipopolysaccharide (LPS), with the activation of a well-characterized pathogen-associated molecular pattern (PAMPs). LPS activates Kupffer cells, the liver's resident macrophages, are highly sensitive to LPS, that activate it.[45] LPS-activated Kupffer cells promote liver inflammation and fibrosis by driving the transcription of pro-inflammatory cytokines and the activation of the stellate cells into the Disse's space.[31,46] Under healthy conditions, the portal vein carries small amounts of pathogens and bacteria, which are effectively managed by the liver's immune system. However, pathological states can result in an excessive influx of microorganisms into the portal vein, contributing to liver disease.[47,48]

In neurodegenerative conditions, α-syn aggregates can travel via portal circulation from the gut to the liver. Moreover, aggregated α-syn can be either a consequence as a driver of bowel inflammation with alteration of the intestinal barrier and increased passage of LPS to the liver.[49,50]

Bile

Bile is a digestive fluid secreted by the hepatocytes and stored in the gallbladder to reach the duodenum. Within the context of the GLA, bile acids play a crucial signalling role. The gut microbiota converts primary bile acids, such as cholic acid (CA) and chenodeoxycholic acid (CDCA), into secondary bile acids, including lithocholic acid (LCA) and deoxycholic acid (DCA).[51] Both primary and secondary bile acids are absorbed by enterocytes and enter the portal circulation. Bile acids act as signalling molecules by interacting with nuclear farnesoid X receptors (FXR) in both intestine and liver, regulating cholesterol, lipid, and energy metabolism.[52] Reabsorbed bile acids can also activate Takeda G protein-coupled receptor 5 (TGR5 a membrane receptor for bile acid), causing multiple effects in hepatic stellate cells, Kupffer cells, cholangiocytes, and enterocytes.[53,54] Activation and transdifferentiation of hepatic stellate cells into myofibroblasts can promote liver fibrosis.[55] Another important receptor, Shingosine-1-phosphate receptor 2 (S1PR2), is present in the liver and bile ducts and is activated by conjugated bile acids such as taurine or glycine-conjugated bile acids[53] Inhibition of S1PR2 has shown promising results as a potential treatment for cholestatic liver diseases. Knockout mice for S1PR2 showed reduced inflammation and hepatic fibrosis in liver.[56] Dysregulation of the gut-liver circulation is evident in cirrhotic patients, where depletion of bacterial populations responsible for bile acid dehydroxylation has been observed.[57] Additionally, gut microbiota can convert choline, a bile component, into trimethylamine N-oxide (TMAO), a toxic metabolite associated with dysbiosis and hepatic steatosis.[53,58] Lastly, bile contains IgA, bicarbonate, and antibacterial molecules, which have bacteriostatic properties and contribute to the regulation of gut microbiota composition.[47]

Mucosal hormones

The gut mucosa contains cells capable of releasing hormones, such as substance P, vasoactive intestinal peptide (VIP) and serotonin as well as fibroblast growth factor 15 (FGF15), which regulates bile-acids synthesis, hepatic glucose, and lipid metabolism.[59] FGF15 (which is equivalent in humans to FGF19)[60] also plays a crucial role in regulating postprandial glucose and energy metabolism by modulating gluconeogenesis.[61] The glucagon-like peptide 1 (GLP-1) is an incretin hormone secreted by L cells of ileum and colon. GLP-1 is involved in the regulation of glucose metabolism in the liver, stomach emptying and feeding.[62] Secretin, another crucial hormone, secreted by S cells in the duodenum, has been shown: (i) to regulate biliary secretion and proliferation[63]and, (ii) to modulate the brown adipose tissue (BAT)-brain metabolic crosstalk.[64] Moreover, one of the endocrine mechanisms responsible for weight regain includes the brain-gut axis, which supports food intake via the production of several gastrointestinal hormones, such as ghrelin, leptin and cholecystokinin (CKK).[65]

2.2. The gut-brain axis

The concept of the gut-brain axis (GBA) was first proposed by Michael D. Gershon in the late 20th century. The idea suggested a bidirectional interaction between the GI tract and brain. The importance of this axis is now emerging. Changes in GI biochemical and physiological pathways have been observed in a growing range of CNS disorders, such as PD, in which GI dysfunction often precedes of decades the onset of neurological symptoms.[66] Generally, the gut-brain axis is mediated by the enteric nervous system (ENS), autonomic nervous system (ANS), hypothalamus-pituitary-adrenal (HPA) axis, the enteroendocrine systems, and the immune system.[53]

ENS anatomy

The GI tract is innervated by number of neurons (estimated at 200-600 million) that exceeds the total number of neurons in the spinal cord. This neuronal system, specific of the gut, is classified as the ENS, also known as the meta sympathetic nervous system. Studies suggested that these neurons are evolutionarily older than those of the central nervous system, and the ENS is capable of functioning independently through various reflexes without input from the CNS and the ANS. Consequently, the ENS is often referred to as the body's "second brain".[67–69] Anatomically, the ENS can be considered a complex network of neuronal connections and ganglia embedded in the layers of the gut wall. These groups of neurons can be subdivided into two plexuses: the Auerbach's (myenteric) plexus, located between the circular and longitudinal layers of the muscularis externa, and the Meissner's (submucosal) plexus, situated within the submucosa.[70] The ENS comprises a complex network of neurons, some of which have been classified, such as: intrinsic primary afferent neurons, excitatory and inhibitory motor neurons, ascending and descending interneurons, secretomotor/vasodilator neurons, and intestinofugal neurons. [71,72]

ENS - ANS cross talk

Although the ENS can function independently, it is still strongly influenced by the ANS (both sympathetic and parasympathetic). The sympathetic system reaches mostly the myenteric plexus, whereas the post ganglionic neurons of the parasympathetic nervous system (mostly constituted by hepatic and celiac branches of the vagus nerve) are found both within the myenteric and submucosal plexuses (Figure 4). The importance of the ANS and ENS in the context of the gut can be understood by considering the numerous functions in which they are involved: gut motility, gut permeability, epithelial fluid homeostasis, luminal osmolarity, bile secretion, carbohydrate concentration, mechanical distortion of the mucosa, bicarbonate production, mucus production and secretion, as well as mucosal immune responses and handling of intestinal fluids.[73,74]

The neuroactive components of the GBA

A diverse array of neuroactive substances exists within the GBA, encompassing gut-derived hormones, neuroactive molecules, metabolites produced by gut microbiota, and various microbial products.[75] Notable examples include bacteria-derived metabolites such as short-chain-fatty-acids (SCFAs), gamma-aminobutyric acid (GABA), serotonin (5-HT), glutamate, acetylcholine, dopamine, norepinephrine, and gut neuropeptides, including peptide YY (PYY), GLP-1, CCK, and ghrelin.[53] A central role in detecting these substances is played by vagal terminal afferent fibres, which have been described in three locations: in the terminals ending of the intestinal muscular layers, in the GI mucosa, and in a subset of enteroendocrine cells (now referred as neuropods) that form synapses with vagal neurons.[76] Due to their wide range of receptor expression, vagal afferents are considered polymodal, meaning that they can detect multiple types of stimuli, including mechanical, chemical, and hormonal signals.[77] Signals from these afferent nerves ascend towards the nucleus tractus solitarius (NTS) in the CNS[78] where they are relayed to other brainstem nuclei and forebrain structures.[79] Nervous communica-

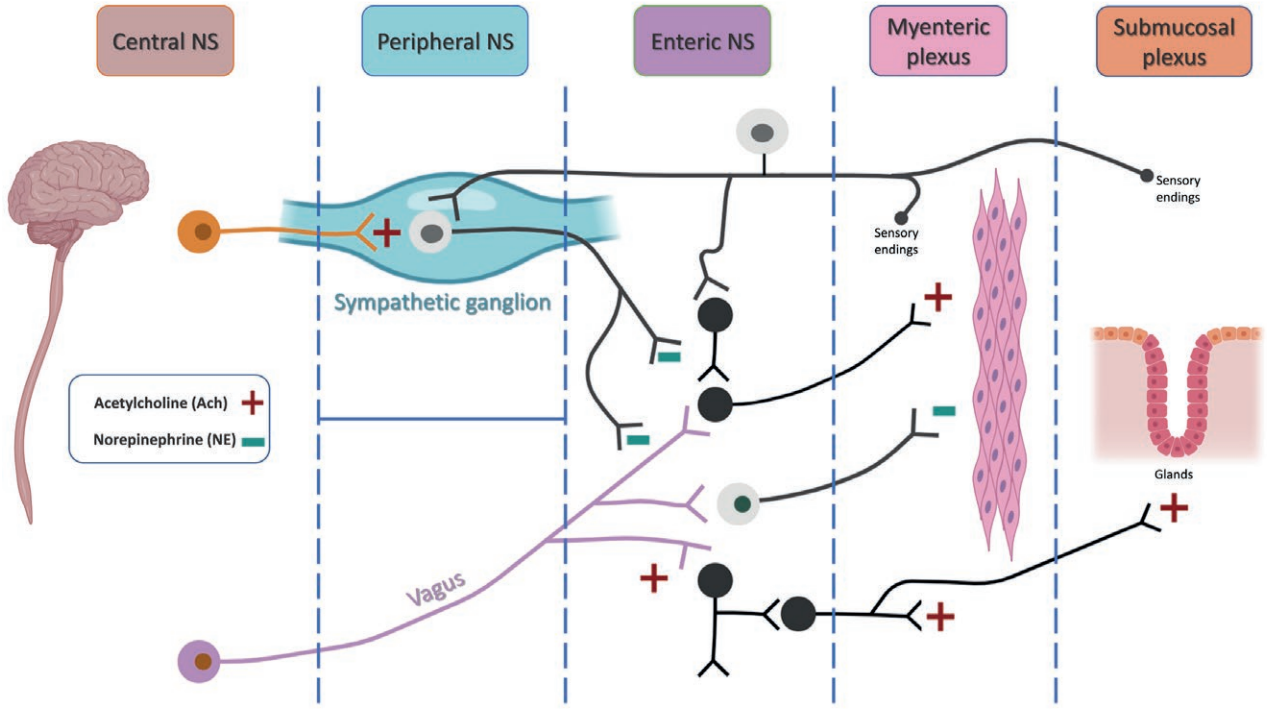

Figure 4. Representative scheme of the anatomical nervous stations. Organization of the myenteric and submucosal plexuses in which are evident the sites of synaptic excitation (+) and inhibition (-). Scheme modified by Kleman JA 1995. Barr's The Human Nervous System: An Anatomical Viewpoint.

tion is bilateral, thus substances targeting the CNS are also released by the ENS and ANS, including GABA, glutamate, acetylcholine, dopamine, norepinephrine, and other bioactive amines.[80]

The microbiota in the gut brain axis

As previously mentioned, the role of gut microbiota is becoming increasingly central in biomedical research, evolving the concept of the GBA into the microbiota-gut-brain axis.[81,82] In addition to interacting with neuronal terminals in the gut, microbial metabolites can enter the circulation and directly affect the CNS. Therefore, the composition of the gut microbiota and its related products, are crucial for the interactions between gut and brain, as well as for the determination of different neurological and psychiatric disorders. Several examples emphasize the molecular pathways involved in this interaction: SCFAs can cross the blood-brain-barrier (BBB) and reduce LPS-induced neurological inflammation in primary microglia and the hippocampus, as well as decrease circulating pro-inflammatory cytokines.[83–85] When imbalances in gut microbiota occur, like in patients affected by irritable bowel syndrome (IBS), the production of secondary bile acids decreases, leading to increased inflammation in the brain.[53] Lastly, it has been observed that trimethylamine N-oxide (TMAO, a metabolite of the gut microbiota) accelerates brain aging and causes age-associated cognitive impairments. [86]

The HPA system in the gut brain axis

The HPA axis is one of the body's primary systems for regulating the release of cortisol and other stress hormones. This response is also mediated by several components, including gut microbiota, the vagus nerve, and the immune system. Studies on germ-free (GF) mice have demonstrated that these mice exhibit an exaggerated HPA response when exposed to stress, releasing more adrenocorticotropic hormone (ACTH) and cortisol.[87,88] In humans, patients with IBS show higher levels of ACTH and cortisol in response to stress, along with altered microbiota composition.[89–91] The HPA axis interacts with other gut-brain communication routes, including the vagus nerve. Studies in rodents indicate that stimulating the vagus nerve increases corticotropin-releasing factor (CRF) production in the brain and raises ACTH and corticosterone levels.[92] The HPA axis also connects to the immune system, where stress and inflammation can influence gut-brain signalling. Stress increases gut permeability, allowing bacteria to cross

into the body, triggering an immune response that activates in turn the HPA axis.[93]

Enteroendocrine system

Enteroendocrine cells (EECs), though comprising only 1% of all gut epithelial cells, are vital for maintaining gut balance due to the various functions of the molecules they release.[94] There are multiple types of EECs, all of which act as sensors that help in regulating the processes such as insulin secretion and food intake based on gut contents.[94] Two well-studied types of EECs in the context of the gut-brain axis are enteroendocrine L cells and enterochromaffin cells.

L cells release hormones like GLP-1 and PYY, which reduce hunger and regulate food intake.[95] These hormones act on receptors in both gut and brain, either directly or indirectly through the vagus nerve, to signal feelings of satiety also involving the circuits of the parabrachial nucleus.[96,97] L cells also communicate with the ENS through neuropods, allowing for fast and precise signalling between the gut and brain.[97–99] The activation of L cells in different parts of the gut depends on what is contained in the lumen: in the upper gut, they are triggered by nutrients like carbohydrates and fats, while in the lower gut they are driven by bacterial metabolites like SCFAs, which can stimulate GLP-1 and PYY secretion.[100–102]

Enterochromaffin cells produce most of the serotonin (5-HT) out of the CNS, which is important for intestinal motility, pain perception, and inflammatory response.[103] Although serotonin from the gut doesn't directly affect the brain due to the BBB, it may influence gut-brain communication through vagal signals[103] and inflammation [104–106]

2.3. The liver-brain axis

Increasing attention is being given to the liver's connection with the brain, which occurs primarily through two main routes: neuronal connections and vascular pathways.[107] Understanding these complex neural circuits is essential to appreciate the liver's involvement in conditions that affect both the liver and brain, including neurodegenerative disorders.[108,109]

Liver brain nervous anatomical connection

The liver, a vital organ for metabolism, detoxification, and nutrient storage, is regulated by the ANS, comprising the sympathetic and parasympathetic branches. Autonomic nerve fibers enter the liver through the hilum, forming plexuses around the liver's primary blood vessels – an anterior plexus encircling the hepatic artery and a posterior plexus surrounding the portal vein.[108]

Sympathetic fibers to the liver originate from preganglionic neurons in the thoracic spinal cord (T7–T12), traveling through the splanchnic nerves and synapsing in the celiac and superior mesenteric ganglia. From there, postganglionic sympathetic fibers innervate various structures, including the hepatic artery, portal vein, and bile ducts.[110,111] Parasympathetic innervation occurs via the hepatic branches of the left vagus nerve, which also innervates the bile ducts, portal vein, duodenum, and portions of the pancreas.[112–114]

In animal species, parasympathetic innervation is generally limited to the portal triad, while sympathetic innervation varies. In humans they reach the hepatocytes.[115]

The sympathetic nervous system predominantly regulates catabolic processes, while the parasympathetic system supports anabolic functions.[116] For example, vagal nerve pathways modulate hepatic lipid metabolism, influencing very low-density lipoprotein (VLDL) triglyceride secretion and reducing lipid accumulation in the liver.[117]

Additionally, to adrenaline, noradrenaline and Ach, hepatic neurons synthesize and release various neurotransmitters and neuropeptides, including neuropeptide Y, substance P, VIP, glucagon-like peptide, somatostatin, neurotensin, and serotonin, all of which further influence liver and systemic homeostasis.[118,119]

Hepatic afferent nerves, particularly from the vagus nerve, sense the liver's microenvironment and relay signals to the NTS, where feedback is sent to the liver via parasympathetic and sympathetic nerves.[120,121] These signals are also transmitted to higher brain regions, such as the hypothalamus and limbic system, influencing metabolic regulation and organ function.[122]

Liver brain vascular communication

In addition to neural circuits, liver and brain communicate through several vascular mechanisms, including BBB permeability, immune modulation, epigenetic alterations and amyloid β metabolism.

BBB permeability: Pro-inflammatory cytokines, including TNF-α and IL-1β, increase BBB permeability, allowing substances like ammonia, xenobiotics, and inflammatory cytokines to penetrate the brain, exacerbating neuroinflammation.[123] Excessive activation of microglia due to these cytokines attracts monocytes to the brain parenchyma, creating chronic inflammation in conditions as liver failure.[124,125] This is evident in chronic liver diseases, where neuroinflammatory processes contribute to neurological pathologies, such as hepatic encephalopathy, which occurs in approximately 30–45% of patients with cirrhosis.[126] Cholestatic mouse models,

such as BDL, show debilitating CNS symptoms defined as sickness behaviors. This behavior appears to be related to elevated levels of circulating and liver-synthesized IL-6. Regulatory T cells (T-regs) appear to be responsible for modulating IL-6 synthesis and inhibiting the activity of circulating monocytes.[127]

Epigenetic alterations: An example of how a metabolite produced by the liver can act centrally is β-hydroxybutyrate, a ketone body capable of crossing the BBB via specific monocarboxylate transporters and able to inhibit histone deacetylases (HDACs) the most important epigenetic control enzymes.[128] Elevated β-hydroxybutyrate levels in the brain increase brain-derived neurotrophic factor (BDNF), which plays a therapeutic role in neurodegenerative diseases and mental health disorders like depression.[129,130]

Amyloid β: The liver is central to the peripheral metabolism of Aβ, and dysregulation of Aβ clearance is a critical factor in the pathogenesis of AD. The connection between the liver and brain is thus closely linked to the progression of AD.[131,132]

α-Synuclein: Accumulation of α-synuclein in the liver may start liver inflammation and fibrosis[133] or represents a mechanism of clearance, which prevent a massive transmission of α-synuclein aggregates from the gut to the brain.[134,135] For this reason, liver could be directly involved in progression of PD either by cytokines release as by regulation of the transmission and clearance of α-synuclein aggregates.

2.4. The gut - liver - brain axis (GLBA)

The GLBA represents a network of bidirectional communication among the GI tract, the liver, and the brain, highlighting the interdependence of these organs in maintaining homeostasis and in contributing also to cognitive process. Understanding the GLBA is primary to elucidate the pathophysiology and the mechanisms of certain diseases, and to develop innovative therapeutic strategies that target this multifaceted network.

Studies suggested that different pathological conditions inducing dysbiosis could have acute or chronic systemic consequences, such as a weakened of the immune system, inflammation or central disorders, as well as neuropsychiatric disorders, including anxiety, depression or neurodegenerative conditions.[136,137] Furthermore, events, such as maternal stress to lack of breastfeeding, mode of delivery (vaginal VS cesarean) and antibiotic exposure, are major players in the development of acute infections and long-term dysbiosis that are associated to chronic pathological conditions, including asthma, diabetes, neurodevelopmental disorders and IBS.[138,139]

In addition, dysbiosis can also impact the function of the HPA, a fundamental part of the limbic system, involved in both emotional behavior and memory consolidation[140,141]. At last, the role of dysbiosis in both a cause and consequence of the "leaky gut", a condition associated to many autoimmune disorders where intestinal permeability is increased and pathogens as well as toxins can enter more freely into the human body, is well documented.[142]

3. PRINCIPAL BIOCHEMICAL MODULATORS ALONG THE GUT-BRAIN AXIS

3.1. Serotonin

Serotonin, also known as 5-hydroxytryptamine (5-HT), is a monoamine neurotransmitter.[143] Historically, its roles have been mostly associated with the regulation of basic functions of the CNS, including sleep, mood and body temperature. Its deficits are present in numerous mental disorders.[144] Despite this common knowledge, it has been demonstrated that less than 5% of the total body's serotonin is in the CNS,[145] while most of it is hosted by the intestine.[146] 5-HT is produced mostly by enterochromaffin cells in the intestinal lining, which regulates many functions of the GI tract, including motility and permeability, as well as local secretions and ENS development [147].

Alterations of serotonin levels have been found in several diseases, including IBS,[148] hepatic conditions[149] and psychiatric disorders,[150] underlying the importance of the GBA and how serotonin pathways affect it. Recent studies have shown that commensal bacteria participate in the production and modulation of intestinal serotonin.[151] Consequently, prebiotics and probiotics can alter both synthesis and release of serotonin, actively impacting both GI and nervous system.[152] Moreover, although enteric 5-HT can both act locally and enter the bloodstream, divergent data on the capacity of 5-HT to cross the BBB are available.[153,154] Despite this, 5-HT has been shown to alter the permeability of the BBB.[155] Study demonstrated that the endothelium of the choroid plexus, which in healthy conditions is permeable to large (70 kDa) circulating molecules, upon intestinal inflammation acts as a vascular barrier (PVB), by closing its accessibility to inflammatory and bacterial molecules.[156] Recent study hypothesizes the capacity of neurotransmitters produced in the gut to cross the choroid plexus.[157] Therefore, it can be said that alterations in serotonin pathways can be both the cause and the consequence of GI or CNS diseases, as GI tract and brain are deeply linked, regulate each other, and are in charge for the control of emotional and stress responses.

As previously mentioned, numerous therapeutic options for several diseases affect serotonin metabolism, from its secretion to its release or reuptake. Due to the high prevalence of serotonin in the GI tract, such therapies can significantly impact GI functions as the use of serotonin reuptake inhinitors.[158] People affected by IBS exhibit altered levels of post-prandial plasma serotonin, both in children [159] and adults,[160] and it has been hypothesized that such individuals may have a genetic predisposition for decreased serotonin reuptake transporter (SERT) expression.[160] Potential therapeutic options are being studied via serotonin-related signaling pathways and the gut-liver axis, in the regulation of obesity,[161] MASLD, and hepatic steatosis. [162] Studies involving serotonin agonists have been shown to benefit patients affected by IBS suffering from constipation, by increasing intestinal mobility and secretion.[103] Moreover, tricyclic antidepressants that were used in numerous psychiatric conditions play a role in both mood and GI symptoms in patients affected by depression as well as IBD[163]. Furthermore, alterations in serotonin signaling can exacerbate gastrointestinal symptoms in stressed individuals, emphasizing the connection between psychological mechanisms and GI function.[164] The serotonin produced by guts significantly influences the brain through immune function, vagal nerve stimulation, neuroendocrine feedback, and the HPA axis, but the relationship between serotonin levels in the brain and depression remains unclear.[165]

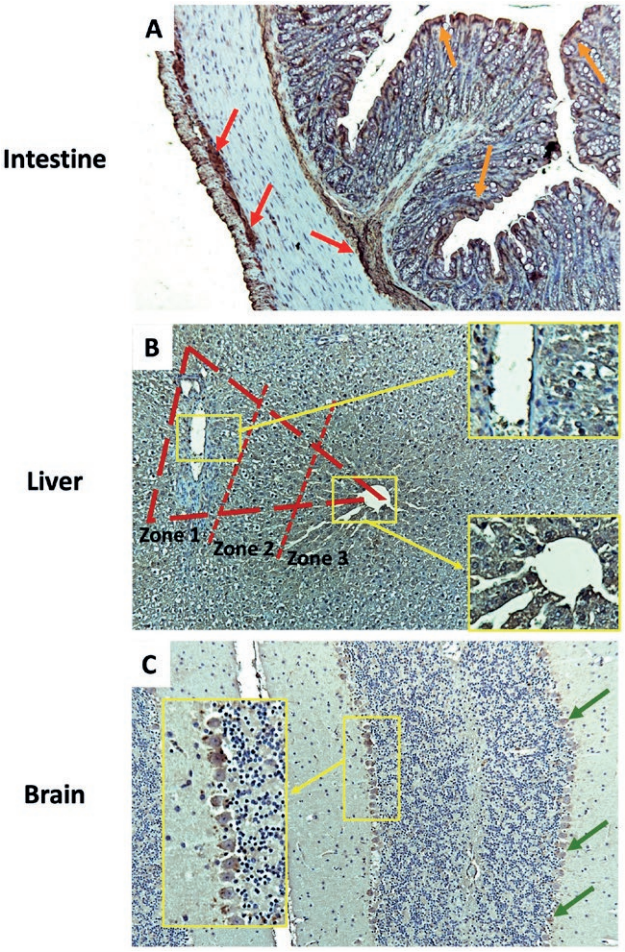

Figure 5. GLP-1 expression (Abcam AB22625) along the gut - liver - brain axis. GLP-1 is released from enteroendocrine cells of the lower intestine and exerts anorectic and antimotility actions.[167] In fact, GLP-1 expression at the level of colon is high in the intestinal epithelium (orange arrows) and in the myenteric and submucosal plexes (red arrows) **[A]**. In the hepatic parenchima exists a different gradient of expression inside the acinus, with an increase from the zone 1 towards zone 3, where it has an insulin-like activity, on glucagon-induced glycogenolysis[168] **[B]**. In the brain, dense immunoreactivity fills the cell bodies of the efferent neurons, such as the Purkinje cells in the cerebellum (green arrows) **[C]**. OM 10x

3.2. GLP-1 and GIP

GLP-1 and glucose dependent insulinotropic polypeptide (GIP) are incretin hormones secreted by their EECs.[166] These cells constitute a small portion of the total intestinal cell population (about 1%). Despite this, they represent the largest endocrine organ of the human body, and they are distributed along the entire GI tract (Figure 5). These are divided into three different subgroups, each specialized in the production of a different gut hormone: (i) L cells, which secrete (secreting GLP-1), (ii) I cell (secreting cholecystokinin [CCK]), and (iii) K cells, which secrete (secreting GIP).

Incretin GLP-1 is present at low levels in a fasting state, and it increases within the first few minutes after food ingestion, reaching a peak of about 15 *p*mol/l at around 60-90 minutes after a meal.[166] The GLP-1 incretin is characterized by a very short half-life, corresponding to about 1 to 2 minutes. Therefore, only about 12% of gut-derived GLP-1 enters the systemic circulation.[167] This could relate to the possibility that GLP-1 could activate vagal terminals innervating, the gut and the hepato-portal region, mediating also a signal from the brain to the pancreatic β-cells through vasovagal reflexes that induce insulin secretion.[168] In fact, the common hepatic, celiac and gastric branches have been shown to contribute to the glucoregulatory effects of gut GLP-1.[169]

GIP is involved in the regulation of glucose in the circulation by actin on islet of Langerhans to release insulin and glucagone.[170] However, different studies demostrated contradictory data on the role of GIP in human energy homeostasis.[171] GIP receptors are expressed on the adipocytes to promote lipid storage,

on neurons in the arcuate nucleus (ARC), dorsomedial nucleus, and paraventricular nucleus of the hypothalamus to control food intake.[172] An array of studies has shown the possible correlation between central GIP signaling, body weight gain and adiposity, through a possible induction of neural leptin resistance. GIP has also been shown to have a direct relation to obesity.[173]

3.3. CCK and lipids

CCK is released by I cells, which are a subgroup of the enteroendocrine cell family. It is secreted in the proximal small intestine because of protein and lipid ingestion. CCK is released following lipid ingestion through a G-protein-coupled receptor 40 (GPR40) mediated mechanism, while it is released because of protein ingestion through calcium-sensing receptor (CaSR).

After being released by ECCs, CCK enters the bloodstream and reaches a peak in concentration of between 6 and 15 *p*mol/L, about 90 to 120 minutes after eating, timing being influenced by fat and protein content of the chymus.[174] CCK is released as a pro-hormone, or pro-CCK, which is then cleaved and activated by prohormone that converts pro-CCK into various forms giving rise to different types of CCK.[175] For instance, CCK8 is the most abundantly utilized form, followed by other types such as CCK58, CCK33 and CCK58, each acting at a different site along the gastrointestinal tract.[176] Different studies have demonstrated the ability of CCK to activate vagal afferent pathways, showing for instance that CCK receptor 1 activation increased cAMP/PKA pathway, which is crucial for CCK activation of central afferent terminals. Furthermore, the activation of CCK receptor1/cAMP/PKA signaling in the small intestine eventually results into vagal afferent firing.[177]

Gut microbiota can affect lipid metabolism acting on bile acids, cholesterol and lipoprotein production. Some bacteria can produce enzymes to deconjugate bile acids, modifying their enterohepatic circulation and altering cholesterol levels.[178] Lipids can increase CCK release and CCK receptor antagonists are used as therapeutic targets to reduce the satiety senses after the intestinal passage of lipid in both humans and experimental models.[179,180] In detail, lipids promote the secretion of CCK and activate VANs to decrease food intake maybe be due to chylomicron formation and activation of a sensory mechanism on the basolateral region of EECs.[181,182] In addition, Pluronic L-81, that can block chylomicron formation, significantly reduces the anorexigenic effects of lipid administration decreasing CCK release, celiac and cervical vagal afferent activation, which are typical effects after lipid infusion.[183,184]

In summary, EECs in the GI tract can secrete different gut peptides affecting energy and glucose homeostasis. Overall, there is strong evidence that suggests how CCK can impact on energy and glucose homeostasis through the activation of a gut-brain vagal pathway, and more studies are required to analyze the mechanism of the process.[185]

4. INVOLVEMENT OF FERROPTOSIS IN THE GUT-LIVER-BRAIN AXIS

Iron dysregulation and ferroptosis have been shown to be active players in the progression of different neurodegenerative disorders, including Amyotrophic Lateral Sclerosis (ALS), multiple sclerosis (MS) and PD.[186-188-189] In neurodegeneration, multiple features of ferroptosis are reported, such as accumulation of lipid peroxidation products, depletion of glutathione, excess of extracellular glutamate and increased lipoxygenase (LOX) activity.[190,191] Microglia are sensitive to iron overload-induced ferroptosis and clinical investigations suggest how ferroptosis inhibitors may represent a therapeutic approach in these types of diseases. In fact, in a human induced pluripotent stem cell-derived tri-culture system containing neurons, astrocytes and microglia, the latter showed the highest transcriptional response to iron accumulation identifying a subgroup of microglia with a distinct ferroptosis-associated transcriptomic signature (FAS). The removal of microglia in the culture system decreased neuronal lipid peroxidation and reduced the death of neurons.[192] Microglia may induce ferroptosis in neurons through the production of pro-inflammatory cytokines, such as IL-1β, IL-6 and IL-8.[193] Microglial uptake of iron may be protective at the beginning of the disease, while a neurotoxic state is later established and leads to the cellular damage. In addition, several data strongly support the concept that the dying microglia may release factors that escalate neuronal death. Moreover, it has been demonstrated that increased endogenous levels of α-syn oligomers are correlated with high cytosolic calcium influx by changes in plasmalemmal membrane potential or activation of glutamate receptor.[194] In the absence of lipid peroxidation, the α-syn-induced calcium dysregulation is also abolished, and physiological calcium signalling is restored.[195]

On these bases, ferroptosis can induce and promote diseases by affecting the GLA and the interaction among these organs, microbiota and environmental factors. For example, the imbalance of intestinal microbiota can enhance microbial metabolites, such as SCFAs, and gut permeability, thereby inducing inflammatory

response and NAFLD.[196] The involvement of ferroptosis in NAFLD is mainly linked to the increase of lipid peroxidation. Moreover, the most important signaling pathways may incorporate Nrf2- GPX4 and AKT-GSK3β-Nrf2 pathways.[197] These imbalances of gut microbiota can be modulated by *Pleurotus geesteranus* polysaccharides through the reduction of oxidative stress acting on Nrf2/HO-1 and TLR4/NF-kB signaling pathways with the result to protect the intestinal barrier.[198] Furthermore, ferroptosis can mediate liver-brain axis affecting the hepatic metabolism level of amino acids and causing neuroinflammation through AKT/Nrf2/GPX4 and Nrf2-ARE pathways leading to ROS production.[199] Nrf2 can block the process of ferroptosis by its nuclear translocation and production of proteins related to iron metabolism, such as ferritin, ferroportin and SLC7A11.[200]

In summary, ferroptosis may modulate the gut-brain axis influencing the progression of the neurodegenerative disorders, acting on two main targets: Nrf2 and HO-1.[201,202] Nrf2 play a crucial role in the preservation of epithelial tight junction and gut barrier,[203,204] whereas, HO-1 represents an important factor regulating the antioxidant and neuro-protective responses.[205] The deposition of iron, GPX4 inactivation and lipid peroxidation accumulation cause damage of cell membrane, cellular junctions and subcellular organelles that contribute to: (i) the pathogenesis of IBD, (ii) initiate and continue liver injury, and (iii) to induce neurodegenerative disease onset mainly reaching the brainstem through the hepatic afferent vagus nerve.[206,207] For all these reasons, iron chelators represent an important approach for the process of ferroptosis, but many of them may have difficulties in the progression along the GLBA and may disrupt homeostatic redox functions.[208] However, some preclinical studies have used lipid peroxidation inhibitors targeting lipid peroxidation and oxidative stress, such as vitamin E derivative vatiquinone acid and activators of the antioxidant NRF2 pathway.[209]

4.1. Specific neuronal territories as main targets of ferroptosis and neurodegeneration along the gut-liver-brain axis

Ferroptosis has been demonstrated to be an important factor in the development of pathological processes in the brain. This is arguably secondary to the relatively higher susceptibility of the CNS to iron-induced lipid peroxidation, because of an intrinsic increased energy consumption and lipid content, as well as lower tolerance to ROS.[210]

Specifically, hippocampal neurons show increased levels of mitochondrial ferroptosis following general anesthesia, partially explaining the mechanism of anesthesia-induced ischemia-reperfusion injury.[211] As isoflurane is often used in general anesthesia, ferroptosis inhibitors and mitochondrial activators (such as ferrostatin-1 and dimethyl fumarate, respectively) could be used to decrease hippocampal susceptibility to ferroptosis.[212] Moreover, ferroptosis significantly induces memory decline. Very interestingly, this seems to be slowed down by hormone-replacement therapy in post-menopausal women,[213] possibly via anti-neuroinflammation and anti-oxidative stress mechanisms.[214]

The importance of ferroptosis in neurological diseases is underlined by the potential treatment strategies that can be utilized in future. For instance, in the hippocampus of animal model experiments mimicking diabetes-related cognitive dysfunction, *sinomenine* showed a neuroprotective potential against erastin-induced ferroptosis via the GBA[215] and by increasing EGF expression (known to reduce oxidative stress via the Nrf2/HO-1 signaling pathway).[216] Moreover, another study showed the potential to slow down diabetes-induced cognitive impairment by inhibition of ferroptosis via activation of AMPK.[217] The hippocampus is also highly susceptible to sepsis-associated encephalopathy (SAE), secondarily to ROS formation and altered ferroptosis-related protein expressions[218]. Similarly, ferroptosis has been shown to have a causative effect in traumatic brain injury (TBI)[219] as well as hemorrhagic and ischemic strokes.[220,221] Reduction of ferroptosis and improved mitochondrial dysfunction were achieved by administration of irisin,[218] a molecule proven to be a potential therapeutic target for cerebral ischemia,[222] neurodegenerative diseases[223] and TBI,[224] through its anti-oxidative, anti-inflammatory and anti-ferroptotic activities. Interestingly, also low-dose acetaminophen prevents hippocampal ferroptosis in septic mice via the GPX4 and FSP1 pathways.[225] In the hippocampus, ferroptosis is significantly involved in AD,[226,227] opening new potential diagnostic and therapeutic possibilities against the most prevalent neurodegenerative disease in the general population.[228]

Moreover, putamen and globus pallidus are particularly susceptible to iron accumulation in PD[229] and in other diseases that involve iron accumulation in the brain.[230] Progressive loss of spontaneous activity in the putamen also contributes to impaired task performance in patients with PD.[231] In a metanalysis of post-mortem measurements of iron levels in the brain of PD patients, significantly high levels of iron deposition were observed in the whole Basal Ganglia system, including the substantia nigra, the caudate nucleus and the globus pallidus, suggesting a crucial role of ferroptosis in the pathogenesis of PD.[232] Ferroptosis plays a role also in the development of Huntington's disease (HD), an inher-

ited, neurodegenerative disorder. This neuro-disorder involves striatum, and it is characterized by the gradual development of choreic movements. Studies suggested high levels of iron in HD patients.[233,234] Unsurprisingly, ferrostatin-1 showed the potential to prevent iron-dependent oxidative stress and the capacity to reverse decrease neuronal cell death in cellular models of HD.[235] Moreover, laduviglusib, a highly selective inhibitor of Glycogen synthase kinase 3, was demonstrated to target ferroptosis-related genes in striatal neurons in the setting of HD.[236]

Doublecortin deficiency and the presence of ferroptosis were observed in a post-mortem analysis of the caudate nucleus of AD patients.[237] Also, the nigrostriatal system can be specifically pathologically affected by ferroptosis. This can be perhaps exemplified by the effect of methamphetamine (the second most used recreational drug, that works through an amphetamine-type neuronal stimulation),[238] whose use was associated to increased iron deposits in both the substantia nigra and caudate nucleus. Very interestingly, the administration of iron chelators in the setting of methamphetamines use proved to decrease the pathological nigrostriatal changes via attenuated iron deposition and ROS formation, as well as dopaminergic cell death.[239]

Several studies have demonstrated that neuroinflammation, or rather the activation of the neuroimmune cells into proinflammatory states, is implicated in neurodegenerative diseases, such as AD, Synucleinopathies, ALS and HD not only because of neurodegeneration but also as a pivotal player in this process.[240] In this context, CNS inflammatory response is orchestrated by an interaction of microglial cells, infiltrating myeloid cells, astrocytes, the BBB cells (endothelial cells, pericytes, astrocytes) and the action of signaling molecules (cytokines, chemokines, and growth factors), which produce both central and peripheral reaction.[241]

Interestingly, the process of neuroinflammation could be triggered and highlighted by both gut and liver produced molecules as well as by ferroptosis.[242–244] Therefore, ferroptosis contributes to the connections of the gut-liver-brain axis, as well as to the interplay between neuroinflammation and neurodegeneration in the context of different brain areas.

CONCLUDING REMARKS

Ferroptosis, an iron-dependent form of programmed cell death, is emerging as a critical factor in neurodegeneration, intricately linked with neuroinflammation and the GLBA. The process of ferroptosis is characterized by the accumulation of lethal lipid peroxides, leading to cell death and dysfunction. In neurodegenerative diseases like AD and PD,[245–247] this pathway is significantly activated, contributing to the degeneration of vulnerable neuronal populations.

Neuroinflammation, characterized by the activation of the brain's immune cells and the release of proinflammatory cytokines, exacerbates ferroptotic mechanisms. The inflammatory milieu enhances oxidative stress, fuelling iron accumulation and lipid peroxidation,[248] thereby contributing to neuronal death. This implies a vicious cycle where neuroinflammation and ferroptosis amplify each other.

Furthermore, the GLBA plays a substantial role in modulating these interactions. The gut microbiota influences systemic inflammation and oxidative stress through the production of metabolites and the modulation of immune responses. Dysbiosis can lead to increased gut permeability, allowing inflammatory mediators to enter circulation and reach the brain,[249,250] thereby directly affecting neuroinflammatory states and potentially triggering ferroptotic pathways.[250,251]

The liver also contributes to this axis, as it regulates systemic iron metabolism and inflammatory responses. Liver dysfunction can lead to altered iron homeostasis and increased production of inflammatory mediators, both of which can influence ferroptotic activity in the brain.[252]

This interplay suggests that targeting the GLBA could potentially offer therapeutic strategies to mitigate ferroptosis and neuroinflammation. By maintaining gut microbiota balance and ensuring proper liver function, it may be possible to modulate systemic inflammation and oxidative stress, thus reducing neuronal vulnerability to ferroptosis and slowing the progression of different neurodegenerative disorders. Understanding these complex interactions underscores the need for integrated therapeutic approaches that address the multifaceted nature of GLBA.

REFERENCES

1. Yang, W., Li, X., Li, X., Li, X. & Yu, S. Neuronal hemoglobin in mitochondria is reduced by forming a complex with α-synuclein in aging monkey brains. *Oncotarget* **7**, 7441–7454 (2016).
2. Galluzzi, L. *et al.* Molecular mechanisms of cell death: recommendations of the Nomenclature Committee on Cell Death 2018. *Cell Death Differ* **25**, 486–541 (2018).
3. Stockwell, B. R. Ferroptosis turns 10: Emerging mechanisms, physiological functions, and therapeutic applications. *Cell* **185**, 2401–2421 (2022).

4. Yang, W. S. & Stockwell, B. R. Ferroptosis: Death by Lipid Peroxidation. *Trends Cell Biol* **26**, 165–176 (2016).
5. Ward, R. J., Zucca, F. A., Duyn, J. H., Crichton, R. R. & Zecca, L. The role of iron in brain ageing and neurodegenerative disorders. *Lancet Neurol* **13**, 1045–60 (2014).
6. Stockwell, B. R. *et al.* Ferroptosis: A Regulated Cell Death Nexus Linking Metabolism, Redox Biology, and Disease. *Cell* **171**, 273–285 (2017).
7. Stockwell, B. R. Ferroptosis turns 10: Emerging mechanisms, physiological functions, and therapeutic applications. *Cell* **185**, 2401–2421 (2022).
8. Linkermann, A. *et al.* Synchronized renal tubular cell death involves ferroptosis. *Proc Natl Acad Sci U S A* **111**, 16836–41 (2014).
9. Chng, C.-P., Sadovsky, Y., Hsia, K. J. & Huang, C. Site-Specific Peroxidation Modulates Lipid Bilayer Mechanics. *Extreme Mech Lett* **42**, (2021).
10. Hao, L., Zhong, Y.-M., Tan, C.-P. & Mao, Z.-W. Quantitative tracking of endoplasmic reticulum viscosity during ferroptosis by an iridium complex via TPPLM. *Chem Commun (Camb)* **57**, 5040–5042 (2021).
11. Nie, Q., Hu, Y., Yu, X., Li, X. & Fang, X. Induction and application of ferroptosis in cancer therapy. *Cancer Cell Int* **22**, 12 (2022).
12. Chen, X., Yu, C., Kang, R. & Tang, D. Iron Metabolism in Ferroptosis. *Front Cell Dev Biol* **8**, 590226 (2020).
13. Koppula, P., Zhuang, L. & Gan, B. Cytochrome P450 reductase (POR) as a ferroptosis fuel. *Protein Cell* **12**, 675–679 (2021).
14. Cobler, L., Zhang, H., Suri, P., Park, C. & Timmerman, L. A. xCT inhibition sensitizes tumors to γ-radiation via glutathione reduction. *Oncotarget* **9**, 32280–32297 (2018).
15. Feng, H. & Stockwell, B. R. Unsolved mysteries: How does lipid peroxidation cause ferroptosis? *PLoS Biol* **16**, e2006203 (2018).
16. Ganz, T. Hepcidin, a key regulator of iron metabolism and mediator of anemia of inflammation. *Blood* **102**, 783–8 (2003).
17. Vogt, A.-C. S. *et al.* On Iron Metabolism and Its Regulation. *Int J Mol Sci* **22**, (2021).
18. Epsztejn, S. *et al.* H-ferritin subunit overexpression in erythroid cells reduces the oxidative stress response and induces multidrug resistance properties. *Blood* **94**, 3593–603 (1999).
19. Nie, Q., Hu, Y., Yu, X., Li, X. & Fang, X. Induction and application of ferroptosis in cancer therapy. *Cancer Cell Int* **22**, 12 (2022).
20. Quiles Del Rey, M. & Mancias, J. D. NCOA4-Mediated Ferritinophagy: A Potential Link to Neurodegeneration. *Front Neurosci* **13**, 238 (2019).
21. Yang, W. S. & Stockwell, B. R. Synthetic lethal screening identifies compounds activating iron-dependent, nonapoptotic cell death in oncogenic-RAS-harboring cancer cells. *Chem Biol* **15**, 234–45 (2008).
22. Kwon, M.-Y., Park, E., Lee, S.-J. & Chung, S. W. Heme oxygenase-1 accelerates erastin-induced ferroptotic cell death. *Oncotarget* **6**, 24393–403 (2015).
23. Koppula, P., Zhuang, L. & Gan, B. Cytochrome P450 reductase (POR) as a ferroptosis fuel. *Protein Cell* **12**, 675–679 (2021).
24. Lin, L.-S. *et al.* Simultaneous Fenton-like Ion Delivery and Glutathione Depletion by MnO2 -Based Nanoagent to Enhance Chemodynamic Therapy. *Angew Chem Int Ed Engl* **57**, 4902–4906 (2018).
25. Reis, A. & Spickett, C. M. Chemistry of phospholipid oxidation. *Biochim Biophys Acta* **1818**, 2374–87 (2012).
26. Kagan, V. E. *et al.* Oxidized arachidonic and adrenic PEs navigate cells to ferroptosis. *Nat Chem Biol* **13**, 81–90 (2017).
27. Gijón, M. A., Riekhof, W. R., Zarini, S., Murphy, R. C. & Voelker, D. R. Lysophospholipid acyltransferases and arachidonate recycling in human neutrophils. *J Biol Chem* **283**, 30235–45 (2008).
28. Pabst, O. *et al.* Gut-liver axis: barriers and functional circuits. *Nat Rev Gastroenterol Hepatol* **20**, 447–461 (2023).
29. Tilg, H., Adolph, T. E. & Trauner, M. Gut-liver axis: Pathophysiological concepts and clinical implications. *Cell Metab* **34**, 1700–1718 (2022).
30. Milosevic, I. *et al.* Gut-Liver Axis, Gut Microbiota, and Its Modulation in the Management of Liver Diseases: A Review of the Literature. *Int J Mol Sci* **20**, (2019).
31. He, J. *et al.* Short-Chain Fatty Acids and Their Association with Signalling Pathways in Inflammation, Glucose and Lipid Metabolism. *Int J Mol Sci* **21**, (2020).
32. Coppola, S., Avagliano, C., Calignano, A. & Berni Canani, R. The Protective Role of Butyrate against Obesity and Obesity-Related Diseases. *Molecules* **26**, (2021).
33. Kawasoe, J. *et al.* Propionic Acid, Induced in Gut by an Inulin Diet, Suppresses Inflammation and Ameliorates Liver Ischemia and Reperfusion Injury in Mice. *Front Immunol* **13**, 862503 (2022).
34. Wright, R. S., Anderson, J. W. & Bridges, S. R. Propionate inhibits hepatocyte lipid synthesis. *Proc Soc Exp Biol Med* **195**, 26–9 (1990).

35. McNabney, S. M. & Henagan, T. M. Short Chain Fatty Acids in the Colon and Peripheral Tissues: A Focus on Butyrate, Colon Cancer, Obesity and Insulin Resistance. *Nutrients* **9**, (2017).
36. Singh, V. *et al.* Dysregulated Microbial Fermentation of Soluble Fiber Induces Cholestatic Liver Cancer. *Cell* **175**, 679-694.e22 (2018).
37. Bäckhed, F. *et al.* The gut microbiota as an environmental factor that regulates fat storage. *Proc Natl Acad Sci U S A* **101**, 15718–23 (2004).
38. van Eenige, R. *et al.* Angiopoietin-like 4 governs diurnal lipoprotein lipase activity in brown adipose tissue. *Mol Metab* **60**, 101497 (2022).
39. Chen, J. & Vitetta, L. Gut Microbiota Metabolites in NAFLD Pathogenesis and Therapeutic Implications. *Int J Mol Sci* **21**, (2020).
40. Israelsen M, Francque S, Tsochatzis EA, Krag A. Steatotic liver disease. *Lancet* **404**(10464), 1761-1778 (2024).
41. Pabst, O. *et al.* Gut-liver axis: barriers and functional circuits. *Nat Rev Gastroenterol Hepatol* **20**, 447–461 (2023).
42. Kuo, W.-T. *et al.* The Tight Junction Protein ZO-1 Is Dispensable for Barrier Function but Critical for Effective Mucosal Repair. *Gastroenterology* **161**, 1924–1939 (2021).
43. Günzel, D. & Fromm, M. Claudins and other tight junction proteins. *Compr Physiol* **2**, 1819–52 (2012).
44. Tsukita, S., Tanaka, H. & Tamura, A. The Claudins: From Tight Junctions to Biological Systems. *Trends Biochem Sci* **44**, 141–152 (2019).
45. Yiu, J. H. C., Dorweiler, B. & Woo, C. W. Interaction between gut microbiota and toll-like receptor: from immunity to metabolism. *J Mol Med (Berl)* **95**, 13–20 (2017).
46. Ciesielska, A., Matyjek, M. & Kwiatkowska, K. TLR4 and CD14 trafficking and its influence on LPS-induced pro-inflammatory signaling. *Cell Mol Life Sci* **78**, 1233–1261 (2021).
47. Yu, X. *et al.* Ferroptosis: An important mechanism of disease mediated by the gut-liver-brain axis. *Life Sci* **347**, 122650 (2024).
48. Albillos, A., de Gottardi, A. & Rescigno, M. The gut-liver axis in liver disease: Pathophysiological basis for therapy. *J Hepatol* **72**, 558–577 (2020).
49. Espinosa-Oliva, A. M. *et al.* Inflammatory bowel disease induces pathological α-synuclein aggregation in the human gut and brain. *Neuropathol Appl Neurobiol* **50**, e12962 (2024).
50. Casini, A. *et al.* TNBS colitis induces architectural changes and alpha-synuclein overexpression in mouse distal colon: A morphological study. *Cell Tissue Res* **399**, 247–265 (2025).
51. Simbrunner, B., Trauner, M. & Reiberger, T. Review article: therapeutic aspects of bile acid signalling in the gut-liver axis. *Aliment Pharmacol Ther* **54**, 1243–1262 (2021).
52. Schoeler, M. & Caesar, R. Dietary lipids, gut microbiota and lipid metabolism. *Rev Endocr Metab Disord* **20**, 461–472 (2019).
53. Yan, M. *et al.* Gut liver brain axis in diseases: the implications for therapeutic interventions. *Signal Transduct Target Ther* **8**, 443 (2023).
54. Guo, C., Chen, W.-D. & Wang, Y.-D. TGR5, Not Only a Metabolic Regulator. *Front Physiol* **7**, 646 (2016).
55. Xie, G. *et al.* Conjugated secondary 12α-hydroxylated bile acids promote liver fibrogenesis. *EBioMedicine* **66**, 103290 (2021).
56. Wang, Y. *et al.* The role of sphingosine 1-phosphate receptor 2 in bile-acid-induced cholangiocyte proliferation and cholestasis-induced liver injury in mice. *Hepatology* **65**, 2005–2018 (2017).
57. Kakiyama, G. *et al.* Modulation of the fecal bile acid profile by gut microbiota in cirrhosis. *J Hepatol* **58**, 949–55 (2013).
58. Arias, N. *et al.* The Relationship between Choline Bioavailability from Diet, Intestinal Microbiota Composition, and Its Modulation of Human Diseases. *Nutrients* **12**, (2020).
59. Gadaleta, R. M. & Moschetta, A. Metabolic Messengers: fibroblast growth factor 15/19. *Nat Metab* **1**, 588–594 (2019).
60. Somm, E. & Jornayvaz, F. R. Fibroblast Growth Factor 15/19: From Basic Functions to Therapeutic Perspectives. *Endocr Rev* **39**, 960–989 (2018).
61. Potthoff, M. J. *et al.* FGF15/19 regulates hepatic glucose metabolism by inhibiting the CREB-PGC-1α pathway. *Cell Metab* **13**, 729–38 (2011).
62. Andersen, A., Lund, A., Knop, F. K. & Vilsbøll, T. Glucagon-like peptide 1 in health and disease. *Nat Rev Endocrinol* **14**, 390–403 (2018).
63. Munshi, M. K. *et al.* Regulation of biliary proliferation by neuroendocrine factors: implications for the pathogenesis of cholestatic liver diseases. *Am J Pathol* **178**, 472–84 (2011).
64. Sun, L. *et al.* Secretin modulates appetite via brown adipose tissue-brain axis. *Eur J Nucl Med Mol Imaging* **50**, 1597–1606 (2023).
65. Barrea, L. *et al.* The challenge of weight loss maintenance in obesity: a review of the evidence on the best strategies available. *Int J Food Sci Nutr* **73**, 1030–1046 (2022).

66. Bove, C. & Travagli, R. A. Neurophysiology of the brain stem in Parkinson's disease. *J Neurophysiol* **121**, 1856–1864 (2019).
67. Fleming, M. A., Ehsan, L., Moore, S. R. & Levin, D. E. The Enteric Nervous System and Its Emerging Role as a Therapeutic Target. *Gastroenterol Res Pract* **2020**, 8024171 (2020).
68. Furness, J. B. & Stebbing, M. J. The first brain: Species comparisons and evolutionary implications for the enteric and central nervous systems. *Neurogastroenterology and motility* **30**, (2018).
69. Rao M, Gershon MD. The bowel and beyond: the enteric nervous system in neurological disorders. *Nat Rev Gastroenterol Hepatol.* **13**(9),517–28 (2016).
70. Santucci, N. R. & Velez, A. Physiology of lower gastrointestinal tract. *Aliment Pharmacol Ther* **60 Suppl 1**, S1–S19 (2024).
71. Wallrapp, A. & Chiu, I. M. Neuroimmune Interactions in the Intestine. *Annu Rev Immunol* **42**, 489–519 (2024).
72. Spencer, N. J. & Hu, H. Enteric nervous system: sensory transduction, neural circuits and gastrointestinal motility. *Nat Rev Gastroenterol Hepatol* **17**, 338–351 (2020).
73. Wehrwein, E. A., Orer, H. S. & Barman, S. M. Overview of the Anatomy, Physiology, and Pharmacology of the Autonomic Nervous System. *Compr Physiol* **6**, 1239–78 (2016).
74. Santucci, N. R. & Velez, A. Physiology of lower gastrointestinal tract. *Aliment Pharmacol Ther* **60 Suppl 1**, S1–S19 (2024).
75. Chakrabarti, A. *et al.* The microbiota-gut-brain axis: pathways to better brain health. Perspectives on what we know, what we need to investigate and how to put knowledge into practice. *Cell Mol Life Sci* **79**, 80 (2022).
76. Kaelberer, M. M. *et al.* A gut-brain neural circuit for nutrient sensory transduction. *Science* **361**, (2018).
77. Berthoud, H. R., Blackshaw, L. A., Brookes, S. J. H. & Grundy, D. Neuroanatomy of extrinsic afferents supplying the gastrointestinal tract. *Neurogastroenterology and motility* **16 Suppl 1**, 28–33 (2004).
78. Bonaz, B., Sinniger, V. & Pellissier, S. Vagus Nerve Stimulation at the Interface of Brain-Gut Interactions. *Cold Spring Harb Perspect Med* **9**, (2019).
79. Rinaman, L. Ascending projections from the caudal visceral nucleus of the solitary tract to brain regions involved in food intake and energy expenditure. *Brain Res* **1350**, 18–34 (2010).
80. Doifode, T. *et al.* The impact of the microbiota-gut-brain axis on Alzheimer's disease pathophysiology. *Pharmacol Res* **164**, 105314 (2021).
81. Cryan, J. F. & Dinan, T. G. Mind-altering microorganisms: the impact of the gut microbiota on brain and behaviour. *Nat Rev Neurosci* **13**, 701–12 (2012).
82. Rhee, S. H., Pothoulakis, C. & Mayer, E. A. Principles and clinical implications of the brain-gut-enteric microbiota axis. *Nat Rev Gastroenterol Hepatol* **6**, 306–14 (2009).
83. Kumar, A. *et al.* Gut Microbiota in Anxiety and Depression: Unveiling the Relationships and Management Options. *Pharmaceuticals (Basel)* **16**, (2023).
84. Su, Y.-L. *et al.* Phlorizin alleviates cholinergic memory impairment and regulates gut microbiota in d-galactose induced mice. *Exp Gerontol* **165**, 111863 (2022).
85. Wenzel, T. J., Gates, E. J., Ranger, A. L. & Klegeris, A. Short-chain fatty acids (SCFAs) alone or in combination regulate select immune functions of microglia-like cells. *Mol Cell Neurosci* **105**, 103493 (2020).
86. Li, D. *et al.* Trimethylamine-N-oxide promotes brain aging and cognitive impairment in mice. *Aging Cell* **17**, e12768 (2018).
87. Clarke, G. *et al.* The microbiome-gut-brain axis during early life regulates the hippocampal serotonergic system in a sex-dependent manner. *Mol Psychiatry* **18**, 666–73 (2013).
88. Sudo, N. *et al.* Postnatal microbial colonization programs the hypothalamic-pituitary-adrenal system for stress response in mice. *J Physiol* **558**, 263–75 (2004).
89. Grenham, S., Clarke, G., Cryan, J. F. & Dinan, T. G. Brain-gut-microbe communication in health and disease. *Front Physiol* **2**, 94 (2011).
90. Eisenstein, M. Microbiome: Bacterial broadband. *Nature* **533**, S104-6 (2016).
91. Dinan, T. G. *et al.* Hypothalamic-pituitary-gut axis dysregulation in irritable bowel syndrome: plasma cytokines as a potential biomarker? *Gastroenterology* **130**, 304–11 (2006).
92. Hosoi, T., Okuma, Y. & Nomura, Y. Electrical stimulation of afferent vagus nerve induces IL-1β expression in the brain and activates HPA axis. *American Journal of Physiology-Regulatory, Integrative and Comparative Physiology* **279**, R141–R147 (2000).
93. Demaude, J. Phenotypic changes in colonocytes following acute stress or activation of mast cells in mice: implications for delayed epithelial barrier dysfunction. *Gut* **55**, 655–661 (2006).
94. Gribble, F. M. & Reimann, F. Enteroendocrine Cells: Chemosensors in the Intestinal Epithelium. *Annu Rev Physiol* **78**, 277–99 (2016).
95. De Silva, A. & Bloom, S. R. Gut Hormones and Appetite Control: A Focus on PYY and GLP-1 as Therapeutic Targets in Obesity. *Gut Liver* **6**, 10–20 (2012).

96. Latorre, R., Sternini, C., De Giorgio, R. & Greenwood-Van Meerveld, B. Enteroendocrine cells: a review of their role in brain-gut communication. *Neurogastroenterology and motility* **28**, 620–30 (2016).
97. Steinert, R. E. *et al.* Ghrelin, CCK, GLP-1, and PYY(3-36): Secretory Controls and Physiological Roles in Eating and Glycemia in Health, Obesity, and After RYGB. *Physiol Rev* **97**, 411–463 (2017).
98. Kaelberer, M. M. *et al.* A gut-brain neural circuit for nutrient sensory transduction. *Science* **361**, (2018).
99. Bohórquez, D. V *et al.* Neuroepithelial circuit formed by innervation of sensory enteroendocrine cells. *J Clin Invest* **125**, 782–6 (2015).
100. Tolhurst, G. *et al.* Short-chain fatty acids stimulate glucagon-like peptide-1 secretion via the G-protein-coupled receptor FFAR2. *Diabetes* **61**, 364–71 (2012).
101. Psichas, A. *et al.* The short chain fatty acid propionate stimulates GLP-1 and PYY secretion via free fatty acid receptor 2 in rodents. *Int J Obes* **39**, 424–429 (2015).
102. Lin, H. V. *et al.* Butyrate and Propionate Protect against Diet-Induced Obesity and Regulate Gut Hormones via Free Fatty Acid Receptor 3-Independent Mechanisms. *PLoS One* **7**, e35240 (2012).
103. Mawe, G. M. & Hoffman, J. M. Serotonin signalling in the gut--functions, dysfunctions and therapeutic targets. *Nat Rev Gastroenterol Hepatol* **10**, 473–86 (2013).
104. Golubeva, A. V *et al.* Microbiota-related Changes in Bile Acid & Tryptophan Metabolism are Associated with Gastrointestinal Dysfunction in a Mouse Model of Autism. *EBioMedicine* **24**, 166–178 (2017).
105. Mawe, G. M., Coates, M. D. & Moses, P. L. Review article: intestinal serotonin signalling in irritable bowel syndrome. *Aliment Pharmacol Ther* **23**, 1067–76 (2006).
106. Shajib, M. S., Baranov, A. & Khan, W. I. Diverse Effects of Gut-Derived Serotonin in Intestinal Inflammation. *ACS Chem Neurosci* **8**, 920–931 (2017).
107. Liu K, Yang L, Wang G, Liu J, Zhao X, Wang Y, Li J, Yang. Metabolic stress drives sympathetic neuropathy within the liver. *J. Cell Metab.* **33**(3), 666-675 (2021).
108. Miller, B. M., Oderberg, I. M. & Goessling, W. Hepatic Nervous System in Development, Regeneration, and Disease. *Hepatology* **74**, 3513–3522 (2021).
109. Matsubara, Y., Kiyohara, H., Teratani, T., Mikami, Y. & Kanai, T. Organ and brain crosstalk: The liver-brain axis in gastrointestinal, liver, and pancreatic diseases. *Neuropharmacology* **205**, 108915 (2022).
110. Berthoud, H. R. & Neuhuber, W. L. Functional and chemical anatomy of the afferent vagal system. *Auton Neurosci* **85**, 1–17 (2000).
111. Magni, F. & Carobi, C. The afferent and preganglionic parasympathetic innervation of the rat liver, demonstrated by the retrograde transport of horseradish peroxidase. *J Auton Nerv Syst* **8**, 237–60 (1983).
112. Waise, T. M. Z., Dranse, H. J. & Lam, T. K. T. The metabolic role of vagal afferent innervation. *Nat Rev Gastroenterol Hepatol* **15**, 625–636 (2018).
113. Berthoud, H.-R. & Neuhuber, W. L. Vagal mechanisms as neuromodulatory targets for the treatment of metabolic disease. *Ann N Y Acad Sci* **1454**, 42–55 (2019).
114. Berthoud, H. R., Carlson, N. R. & Powley, T. L. Topography of efferent vagal innervation of the rat gastrointestinal tract. *Am J Physiol* **260**, R200-7 (1991).
115. Fukuda, Y., Imoto, M., Koyama, Y., Miyazawa, Y. & Hayakawa, T. Demonstration of Noradrenaline-Immunoreactive Nerve Fibres in the Liver. *Journal of International Medical Research* **24**, 466–472 (1996).
116. Imai, J. & Katagiri, H. Regulation of systemic metabolism by the autonomic nervous system consisting of afferent and efferent innervation. *Int Immunol* **34**, 67–79 (2022).
117. Metz, M. *et al.* Leptin increases hepatic triglyceride export via a vagal mechanism in humans. *Cell Metab* **34**, 1719-1731.e5 (2022).
118. Stoyanova, I. I. & Gulubova, M. V. Peptidergic nerve fibres in the human liver. *Acta Histochem* **100**, 245–56 (1998).
119. Akiyoshi, H., Gonda, T. & Terada, T. A comparative histochemical and immunohistochemical study of aminergic, cholinergic and peptidergic innervation in rat, hamster, guinea pig, dog and human livers. *Liver* **18**, 352–9 (1998).
120. Patterson, T. T., Nicholson, S., Wallace, D., Hawryluk, G. W. J. & Grandhi, R. Complex Feed-Forward and Feedback Mechanisms Underlie the Relationship Between Traumatic Brain Injury and the Gut-Microbiota-Brain Axis. *Shock* **52**, 318–325 (2019).
121. Coulter, A. A., Rebello, C. J. & Greenway, F. L. Centrally Acting Agents for Obesity: Past, Present, and Future. *Drugs* **78**, 1113–1132 (2018).
122. Sawchenko, P. E. Central connections of the sensory and motor nuclei of the vagus nerve. *J Auton Nerv Syst* **9**, 13–26 (1983).
123. Cheon, S. Y. & Song, J. The Association between Hepatic Encephalopathy and Diabetic Encephalopathy: The Brain-Liver Axis. *Int J Mol Sci* **22**, (2021).

124. Kerfoot, S. M. *et al.* TNF-alpha-secreting monocytes are recruited into the brain of cholestatic mice. *Hepatology* **43**, 154–62 (2006).
125. D'Mello, C., Le, T. & Swain, M. G. Cerebral microglia recruit monocytes into the brain in response to tumor necrosis factoralpha signaling during peripheral organ inflammation. *J Neurosci* **29**, 2089–102 (2009).
126. Cheon, S. Y. & Song, J. The Association between Hepatic Encephalopathy and Diabetic Encephalopathy: The Brain-Liver Axis. *Int J Mol Sci* **22**, (2021).
127. Nguyen, K., D'Mello, C., Le, T., Urbanski, S. & Swain, M. G. Regulatory T cells suppress sickness behaviour development without altering liver injury in cholestatic mice. *J Hepatol* **56**, 626–31 (2012).
128. Sleiman, S. F. *et al.* Exercise promotes the expression of brain derived neurotrophic factor (BDNF) through the action of the ketone body β-hydroxybutyrate. *Elife* **5**, (2016).
129. Ieraci, A., Mallei, A., Musazzi, L. & Popoli, M. Physical exercise and acute restraint stress differentially modulate hippocampal brain-derived neurotrophic factor transcripts and epigenetic mechanisms in mice. *Hippocampus* **25**, 1380–92 (2015).
130. Sleiman, S. F. *et al.* Exercise promotes the expression of brain derived neurotrophic factor (BDNF) through the action of the ketone body β-hydroxybutyrate. *Elife* **5**, (2016).
131. Ray, W. J. & Buggia-Prevot, V. Novel Targets for Alzheimer's Disease: A View Beyond Amyloid. *Annu Rev Med* **72**, 15–28 (2021).
132. Cheng, Y. *et al.* Physiological β-amyloid clearance by the liver and its therapeutic potential for Alzheimer's disease. *Acta Neuropathol* **145**, 717–731 (2023).
133. Mao, Z., Zhang, Y., Liang, Y., Xia, C. & Tang, L. Liver X receptor α contribution to neuroinflammation and glial cells activation induced by MPTP: Implications for Parkinson's disease. *Neuroscience* **560**, 109–119 (2024).
134. Reyes, J. F. *et al.* Accumulation of alpha-synuclein within the liver, potential role in the clearance of brain pathology associated with Parkinson's disease. *Acta Neuropathol Commun* **9**, 46 (2021).
135. Hallbeck, M., Ekmark-Lewén, S., Kahle, P. J., Ingelsson, M. & Reyes, J. F. Accumulation of alpha-synuclein pathology in the liver exhibits post-translational modifications associated with Parkinson's disease. *iScience* **27**, 111448 (2024).
136. Góralczyk-Bińkowska, A., Szmajda-Krygier, D. & Kozłowska, E. The Microbiota-Gut-Brain Axis in Psychiatric Disorders. *Int J Mol Sci* **23**, (2022).
137. Socała, K. *et al.* The role of microbiota-gut-brain axis in neuropsychiatric and neurological disorders. *Pharmacol Res* **172**, 105840 (2021).
138. Ancona, A. *et al.* The gut-brain axis in irritable bowel syndrome and inflammatory bowel disease. *Dig Liver Dis* **53**, 298–305 (2021).
139. Hummel, S. *et al.* Associations of breastfeeding with childhood autoimmunity, allergies, and overweight: The Environmental Determinants of Diabetes in the Young (TEDDY) study. *Am J Clin Nutr* **114**, 134–142 (2021).
140. Ilie, O.-D., Ciobica, A., McKenna, J., Doroftei, B. & Mavroudis, I. Minireview on the Relations between Gut Microflora and Parkinson's Disease: Further Biochemical (Oxidative Stress), Inflammatory, and Neurological Particularities. *Oxid Med Cell Longev* **2020**, 4518023 (2020).
141. Christovich, A. & Luo, X. M. Gut Microbiota, Leaky Gut, and Autoimmune Diseases. *Front Immunol* **13**, 946248 (2022).
142. Moser, G., Fournier, C. & Peter, J. Intestinal microbiome-gut-brain axis and irritable bowel syndrome. *Wien Med Wochenschr* **168**, 62–66 (2018).
143. Green, A. R. Neuropharmacology of 5-hydroxytryptamine. *Br J Pharmacol* **147 Suppl 1**, S145-52 (2006).
144. Lin, S.-H., Lee, L.-T. & Yang, Y. K. Serotonin and mental disorders: a concise review on molecular neuroimaging evidence. *Clin Psychopharmacol Neurosci* **12**, 196–202 (2014).
145. Khlevner, J., Park, Y. & Margolis, K. G. Brain-Gut Axis: Clinical Implications. *Gastroenterol Clin North Am* **47**, 727–739 (2018).
146. Gershon, M. D. 5-Hydroxytryptamine (serotonin) in the gastrointestinal tract. *Curr Opin Endocrinol Diabetes Obes* **20**, 14–21 (2013).
147. Gross, E. R. *et al.* Neuronal serotonin regulates growth of the intestinal mucosa in mice. *Gastroenterology* **143**, 408–17.e2 (2012).
148. Crowell, M. D. Role of serotonin in the pathophysiology of the irritable bowel syndrome. *Br J Pharmacol* **141**, 1285–93 (2004).
149. Lesurtel, M., Soll, C., Humar, B. & Clavien, P.-A. Serotonin: a double-edged sword for the liver? *Surgeon* **10**, 107–13 (2012).
150. Marazziti, D. Understanding the role of serotonin in psychiatric diseases. *F1000Res* **6**, 180 (2017).
151. Reigstad, C. S. *et al.* Gut microbes promote colonic serotonin production through an effect of short-chain fatty acids on enterochromaffin cells. *FASEB J* **29**, 1395–403 (2015).
152. Sampson, T. R. *et al.* Gut Microbiota Regulate Motor Deficits and Neuroinflammation in a Model of Parkinson's Disease. *Cell* **167**, 1469-1480.e12 (2016).
153. Xie, A. *et al.* Bacterial Butyrate in Parkinson's Disease Is Linked to Epigenetic Changes and Depressive Symptoms. *Mov Disord* **37**, 1644–1653 (2022).

154. Desbonnet, L. *et al.* Effects of the probiotic Bifidobacterium infantis in the maternal separation model of depression. *Neuroscience* **170**, 1179–88 (2010).
155. Sittipo, P., Choi, J., Lee, S. & Lee, Y. K. The function of gut microbiota in immune-related neurological disorders: a review. *J Neuroinflammation* **19**, 154 (2022).
156. Carloni, S. *et al.* Identification of a choroid plexus vascular barrier closing during intestinal inflammation. *Science* **374**, 439–448 (2021).
157. Carloni, S. & Rescigno, M. The gut-brain vascular axis in neuroinflammation. *Semin Immunol* **69**, 101802 (2023).
158. Sjöstedt, P., Enander, J. & Isung, J. Serotonin Reuptake Inhibitors and the Gut Microbiome: Significance of the Gut Microbiome in Relation to Mechanism of Action, Treatment Response, Side Effects, and Tachyphylaxis. *Front Psychiatry* **12**, 682868 (2021).
159. Faure, C., Patey, N., Gauthier, C., Brooks, E. M. & Mawe, G. M. Serotonin Signaling Is Altered in Irritable Bowel Syndrome With Diarrhea but Not in Functional Dyspepsia in Pediatric Age Patients. *Gastroenterology* **139**, 249–258 (2010).
160. Sikander, A., Rana, S. V. & Prasad, K. K. Role of serotonin in gastrointestinal motility and irritable bowel syndrome. *Clin Chim Acta* **403**, 47–55 (2009).
161. Li, H.-Y. *et al.* Theabrownin inhibits obesity and non-alcoholic fatty liver disease in mice via serotonin-related signaling pathways and gut-liver axis. *J Adv Res* **52**, 59–72 (2023).
162. Ko, M. *et al.* Correction: Modulation of serotonin in the gut-liver neural axis ameliorates the fatty and fibrotic changes in non-alcoholic fatty liver. *Dis Model Mech* **16**, (2023).
163. Ford, A. C. *et al.* American College of Gastroenterology monograph on the management of irritable bowel syndrome and chronic idiopathic constipation. *Am J Gastroenterol* **109 Suppl 1**, S2-26; quiz S27 (2014).
164. Murnane, K. S. Serotonin 2A receptors are a stress response system: implications for post-traumatic stress disorder. *Behavioural pharmacology* **30**, 151–162 (2019).
165. Lee, S.-H., Han, C. & Shin, C. IUPHAR review: Microbiota-gut-brain axis and its role in neuropsychiatric disorders. *Pharmacol Res* **216**, 107749 (2025).
166. Nauck, M. A. & Meier, J. J. Incretin hormones: Their role in health and disease. *Diabetes Obes Metab* **20 Suppl 1**, 5–21 (2018).
167. Zhang T, Perkins MH, Chang H, Han W, de Araujo IE. An inter-organ neural circuit for appetite suppression. *Cell* **185**(14), 2478-2494 (2022).
168. Ikezawa Y, Yamatani K, Ohnuma H, Daimon M, Manaka H , Sasaki H. Glucagon-like peptide-1 inhibits glucagon-induced glycogenolysis in perivenous hepatocytes specifically. *Regul Pept.* **111**(1-3), 207-10 (2003).
169. Ionut, V. *et al.* Hepatic portal vein denervation impairs oral glucose tolerance but not exenatide's effect on glycemia. *Am J Physiol Endocrinol Metab* **307**, E644-52 (2014).
170. Taminato, T., Seino, Y., Goto, Y., Inoue, Y. & Kadowaki, S. Synthetic gastric inhibitory polypeptide. Stimulatory effect on insulin and glucagon secretion in the rat. *Diabetes* **26**, 480–4 (1977).
171. Ebert, R., Nauck, M. & Creutzfeldt, W. Effect of exogenous or endogenous gastric inhibitory polypeptide (GIP) on plasma triglyceride responses in rats. *Horm Metab Res* **23**, 517–21 (1991).
172. Adriaenssens, A. E. *et al.* Glucose-Dependent Insulinotropic Polypeptide Receptor-Expressing Cells in the Hypothalamus Regulate Food Intake. *Cell Metab* **30**, 987-996.e6 (2019).
173. Vilsbøll, T., Krarup, T., Deacon, C. F., Madsbad, S. & Holst, J. J. Reduced postprandial concentrations of intact biologically active glucagon-like peptide 1 in type 2 diabetic patients. *Diabetes* **50**, 609–13 (2001).
174. Burton-Freeman, B., Davis, P. A. & Schneeman, B. O. Interaction of fat availability and sex on postprandial satiety and cholecystokinin after mixed-food meals. *Am J Clin Nutr* **80**, 1207–14 (2004).
175. Sayegh, A. I. The role of cholecystokinin receptors in the short-term control of food intake. *Prog Mol Biol Transl Sci* **114**, 277–316 (2013).
176. Sayegh, A. I., Washington, M. C., Raboin, S. J., Aglan, A. H. & Reeve, J. R. CCK-58 prolongs the intermeal interval, whereas CCK-8 reduces this interval: not all forms of cholecystokinin have equal bioactivity. *Peptides (N.Y.)* **55**, 120–5 (2014).
177. Rasmussen, B. A. *et al.* Duodenal activation of cAMP-dependent protein kinase induces vagal afferent firing and lowers glucose production in rats. *Gastroenterology* **142**, 834-843.e3 (2012).
178. Cani, P. D. *et al.* Metabolic endotoxemia initiates obesity and insulin resistance. *Diabetes* **56**, 1761–72 (2007).
179. Matzinger, D. The role of long chain fatty acids in regulating food intake and cholecystokinin release in humans. *Gut* **46**, 689–694 (2000).
180. Duca, F. A. & Lam, T. K. T. Gut microbiota, nutrient sensing and energy balance. *Diabetes Obes Metab* **16 Suppl 1**, 68–76 (2014).
181. Beglinger, S. *et al.* Role of fat hydrolysis in regulating glucagon-like Peptide-1 secretion. *J Clin Endocrinol Metab* **95**, 879–86 (2010).

182. Degen, L. *et al.* Effect of CCK-1 receptor blockade on ghrelin and PYY secretion in men. *Am J Physiol Regul Integr Comp Physiol* **292**, R1391-9 (2007).
183. Lu, W. J. *et al.* Chylomicron formation and secretion is required for lipid-stimulated release of incretins GLP-1 and GIP. *Lipids* **47**, 571–80 (2012).
184. Randich, A. *et al.* Responses of celiac and cervical vagal afferents to infusions of lipids in the jejunum or ileum of the rat. *Am J Physiol Regul Integr Comp Physiol* **278**, R34-43 (2000).
185. Wachsmuth, H. R., Weninger, S. N. & Duca, F. A. Role of the gut-brain axis in energy and glucose metabolism. *Exp Mol Med* **54**, 377–392 (2022).
186. Kwan, J. Y. *et al.* Iron accumulation in deep cortical layers accounts for MRI signal abnormalities in ALS: correlating 7 tesla MRI and pathology. *PLoS One* **7**, e35241 (2012).
187. Angelova, P. R. *et al.* Alpha synuclein aggregation drives ferroptosis: an interplay of iron, calcium and lipid peroxidation. *Cell Death Differ* **27**, 2781–2796 (2020).
188. Ryan, S. K. *et al.* Therapeutic inhibition of ferroptosis in neurodegenerative disease. *Trends Pharmacol Sci* **44**, 674–688 (2023).
189. Agmon, E., Solon, J., Bassereau, P. & Stockwell, B. R. Modeling the effects of lipid peroxidation during ferroptosis on membrane properties. *Sci Rep* **8**, 5155 (2018).
190. Angelova, P. R. *et al.* Alpha synuclein aggregation drives ferroptosis: an interplay of iron, calcium and lipid peroxidation. *Cell Death Differ* **27**, 2781–2796 (2020).
191. Lei, P., Bai, T. & Sun, Y. Mechanisms of Ferroptosis and Relations With Regulated Cell Death: A Review. *Front Physiol* **10**, 139 (2019).
192. Ryan, S. K. *et al.* Microglia ferroptosis is regulated by SEC24B and contributes to neurodegeneration. *Nat Neurosci* **26**, 12–26 (2023).
193. Li, J. *et al.* Ferroptosis: past, present and future. *Cell Death Dis* **11**, 88 (2020).
194. Galvagnion, C. *et al.* Chemical properties of lipids strongly affect the kinetics of the membrane-induced aggregation of α-synuclein. *Proc Natl Acad Sci U S A* **113**, 7065–70 (2016).
195. Angelova, P. R. *et al.* Alpha synuclein aggregation drives ferroptosis: an interplay of iron, calcium and lipid peroxidation. *Cell Death Differ* **27**, 2781–2796 (2020).
196. Ji, J., Wu, L., Wei, J., Wu, J. & Guo, C. The Gut Microbiome and Ferroptosis in MAFLD. *J Clin Transl Hepatol* **11**, 174–187 (2023).
197. Ye, Q. *et al.* Atractylodin alleviates nonalcoholic fatty liver disease by regulating Nrf2-mediated ferroptosis. *Heliyon* **9**, e18321 (2023).
198. Song, X. *et al.* Glucopyranose from Pleurotus geesteranus prevent alcoholic liver diseases by regulating Nrf2/HO-1-TLR4/NF-κB signalling pathways and gut microbiota. *Food Funct* **13**, 2441–2455 (2022).
199. Matsubara, Y., Kiyohara, H., Teratani, T., Mikami, Y. & Kanai, T. Organ and brain crosstalk: The liver-brain axis in gastrointestinal, liver, and pancreatic diseases. *Neuropharmacology* **205**, 108915 (2022).
200. Ren, B. *et al.* Protective effects of sesamol on systemic oxidative stress-induced cognitive impairments via regulation of Nrf2/Keap1 pathway. *Food Funct* **9**, 5912–5924 (2018).
201. Wei, X. *et al.* Astragalus polysaccharide ameliorated complex factor-induced chronic fatigue syndrome by modulating the gut microbiota and metabolites in mice. *Biomed Pharmacother* **163**, 114862 (2023).
202. Zhang, H. *et al.* Gut Microbiota Mediates the Susceptibility of Mice to Sepsis-Associated Encephalopathy by Butyric Acid. *J Inflamm Res* **15**, 2103–2119 (2022).
203. Singh, R. *et al.* Enhancement of the gut barrier integrity by a microbial metabolite through the Nrf2 pathway. *Nat Commun* **10**, 89 (2019).
204. Singh, R. *et al.* Enhancement of the gut barrier integrity by a microbial metabolite through the Nrf2 pathway. *Nat Commun* **10**, 89 (2019).
205. Cai, Y. *et al.* Vitamin D suppresses ferroptosis and protects against neonatal hypoxic-ischemic encephalopathy by activating the Nrf2/HO-1 pathway. *Transl Pediatr* **11**, 1633–1644 (2022).
206. Margolis, K. G., Cryan, J. F. & Mayer, E. A. The Microbiota-Gut-Brain Axis: From Motility to Mood. *Gastroenterology* **160**, 1486–1501 (2021).
207. Benarroch, E. What Is the Role of Ferroptosis in Neurodegeneration? *Neurology* **101**, 312–319 (2023).
208. Nuñez, M. T. & Chana-Cuevas, P. New Perspectives in Iron Chelation Therapy for the Treatment of Neurodegenerative Diseases. *Pharmaceuticals (Basel)* **11**, (2018).
209. Kahn-Kirby, A. H. *et al.* Targeting ferroptosis: A novel therapeutic strategy for the treatment of mitochondrial disease-related epilepsy. *PLoS One* **14**, e0214250 (2019).
210. Pekkurnaz, G. & Wang, X. Mitochondrial heterogeneity and homeostasis through the lens of a neuron. *Nat Metab* **4**, 802–812 (2022).
211. Yu, X. *et al.* Ferroptosis involved in sevoflurane-aggravated young rats brain injury induced by liver transplantation. *Neuroreport* **33**, 705–713 (2022).
212. Liu, P. *et al.* Ferroptosis contributes to isoflurane-induced neurotoxicity and learning and memory impairment. *Cell Death Discov* **7**, 72 (2021).
213. Tian, Y. *et al.* 17β-oestradiol inhibits ferroptosis in the hippocampus by upregulating DHODH and fur-

ther improves memory decline after ovariectomy. *Redox Biol* **62**, 102708 (2023).
214. Kouhestani, S., Jafari, A. & Babaei, P. Kaempferol attenuates cognitive deficit via regulating oxidative stress and neuroinflammation in an ovariectomized rat model of sporadic dementia. *Neural Regen Res* **13**, 1827–1832 (2018).
215. Chen, J. *et al.* Cognitive protection of sinomenine in type 2 diabetes mellitus through regulating the EGF/Nrf2/HO-1 signaling, the microbiota-gut-brain axis, and hippocampal neuron ferroptosis. *Phytother Res* **37**, 3323–3341 (2023).
216. Ding, C. *et al.* EGF released from human placental mesenchymal stem cells improves premature ovarian insufficiency via NRF2/HO-1 activation. *Aging* **12**, 2992–3009 (2020).
217. Xie, Z. *et al.* Activated AMPK mitigates diabetes-related cognitive dysfunction by inhibiting hippocampal ferroptosis. *Biochem Pharmacol* **207**, 115374 (2023).
218. Wang, J. *et al.* Irisin protects against sepsis-associated encephalopathy by suppressing ferroptosis via activation of the Nrf2/GPX4 signal axis. *Free Radic Biol Med* **187**, 171–184 (2022).
219. Fang, J. *et al.* Overexpression of GPX4 attenuates cognitive dysfunction through inhibiting hippocampus ferroptosis and neuroinflammation after traumatic brain injury. *Free Radic Biol Med* **204**, 68–81 (2023).
220. Zhang, Y., Zhang, X., Wee Yong, V. & Xue, M. Vildagliptin improves neurological function by inhibiting apoptosis and ferroptosis following intracerebral hemorrhage in mice. *Neurosci Lett* **776**, 136579 (2022).
221. Xie, B.-S. *et al.* Inhibition of ferroptosis attenuates tissue damage and improves long-term outcomes after traumatic brain injury in mice. *CNS Neurosci Ther* **25**, 465–475 (2019).
222. Liu, Y., Zhu, C., Guo, J., Chen, Y. & Meng, C. The Neuroprotective Effect of Irisin in Ischemic Stroke. *Front Aging Neurosci* **12**, 588958 (2020).
223. Young, M. F., Valaris, S. & Wrann, C. D. A role for FNDC5/Irisin in the beneficial effects of exercise on the brain and in neurodegenerative diseases. *Prog Cardiovasc Dis* **62**, 172–178 (2019).
224. Guo, P., Jin, Z., Wang, J., Sang, A. & Wu, H. Irisin Rescues Blood-Brain Barrier Permeability following Traumatic Brain Injury and Contributes to the Neuroprotection of Exercise in Traumatic Brain Injury. *Oxid Med Cell Longev* **2021**, 1118981 (2021).
225. Chu, J. *et al.* Acetaminophen impairs ferroptosis in the hippocampus of septic mice by regulating glutathione peroxidase 4 and ferroptosis suppressor protein 1 pathways. *Brain Behav* **13**, e3145 (2023).
226. Hambright, W. S., Fonseca, R. S., Chen, L., Na, R. & Ran, Q. Ablation of ferroptosis regulator glutathione peroxidase 4 in forebrain neurons promotes cognitive impairment and neurodegeneration. *Redox Biol* **12**, 8–17 (2017).
227. Wang, B. *et al.* Ferroptosis-related biomarkers for Alzheimer's disease: Identification by bioinformatic analysis in hippocampus. *Front Cell Neurosci* **16**, 1023947 (2022).
228. Yuan, H., Pratte, J. & Giardina, C. Ferroptosis and its potential as a therapeutic target. *Biochem Pharmacol* **186**, 114486 (2021).
229. Wang, J.-Y. *et al.* Meta-analysis of brain iron levels of Parkinson's disease patients determined by postmortem and MRI measurements. *Sci Rep* **6**, 36669 (2016).
230. Hayflick, S. J., Kurian, M. A. & Hogarth, P. Neurodegeneration with brain iron accumulation. *Handb Clin Neurol* **147**, 293–305 (2018).
231. Liu, A. *et al.* Decreased subregional specificity of the putamen in Parkinson's Disease revealed by dynamic connectivity-derived parcellation. *Neuroimage Clin* **20**, 1163–1175 (2018).
232. Wang, J.-Y. *et al.* Meta-analysis of brain iron levels of Parkinson's disease patients determined by postmortem and MRI measurements. *Sci Rep* **6**, 36669 (2016).
233. Chen, J. *et al.* Iron accumulates in Huntington's disease neurons: protection by deferoxamine. *PLoS One* **8**, e77023 (2013).
234. Rosas, H. D. *et al.* Alterations in brain transition metals in Huntington disease: an evolving and intricate story. *Arch Neurol* **69**, 887–93 (2012).
235. Skouta, R. *et al.* Ferrostatins inhibit oxidative lipid damage and cell death in diverse disease models. *J Am Chem Soc* **136**, 4551–6 (2014).
236. Liu, M., Zhao, J., Xue, C., Yang, J. & Ying, L. Uncovering the ferroptosis related mechanism of laduviglusib in the cell-type-specific targets of the striatum in Huntington's disease. *BMC Genomics* **25**, 633 (2024).
237. Barrett, E. *et al.* Reduced GLP-1R availability in the caudate nucleus with Alzheimer's disease. *Front Aging Neurosci* **16**, 1350239 (2024).
238. Deng, B. *et al.* MicroRNAs in Methamphetamine-Induced Neurotoxicity and Addiction. *Front Pharmacol* **13**, 875666 (2022).
239. Hu, S. *et al.* Iron chelation prevents nigrostriatal neurodegeneration in a chronic methamphetamine mice model. *Neurotoxicology* **99**, 24–33 (2023).
240. Schain, M. & Kreisl, W. C. Neuroinflammation in Neurodegenerative Disorders-a Review. *Curr Neurol Neurosci Rep* **17**, 25 (2017).

241. Millán Solano, M. V. *et al.* Effect of Systemic Inflammation in the CNS: A Silent History of Neuronal Damage. *Int J Mol Sci* **24**, (2023).
242. Guo, X., Wei, R., Yin, X. & Yang, G. Crosstalk between neuroinflammation and ferroptosis: Implications for Parkinson's disease progression. *Front Pharmacol* **16**, 1528538 (2025).
243. Hu, X. *et al.* Emerging role of STING signalling in CNS injury: inflammation, autophagy, necroptosis, ferroptosis and pyroptosis. *J Neuroinflammation* **19**, 242 (2022).
244. Cui, Y. *et al.* Microglia and macrophage exhibit attenuated inflammatory response and ferroptosis resistance after RSL3 stimulation via increasing Nrf2 expression. *J Neuroinflammation* **18**, 249 (2021).
245. Ward, R. J., Dexter, D. T. & Crichton, R. R. Iron, Neuroinflammation and Neurodegeneration. *Int J Mol Sci* **23**, (2022).
246. Ong, W.-Y. & Farooqui, A. A. Iron, neuroinflammation, and Alzheimer's disease. *J Alzheimers Dis* **8**, 183–200; discussion 209-15 (2005).
247. Zeng, T. *et al.* Nrf2 regulates iron-dependent hippocampal synapses and functional connectivity damage in depression. *J Neuroinflammation* **20**, 212 (2023).
248. Ward, R. J., Zucca, F. A., Duyn, J. H., Crichton, R. R. & Zecca, L. The role of iron in brain ageing and neurodegenerative disorders. *Lancet Neurol* **13**, 1045–60 (2014).
249. Pretorius, L., Kell, D. B. & Pretorius, E. Iron Dysregulation and Dormant Microbes as Causative Agents for Impaired Blood Rheology and Pathological Clotting in Alzheimer's Type Dementia. *Front Neurosci* **12**, 851 (2018).
250. Tizabi, Y., Bennani, S., El Kouhen, N., Getachew, B. & Aschner, M. Heavy Metal Interactions with Neuroglia and Gut Microbiota: Implications for Huntington's Disease. *Cells* **13**, (2024).
251. Kania, B., Sotelo, A., Ty, D. & Wisco, J. J. The Prevention of Inflammation and the Maintenance of Iron and Hepcidin Homeostasis in the Gut, Liver, and Brain Pathologies. *J Alzheimers Dis* **92**, 769–789 (2023).
252. Butterworth, R. F. Metal toxicity, liver disease and neurodegeneration. *Neurotox Res* **18**, 100–5 (2010).

IJAE
ITALIAN JOURNAL OF ANATOMY AND EMBRYOLOGY

Firenze University Press
www.fupress.com/ijae

Citation: Keshelava, G. (2025). Cardiac anatomy in the 'Madonna of the Carnation' attributed to Leonardo da Vinci. *Italian Journal of Anatomy and Embryology* 129(2): 55-59. doi: 10.36253/ijae-16769

Data Availability Statement: All relevant data are within the paper and its Supporting Information files.

Competing Interests: The Author(s) declare(s) no conflict of interest.

Cardiac anatomy in the 'Madonna of the Carnation' attributed to Leonardo da Vinci

Grigol Keshelava

Department of Vascular Surgery; Helsicore; Tevdore Mgvdeli st. 13; Tbilisi, Georgia
E-mail: gagakeshelava@gmail.com
ORCID: 0000-0003-3784-1869

Abstract. Around 1478-1480, the 'Madonna of the Carnation', also known as the 'Madonna with Vase', the 'Madonna with Child', or the 'Virgin with Flower', was produced. Using the program Paint X, we moved one detail (indicated by a bird-like shape drawn by Leonardo himself) ob Mary's left breast and we obtained an image of an ox heart with its aortic arch. The image of the heart obtained by us is identical to the ox's heart described by Leonardo in his anatomical drawing. Comparison reveals a striking resemblence to the heart configuration and arrangement of the branches of an aortic arch. Based on the fact that the heart is symbol of love, in this artwork Leonardo symbolically depicted a mother's love for her son and at the same time he described the anatomy of the heart.

Keywords: Leonardo da Vinci, Madonna of the Carnation, cardiac anatomy, aortic arch.

INTRODUCTION

The aim of this study is to interpret 'The Madonna of the Carnation' (Madonna with a Vase of Flowers) in anatomical aspect. This study provides insight into how Leonardo translated his innovative anatomical knowledge into art.

The 'Madonna of the Carnation' was produced around 1472-1478, (Fig. 1). The thorough study of the painting conducted by Moller eventually allowed the panel to be confidently attributed to Leonardo (Moller, 1937), an attribution that remained unchallenged during the last 30 years and was substantiated afresh by the study conducted by Brown (Brown, 1998). Although some historians believe that Verrocchio produced the original design for the 'Madonna of the Carnation' (Dunkerton, 2011).

The iconography of the Madonna handing a flower to her son is hardly original. The flower can be the symbol of the virtue of the virgin but also that of the death of Jesus. The carnation, by its shape associated with that of a nail and its blood-red color, announces the future of Christ.

The work is stored in the Alte Pinakothek Gallery in Munich, Germany.

Figure 1. The 'Madonna of the Carnation' by Leonardo da Vinci.

INTERPRETATION OF THE PAINTING

In the 'Madonna of the Carnation', our attention was drawn to the shadow drawn by Leonardo himself on Mary's left breast (Fig. 2A – bounded by a red contour). This shadow resembles an arrow indicating the direction of something. But in Leonardo's era, the arrow was not yet used as a direction indicator. The second thing this shadow resembles is a bird depicted in a drawing by Leonardo (Fig. 2B). The 'bird' indicates the detail bordered by author of a painting with a faint contour (Fig. 2 A- blue marked contour).

Using the program Paint X, we moved the detail in the direction of the blue arrow to final location and we got an image of the heart (Fig. 3 A, B). It depicts the left and right subclavian arteries, common carotid arteries, and ventricles (Fig. 3 C)**.** The image of the heart obtained by us is strikingly similar to the ox's heart described by Leonardo in his anatomical drawing (RL 19073-74v; K/P 1 66v) (Fig. 3 D). By comparing them we see a sharp resemblance to the heart configuration and arrangement of the branches of an aortic arch (Fig. 3 C, D).

It is noteworthy that after placing the detail in the correct place, the insignificant contour in the painting acquired the meaning of the second branch of the aortic arch (Fig. 3 B, C).

A similar concept is found in the 'Dreyfus Madonna' attributed to Leonardo da Vinci. Also, by moving one detail in this artwork an image of an ox's heart is obtained. The difference is that in the second painting, the detail is emphasized by the Madonna's hand. In this case too, the obtained image of the heart resembles the heart depicted in Leonardo's anatomical sketch (Keshelava, 2021). Based on the fact that the heart is symbol of love, in the both artwork Leonardo originally depicted the feeling of mother towards her son and at the same time he described the anatomy of the heart.

Peter Paul Rubens's copy of 'The Battle of Anghiari' by Leonardo da Vinci is also an example of the transfer of anatomical knowledge into art (Keshelava, 2023).

It should be noted that there is a discrepancy between the periods of creation of the painting and Leonardo's anatomical studies. It was speculated that Leonardo created this work in 1472-1478 and an important contribution to Leonardo's approach to anatomy was provided after 1510, which meant dissection of animal and human cadavers. The anatomical drawing (RL 19073-74v; K/P 1 66v) similar to image obtained by us is created in 1513. This discrepancy can be explained in only one way: the master could have made changes to the painting later. The fact that Leonardo made changes in his work is confirmed by researchers (Cotte, 2005).

LEONARDO'S INNOVATIONS IN THE CARDIOVASCULAR ANATOMY

Leonardo da Vinci's study in anatomy can be divided into three periods: an early (from c. 1487), a middle (1506-1510) and a late phase (after 1510). The drawings from early phase was not based on the dissection of bodies and meant simply upon information that could be deduced from the surface of the human corps, from the bodies of animals and from the human skeleton. During this period, animal examination, documents from ancient Greece and medieval Italy, and the occasional autopsy of a condemned criminals were the main source of anatomical knowledge in Europe (Park, 1994; Olry, 1997).

Marco Antonio Della Torre, an anatomist and a medical doctor, known mainly for his collaboration with Leonardo da Vinci, made a significant contribution to Leonardo's knowledge and approach in the anatomy (Picardi et al., 2010)

At the time of Leonardo, ideas about the anatomy and physiology of the heart were based on the views of the authorities (Cambiagi, 2019). At the same time, the heart had an almost spiritual role (Heater, 2010).

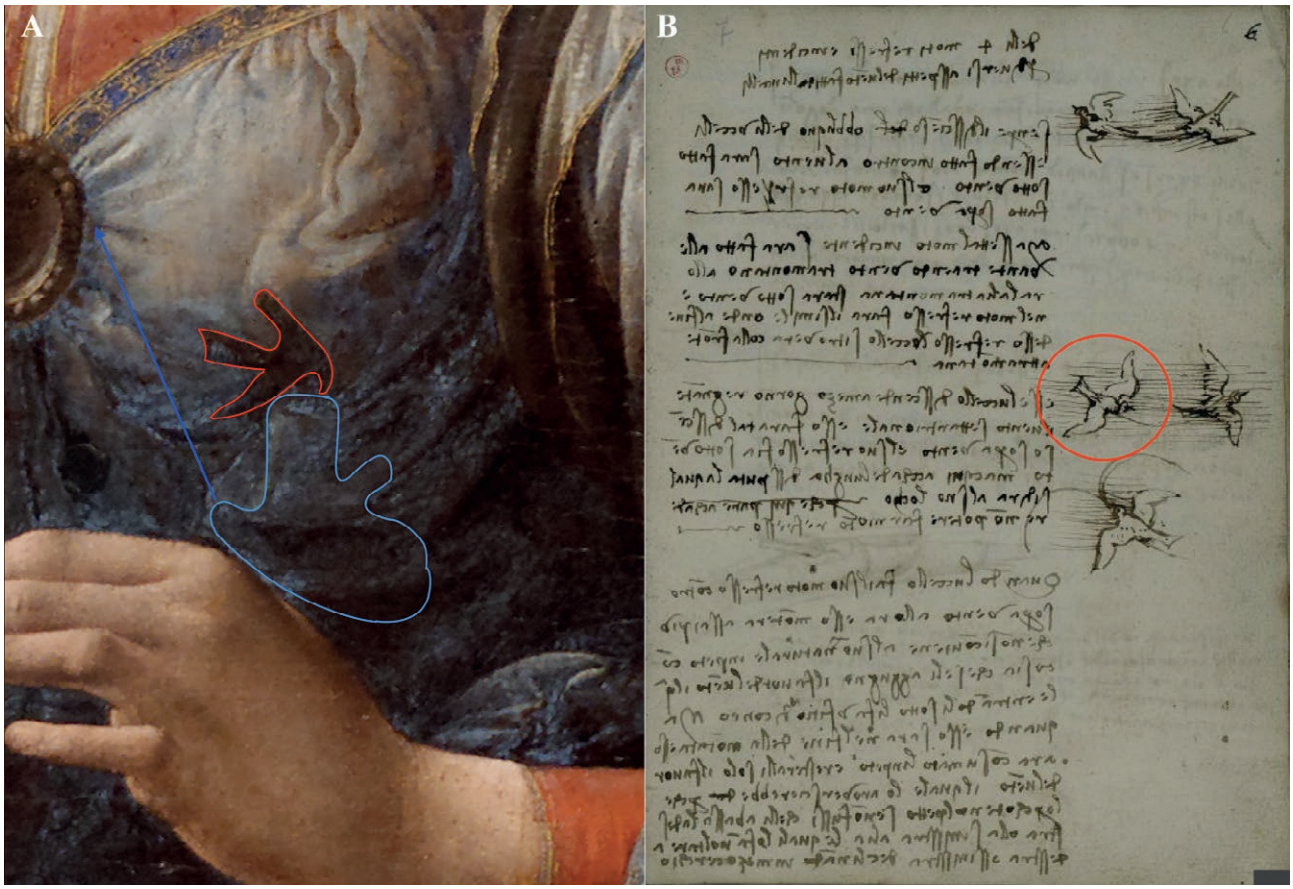

Fig. 2. A) Shadow depicted by Leonardo itself on Mary's left breast (marked in red); Blue arrow indicate the direction and location of the moving detail (marked in blue). B) Drawing of the birds by Leonardo da Vinci; the shape of the bird outlined in red resembles the shape of the shadow on Mary's left breast.

In order to examine the hemodynamic properties of blood flow through the heart and its valve, the master created multiple wax castings of the bull heart. From these casts he built glass models. Leonardo described the characteristic of the sinus of Valsalva. He also studied the dynamics of water flow in rivers, using colors to show the flow patterns. He stated: "...the water is continuously bouncing against the banks... and as time passes the course of the river gets more and more tortuous..." Leonardo da Vinci translated those findings to blood flow in vessels (Boon, 2010; Webb, 2010) and described turbulence formation in the aortic sinus (Keele, 1979).

His first achievement was to describe the heart as a muscle, constantly contracting and expanding. He also noted that this muscle is much stronger than other muscles (Keele, 1952). Leonardo believed that the contraction of the heart causes a wave to propagate along the vessels and concluded that this is the reason for the existence of a pulse in a living organism (Pasipoularides, 2014).

The master also deduced that the blood is supplied to every part of the body by the aorta. He proposed that new blood is received by the bronchial arteries from the bronchi, and that venous blood is freshened in the lungs before to returning to the heart. He came to the notion that the heart feeds itself by looking at the coronary arteries (Keele, 1973; Sterpetti, 2019). "The heart is a vessel made of thick muscle, vivified and nourished by artery and vein as are other muscles" - he made such a conclusion on the background of the dissection of the coronary arteries, which are clearly described in the anatomical sketches. Leonardo da Vinci used his understanding of hydrodynamics and anatomy to highlight the atherosclerotic alterations in arteries.[18] He was also interesting in the tortuosity and elongation of the vessels in old people.

He distinguished between the atria and ventricles based on their function and physical characteristics, and he thought that the heart was composed of four chambers (Sterpetti, 2019). Leonardo adopted Galenic

Fig. 3. A, B) The image of the ox's heart obtained after moving the details; C) 1- right subclavian artery; 2- right common carotid artery; 3- left common carotid artery; 4- left subclavian artery. D) Leonardo's anatomical drawing of an ox' heart (Royal Collection Enterprises Limited 2025 | Royal Collection Trust).

beliefs, unaware of the circulatory system's relationship, which William Harvey would not completely establish until 1628.

Da Vinci's most important findings in cardiovascular anatomy and physiology were as follow (Wells, 2007): the view of the cardiac cycle and asynchronous contraction and dilation of the atria and ventricles; he noted that the heart is a muscle; Leonardo rejected the idea that the heart receives air from the lungs; He solved the mechanism of valves function; His drawings describe the coronary arteries in detail; Leonardo's study on old bodies provided showed the atherosclerotic changes in vessels; da Vinci was the first to describe the trabecula septomarginalis or moderator band of the right ventricle (this anatomical detail is also known as Reil's band, but some scholars proposed the term "Leonardo's band" (Shoja, 2013).

Leonardo da Vinci's own studies in anatomy and physiology were mainly based on empirical observation. As mentioned above, he used simple and reasonable experiments, and based on them, he obtained important conclusions. His achievement are a good example of how logical thinking can be used to understand the physiology of life. It is regrettable that although his art was appreciated by his contemporaries, but he was not known as scientist. After his death the sketches and drawings remained hidden for a century (Dorland, 1922). His vision of the world was logical, using an empiric and unusual method of study. He wrote,"... nature is driven by the intelligence of its law".

During the Renaissance, the artists already saw the heart as a symbol of romantic love and the love of God (Figueredo, 2024). The fact that the heart was a symbol of love in that era logically explains Leonardo's idea and the meaning of hidden heart images in his paintings. The images of the heart in the "Madonna of the Carnation" depict a mother's love for her child.

AUTHORSHIP

Grigol Keshelava has made substantial contribution to all of the following: 1) the conception and design of the study, acquisition of data and interpretation of data; 2) drafting the article and revising it critically for intellectual content; 3) final approval of the version to be submitted.

REFERENCES

Boon B. (2010) Leonardo da Vinci on atherosclerosis and function of the sinuses of Valsalva. Netherlands Heart Journal. 17: 496-499.

Brown D.A. (1998) Leonardo da Vinci. Origins of a Genius. New Haven, London.

Cambiagi M., Hausse H. (2019) Leonardo da Vinci and his study of the heart. European Heart Journal. 40: 1823-1831.

Cotte P. (2005) Lumiere on the Lady with an Ermine. Vinci Edition.

Dorland W.A. (1922) The American illustrated medical dictionary. Philadelphia, Saunders.

Dunkerton J. (2011) Leonardo in Verrocchio's workshop: re-examining the technical evidence. National Gallery Technical Bulletin. 32: 1-31.

Figueredo V.M. (2024) The heart Renaissance. Reviews in Cardiovascular Medicine. 25(3): 91.

Heater W. (2010) The Medieval Heart. New Haven, London: Yale University Press.

Keele K.D. (1952) Leonardo da Vinci on movement of the heart and blood. Philadelphia: Lippincott.

Keele K.D (1973) Leonardo da Vinci's views on atherosclerosis. Medical History. 17(3): 304-308.

Keele K.D., Pedretti C. (1979) Leonardo da Vinci. Corpus of anatomical studies in the Collection of Her Majestry the Queen at Windsor Castle. Harcourt Brace Jovanovich, New York.

Keshelava G. (2021) Cardiac anatomy in the 'Dreyfus Madonna' by Leonardo da Vinci. Interact Cardiovascular and Thoracic Surgery. 32(4): 582-584.

Keshelava G. (2023) Hidden brain anatomy in Peter Paul Rubens's copy of 'The battle of Anghiari' by Leonardo da Vinci. The Neuroscientist. 29(6): 676-680.

Moller E. (1937) Leonardos Madonna mit der Nelke in der Alteren Pinakothek. Muchner Jahrbuck der Bildenden Kunst. 12: 5-40.

Olry R. (1997) Medieval neuroanatomy: the text of Mondino dei Luzzi and the plates of Guido da Vigevano. Journal of the History of the Neurosciences. 6(2): 113-123.

Park K. (1994) The criminal and the sainthly body: autopsy and dissection in Renaissance Italy. Renaissance Quarterly. 47(1): 1-33.

Pasipoularides A. (2014) Historical continuity in the methodology of modern medical science: Leonardo leads the way. International Journal of Cardiology. 171: 103-115.

Picardi E.E., Macchi V., Porzionat A., Boscolo-Berto R., Loukas M., Tubbs S., De Caro R. (2010) Marco Antonio Della Torre and Leonardo da Vinci. Clinical Anatomy. 2(6): 744-748.

Shoja M.M., Agutter P.S., Loukas M., Benninger B., Shokouhi G., Namdar H., Ghabili K., Khalili M., Tubbs R.S (2013) Leonardo da Vini's studies of the heart. International Journal of Cardiology. 167(4): 1126-1138.

Sterpetti A.V. (2019) Cardiovascular research by Leonardo da Vinci (1452-1519). Circulation Research. 124: 189-191.

Wells F. (2007) The Renaissance heart: the drawings of Leonardo da Vinci. In: Peto, J. The Heart. London/ New Haven: Yale University Press: 70-94.

IJAE
ITALIAN JOURNAL OF ANATOMY AND EMBRYOLOGY

Firenze University Press
www.fupress.com/ijae

Citation: Carretti, G., Manetti, M., & Marini, M. (2025). Metamodal proprioceptive intervention to improve sensorimotor control in visually impaired adults: a preliminary study. *Italian Journal of Anatomy and Embryology* 129(2): 61-73. doi: 10.36253/ijae-16799

Data Availability Statement: All relevant data are within the paper and its Supporting Information files.

Competing Interests: The Author(s) declare(s) no conflict of interest.

Metamodal proprioceptive intervention to improve sensorimotor control in visually impaired adults: a preliminary study

Giuditta Carretti[1,2], Mirko Manetti[1], Mirca Marini[1,*]

[1] *Section of Anatomy and Histology, Department of Experimental and Clinical Medicine, University of Florence, Florence, Italy*
[2] *A.S.D. Polisportiva Fiorentina Silvano Dani A.P.S, c/o Unione Italiana Ciechi e Ipovedenti (UICI), Florence, Italy*
*Corresponding author. E-mail: mirca.marini@unifi.it

Abstract. Visual impairment jeopardizes body kinematics and environmental interactions progressively leading to postural instability, coordinative deficits, and quality of life reduction. Although vision plays a key role in motor function, sensorimotor control mostly relies on proprioceptive inputs provided while dynamically interacting with gravity, and its efficiency is frequency dependent. Therefore, targeted proprioceptive training is necessary to counteract the disability-related deficits. The present preliminary study investigated the effects of an adapted proprioceptive intervention on sensorimotor control of blind adults aiming to improve postural stability, body awareness, coordination, and daily functionality. Twenty legally blind adults aged 18-60 voluntarily adhered to the study. Before and after taking part in the targeted 8-week proprioceptive training intervention, sensorimotor control was evaluated by Brief BESTest and a biofeedback-based device (Libra Easytech) able to adapt multimodal high-frequency stimulation to the specific needs of blind subjects. Psychological well-being and quality of life were also assessed using the 18-item Psychological Well-being and 12 item-Short Form questionnaires, respectively. Post-intervention evaluation revealed a statistically significant improvement in ankle stability/mobility and orthostatic postural control/reactivity in micro and macro instability conditions. Our findings suggest that a targeted metamodal sensorimotor protocol conceived, led, and monitored by a specialized kinesiologist may effectively improve proprioceptive control in visually impaired individuals. The present research might also offer innovative methodological hints to apply in further studies aimed at boosting sensorimotor efficiency and daily functionality in this still under investigated population.

Keywords: proprioception, postural re-education, blindness, adapted kinesiology, functionality, biofeedback.

INTRODUCTION

Physical inactivity, increasingly prevalent and identified as the fourth risk factor for global mortality, negatively impacts psychophysical well-being and functionality, causing a dangerous decline in the general health of pop-

ulation in all age groups (Stamatakis et al., 2019). Posture is an important health indicator, consequently, any alterations caused by sedentariness, aging or vulnerable health conditions are often associated with psychophysical disorders that jeopardize autonomy, self-esteem, socioemotional functioning, and quality of life (Harvey et al., 2020). Since humankind assumed upright stance, the postural tonic system is responsible for neuromuscular modulation to actively counteract atmospheric pressure and gravity allowing to maintain verticality. In a broad sense, two macro-components contribute to postural control, namely the musculoskeletal and the neuromotor system. The latter includes sensory (proprioceptive, visual, and vestibular systems), cognitive (adaptive and anticipatory) and motor (finalized motor gesture realization) processes. Concerning the somatosensory aspect, postural control is based on the coordinated and synergistic intervention of three stabilizers, namely proprioceptive, visual, and vestibular systems (Forbes, Chen & Blouin, 2018; Aspell, Lenggenhager & Blanke, 2012). Specifically, the former makes use of a peripheral network of sensors distributed in every muscle-tendon-articular district able to inform at high speed the more archaic structures of the nervous system. It is simultaneously involved in the effector response since the fine muscle tone modulation depends on some of the receptors. Given all these peculiarities, it is referred to as the primary stabilizer because the most precocious postural responses are activated by its afferents. The second one can be likened to a pointing system that allows body anchoring to fixed environment points by integrating and improving the accuracy of archeoproprioceptive postural control; precisely because it prioritizes accuracy over speed, it is termed the secondary stabilizer. Finally, the last one registers linear and angular accelerations of the head and, owing to a higher activation threshold, is the belated stabilizer; a kind of emergency system capable of overriding the previous two only if head movements exceed a certain amplitude and speed (Forbes, Chen & Blouin, 2018; Aspell, Lenggenhager & Blanke, 2012). The abovementioned hierarchical order is generally respected in physiological conditions while in conflicting situations known as sensory mismatch, or in case of deficits, each system is able to compensate for the inefficiency of the others by becoming the primary stabilizer, despite its inherent peculiarities and purposes (Block & Liu, 2023). Optimal functionality can only be ensured if all systems are used according to their potential, and if they are constantly and specifically stimulated and educated for selective integration.

Although the visual system represents the most specialized tool in processing details and environmental topographical aspects and in providing postural anchorage, an efficient and effective sensorimotor control requires the cooperation of all sensory channels in respect of the multimodal nature of reality (Aspell, Lenggenhager & Blanke, 2012). At the functional level, visual apparatus enables the evaluation and processing of information about body position in space, adjusting posture accordingly and ensuring gestures accuracy and a correct motor reaction timing. Therefore, a partial or total sight deficit generates inadequate interaction with the surrounding environment with consequent deficiencies in global and segmental coordination and postural control, ultimately altering gait and balance patterns (Alotaibi et al., 2016). In addition, visual deprivation results in negatively altered global and segmental kinematics, head-trunk-pelvis coordination, and core muscle recruitment, further challenging the safety, autonomy, and mobility of the affected individuals, both in daily and recreational and/or sports activities (West et al., 2002).

In everyday life, human beings maintain upright posture in a dynamic environment that continuously and rapidly changes, globally entailing the sensorimotor sphere in a multimodal way. Hence, in order to investigate postural control in a real setting, it is important to inquire stability in orthostatic position by applying variegated environmental conditions, especially those characterized by perturbations (Chagdes et al., 2013). Since sight crucially contributes to anticipatory and reactive postural control, orientation, and accuracy of motor execution, in case of visual disability, the dynamic interaction with the spatiotemporal dimension is strongly altered (Alghadir, Alotaibi & Iqbal, 2019; Bell et al., 2019). Despite such disability-related deficits, it is crucial to remember that the most efficient and reliable contribution to maintaining static and dynamic balance comes from the proprioceptive stabilizer and from the inputs provided by the foot sole interacting with gravity and the support surface. Under physiological conditions and in the absence of sensorimotor deficits, the nervous system places greater weight on somatosensory inputs, but in the process of learning new motor patterns, prolonged immobility, sedentariness, or disability, reliance on this privileged source may progressively fail until a total inhibition (Canu et al., 2019). Postural control and neuromuscular efficiency are structured and refined throughout life conforming to the psychophysical development degree, the acquired motor background and, above all, the utilization level. As widely demonstrated, the only effective way to stimulate and reinstruct the archeoproprioceptive system is to make it regularly experience disequilibrium and instability with the highest number of biomechanical situations to handle in time

unit, hence providing a high-frequency proprioceptive input flow (Riva et al., 2016, 2019). Therefore, the real challenge is to re-educate functional capacities phylogenetically deputed to sensorimotor control that progress or certain health conditions may relegate to a dangerous disuse hibernation. It has been shown that proprioceptive system efficacy is stimulus- and frequency-specific, and the best motor efficiency predictor is represented by orthostatic monopodalic stability (Riva et al., 2013). For this reason, re-educating the aforementioned stabilizer requires the application of technological tools purposely designed for high-frequency proprioceptive evaluation and training (Riva et al., 2019). Though still poorly applied in scientific research, technological devices to investigate and quantify postural control efficiency have been recently introduced. Specifically, such innovative tools embody sensorized proprioceptive boards provided with a biofeedback-based digital interface designed to assess and train functional stability taking into account the multimodal complex nature of reality (Bronstein, 2016; Cheung & Schmuckler, 2021; Carretti et al., 2023). From an operational perspective, biofeedback technology transduces the micro and macro postural adjustments into real-time multisensory signals consequently bringing undetectable input to a conscious level, thus optimizing sensorimotor control and motor learning timing (Francesconi & Gandini, 2015). The importance of integrating proprioceptive exercises into any type of workout program has long been recognized (Winter et al., 2022). In adults, especially those affected by sensory impairments, proprioceptive re-education assumes a fundamental role in the preservation of functionality, autonomy, and quality of life. However, despite the well-known benefits of regular physical activity in disabled individuals, no specific guidelines are still available for visually impaired, and a substantial percentage of them do not even meet the minimum levels of practice globally established for the general population (Carty et al., 2021). At the same time, increasingly strong evidence can be found in the literature regarding the close link between motor performance, function, and physical activity levels in this target population. In fact, if the vestibular and proprioceptive stabilizers are systematically stimulated through adapted and targeted motor proposals based on these vicarious senses, visually impaired subjects can become as efficient as sighted peers, not only in daily life activities but also in recreational and sport ones (Rogge et al., 2021). Consequently, regular involvement in proprioceptive training protocols can benefit first and foremost those individuals but, in a broader and longer-term perspective, also the community in which they live and which they relate with (Rogge et al., 2021).

On this basis, the purpose of this preliminary study was to investigate and deepen the effects of an adapted proprioceptive training (APT) intervention on balance and sensorimotor control of blind adults to improve their function and perceived quality of life. By applying, for the first time in blind subjects, a biofeedback-based device and a metamodal approach, both for testing and training, our study also provides methodological-didactic hints to be applied in future research concerning this growing but still under investigated target population.

MATERIALS AND METHODS

Participants

The study enrolled 20 subjects who provided their signed informed consent and voluntarily adhered to the training intervention and related assessment procedures. Specifically, the sample comprised 9 women and 11 men aged 19 to 56 years, all acknowledged as totally blind according to the Italian Law n.138/April 3, 2001. Inclusion criteria were age between 18-60 years and the legal certification of absolute blindness, while the presence of any additional concomitant physical and/or intellectual disability constituted exclusion criteria. The request for participation in the study was promoted using the official communication channels made available by some associations specialized in adapted physical/sport activity for visually impaired individuals, specifically, Italian Blind Baseball Association (AIBXC), A.S.D. Polisportiva Fiorentina Silvano Dani A.P.S. and A.S.D. Blind Fighters of Florence and A.S.D. Virtus Tennis of Bologna. The proposed sensorimotor training was carried out in the venues of these associations as a temporary replacement of the activities regularly practiced by the members but suspended due to the COVID-19 restrictions in force in Italy during the adherence to the study. On this basis, the overall study sample of 20 subjects was set up by pooling three groups: two in the Florentine metropolitan area and one in the city of Bologna. Concerning any possible physical risk, all the subjects were in possession of a mandatory valid medical certificate for motor and/or noncompetitive sport practice issued by a sports doctor. Therefore, the study participants could be considered as physically active individuals but not athletes. Figure 1 provides a schematic representation of participant recruitment and inclusion/exclusion criteria.

As commonly provided for Italian sport associations, in the act of renewing the annual membership, each member signed up an informed consent and agreed to participate in the training and testing activities promoted by the technical staff during the

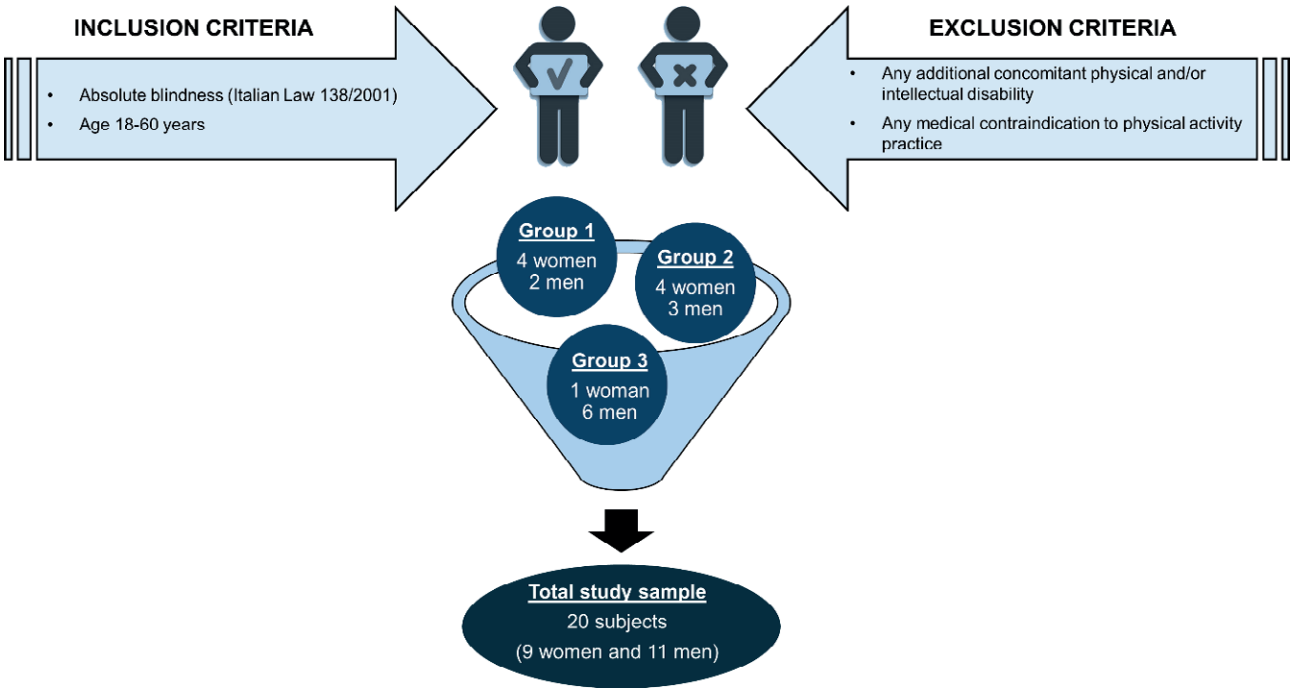

Figure 1. Schematic representation of participant recruitment and inclusion/exclusion criteria to set up the total study sample consisting of 20 legally blind adult subjects.

whole sport season. According to the Italian Legislative Decree 36/2021, our adapted training protocol was designed, proposed, supervised, and carried out, in a non-medicalized context, by a legally acknowledged and staff-integrated kinesiologist. Given the double affiliation, both in the kinesiological and research field, such a professional figure personally managed the protocol administration and data evaluation/collection strictly following the regulations provided and agreed by the management of each sport association adhering to the study. Specifically, since they are private institutions owing long-term expertise in testing and training visually impaired individuals, not comparable to academic or healthcare ones, the study design was carefully examined and approved by the internal review board of each involved sport association constituted by legal and technical experts. All study procedures were conducted following the rules of the Declaration of Helsinki of 1975 (https://www.wma.net/what-we-do/medical-ethics/declaration-of-helsinki/), revised in 2013, and reviewed and approved by the Review Board of A.S.D. Polisportiva Fiorentina Silvano Dani A.P.S, c/o Unione Italiana Ciechi e Ipovedenti, Florence, Italy (approval number 2021/09.09). As clearly reported in the informed consent form signed by all participants, in the act of adhering to the study they deliberately and consciously gave their consent not only to participate in the study procedures but also to data collection, storage, and utilization for scientific publications. In agreement with the above-mentioned form, data was treated, processed, and stored in a completely anonymous way for the purposes of this study. In particular, the obtained information was entered into an electronic datasheet identifying each participant by a unique alphanumeric ID, not mentioning or making any sensitive data accessible.

Methodologies and measurements

The present investigation was conceived as a pre-post study on 20 totally blind adults all performing the same tailored proprioceptive training. Before and after taking part in the adapted protocol, all study participants filled out a structured questionnaire purposely designed using the Google Forms platform and sent by e-mail in the form of a direct access link to the form. Given the visual impairment of the investigated sample, survey compilation was carried out using specific assistive speech synthesis technologies. The first section of the self-administered baseline questionnaire was aimed at collecting sociodemographic data regarding age, gender, educational status, occupation, and visual impairment classification. In addition, to assess the motor background of each participant, the above section also

collected information regarding current and previous motor/sport practice. The second and final section of the questionnaire comprised the 18-item Italian version of the Psychological Well-Being Scale (PWB-18) (Ruini et al., 2003) and the 12-item version of the Short Form questionnaire (SF-12) (Apolone et al., 2001) to investigate psychological well-being and perceived quality of life, respectively. Both these validated and widely applied qualitative tools have been already administered and described in our previous studies addressing visually impaired individuals (Carretti et al., 2022). Moreover, the post-protocol questionnaire also investigated the level of satisfaction concerning the proposed motor contents, the applied leading methodology, and the competence of the adapted physical activity kinesiologist.

Similarly, all the anatomo-functional and sensorimotor assessments were also performed at baseline and post-intervention. Bilateral ankle active range of motion (AROM) was measured, unloading, in the movements of flexion-extension and inversion-eversion using digital postural goniometer and placing the subject in supine and prone decubitus position (Clarkson, 2023). The Knee to wall Test, also referred to as Lunge Test, was also administered, strictly following the official guidelines available in literature (Clanton et al., 2012), to assess the tibio-tarsal joint mobility in dorsiflexion and loading conditions. The Brief BESTest, a shortened version of the original Balance Evaluation Systems Test (BESTest), which involves 8 items assessing postural control in orthostatic position and during walking, was administered to the whole sample. An evaluative scale ranging from 0 to 3 points is applied to each item so the total score ranges between 0 and 24 points, with higher values corresponding to a better static and dynamic postural control (Padgett, Jacobs & Kasser, 2012). Finally, the efficiency of proprioceptive stabilizer in dynamic postural control was tested by making use of the Libra sensorized proprioceptive board (Easytech s.r.l., Borgo San Lorenzo, Florence, Italy), an innovative device capable of providing accurate and reliable quantitative data (Tchórzewski, Jaworski & Bujas, 2010). Specifically, it consists of a sensorized tilting board equipped with interchangeable rolling wedges that allow variable oscillation degrees. Such a tool has been validated for balance assessment, calculation of global stability index in relation to visual anchorage, and ankle sprain risk index. Libra can be connected, via USB, to any computer and the software interface, equipped with biofeedback, allows to set different path patterns which can be displayed on the computer screen as a roadway laterally bounded by two parallel lines. During the board swing, whenever these limits are approached or exceeded, a special graphical and acoustic feedback is played to signal the departure from the equilibrium position (Tchórzewski, Jaworski & Bujas, 2010). The digital interface also offers two validated preset tests, specifically, Spielman-De Gunsch (SDG) Test and Cauquil-De Gunsch (CDG) Test. In both tasks, the subject is asked to stand up in orthostatic position on Libra while trying to control oscillations by keeping it as parallel to the floor as possible, as generally required during balance exercises on traditional proprioceptive board (https://www.easytechitalia.com/prodotti/libra/). The SDG Test allows the assessment of global postural stability and the subsequent fall risk in orthostatic bipodalic support, in relation to three different conditions of visual anchorage: visual feedback with no head coordination constraints, gaze on frontal fixed point, and closed eyes (Adamo, Pociask & Goldberg, 2013). At the end of the entire execution, the software calculates and records in the database the performance index obtained in the different visual conditions applied. According to the reference cut-offs, the stability index ranges from 0 to 100 with lower values corresponding to more efficient postural control. Taking into account the visual impairment of the investigated sample and the associated head-trunk separation deficits, head coordinative constraints only were applied in performing the SDG Test (West et al., 2002; Adamo, Pociask & Goldberg, 2013). The CDG Test allows to assess ankle stability and the related sprain risk during dynamic balance. Specifically, the subject is evaluated in bipodalic and monopodalic stance and at the end of the overall test, the recovery ratio, expressed as a percentage, can be considered a significant predictor of tibio-tarsal stability (Tchórzewski, Jaworski & Bujas, 2010; Riva et al., 2016) with lower values corresponding to a lower risk of ankle sprain. Despite the absolute blindness condition of the study participants, the test performance was possible thanks to the auditory feedback provided by the Libra digital interface.

Adapted proprioceptive training

The targeted 8-week intervention was organized at each of the three locations of the sport associations (i.e. two in the Florentine metropolitan area and one in the city of Bologna) adhering to the study thus avoiding their members any disability-related logistical and mobility difficulties or barriers. Advisably, adapted training interventions for visually impaired individuals must be led in small groups to grant collective/individual support, assistance, and safety. Specifically, it was administered in two 60-min sessions per week per-

formed on non-consecutive days. The main objectives of the APT were set in the sensorimotor re-education, and the postural control, global/segmental coordination and balance improvement, thus positively impacting daily functionality, fall prevention, and quality of life in this particularly vulnerable target population. The whole training protocol was conceived in three progressive macro-phases according to the re-educational focuses and the specific goals set, always avoiding inducing psycho-physical and cognitive overload. Regarding the applied equipment, the main unstable surfaces used were Freeman boards, foampads, skimmies, proprioceptive cushions and wedges, foam rollers, Gibbon Slackrack (https://www.gibbon-slacklines.com/pages/slackline-therapie-landing-page), and Libra Easytech sensorized board. The workout load was progressively increased by varying the instability degree, the exercise performing position, adding coordinative constraints and dual-task assignments, as well as using small fitness tools. To respect the pandemic context in which the intervention was conducted and to grant the best safety and management of participants during the protocol, the circuit training methodology was applied to all training sessions. In general, each of them included an initial phase of respiratory education, total-body activation and consciousness, a middle phase characterized by exercises with proprioceptive focus, and a final phase of cooldown, stretching and conscious listening/internalizing of post-workout sensorimotor sensations. To promote and maximize the perception of proprioceptive inputs arising from the plantar sole interacting with gravity and perturbations, the workout sessions were performed barefoot. In detail, the central phase of the session involved the execution of two distinct circuits, one consisting of monopodalic exercises, therefore repeated twice, changing sides at each turn, and the other comprising exercises with predominantly bipodalic or alternating execution, therefore performed once. The working time on each station was 2 min, with no recovery in the transition between consecutive stations and, in each circuit, one station always involved the Libra board. Given the large number and variety of proprioceptive exercises proposed, the main methodological/motor contents of each protocol phase are represented in synthetic graphic form in Figure 2.

To ease and promote motor contents reproducibility, an exemplifying circuit training schedule is detailed and provided as Supporting Information files, with figures specifically showing the digital interface and exercise settings of the sensorized Libra board.

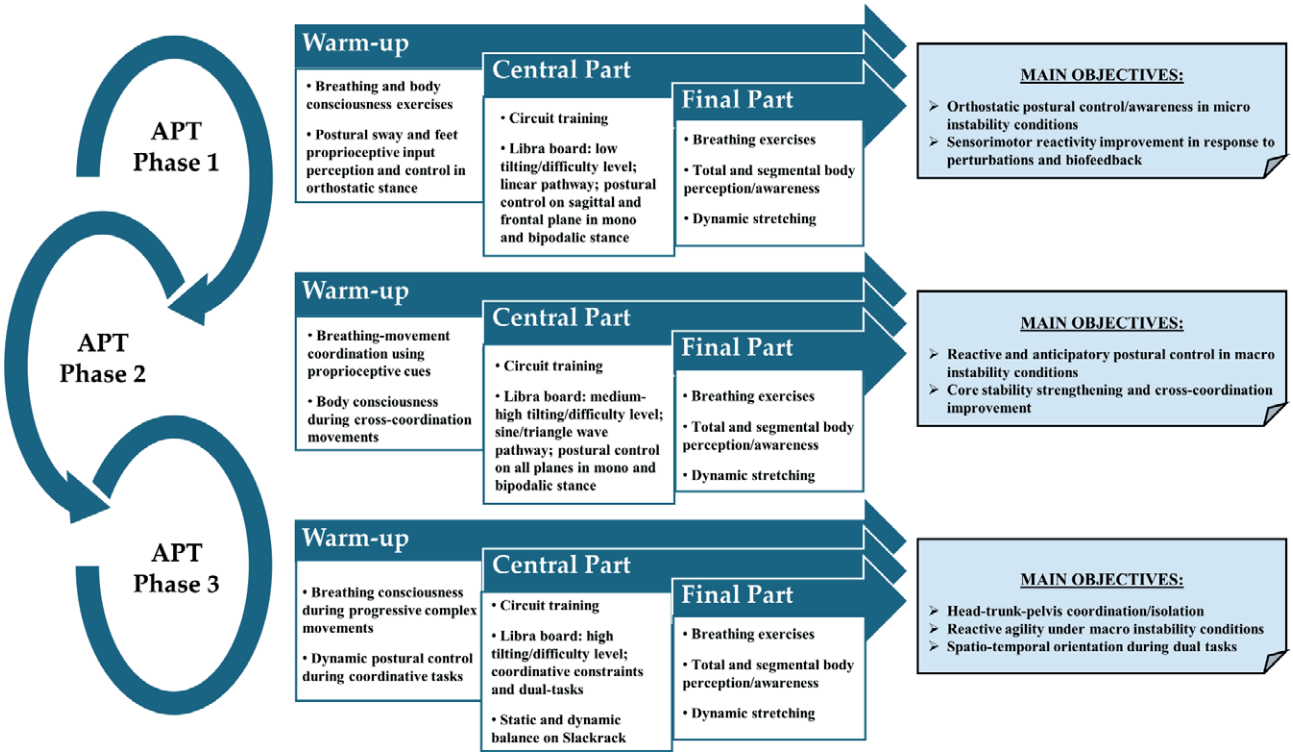

Figure 2. Adapted proprioceptive training (APT) organization.

Statistical analysis

Statistical analysis was performed using SPSS 28.0.1 (Statistical Package for the Social Sciences, Chicago, IL, USA). Data were expressed as mean ± standard error of the mean (SEM), mean ± standard deviation (SD), or number and percentage of subjects participating in the study. Student's *t*-test for paired data was used to compare the baseline vs. post-APT outcomes after verifying the normality of data with a Shapiro–Wilk test. Values of $p < 0.05$ were considered statistically significant.

RESULTS

A sample of 20 totally blind subjects [11 (55.0%) male; mean ± SD age, 45.5 ± 10.64 years] voluntarily took part in this study. The collected data regarding sociodemographic characteristics and visual disability features of the study participants are detailed in Table 1.

Regarding past and current motor/sport activity practice, almost all participants reported consistent adherence over time (Table 1).

Results concerning the investigated anatomo-functional parameters and sensorimotor control assessment at baseline and after ending the structured APT are reported in Table 2.

Table 1. Sociodemographic data of study participants.

Variables	Blind subjects (n = 20)
Age (years), mean ± SD (range)	45.5 ± 10.64 (19–56)
Sex, *n* (%)	
Male	11(55.0)
Female	9 (45.0)
Blindness, *n* (%)	
Congenital	10 (50.0)
Acquired	10 (50.0)
Educational level, *n* (%)	
Middle school degree	2 (10.0)
High school degree	8 (40.0)
University	9 (45.0)
None	1 (5.0)
Employment status, *n* (%)	
Employee	13 (65.0)
Freelance	2 (10.0)
Health profession	2 (10.0)
Retiree	2 (10.0)
Current physical/sport activity, *n* (%)	
Yes	20 (100)
No	0 (0)
Previous physical/sport activity, *n* (%)	
Yes	19 (95.0)
No	1 (5.0)

In detail, ankle AROM values showed a statistically significant post-protocol increase in dorsal/plantar flexion movements, as well as a decrease in bilateral inversion (Table 2). Likewise, the bilateral eversion AROM values, though not statistically significant, revealed a trend toward a decrease post-APT (Table 2). Moreover, bilateral tibio-tarsal joint mobility in loading, measured by the Knee to wall Test, was significantly improved following the APT (Table 2). With respect to the sensorimotor component, a statistically significant increase in the Brief BESTest total score was found after the APT respect to baseline (Table 2). Table 2 also shows the results obtained in the CDG and SDG Test performed on Libra Easytech proprioceptive board. All the parameters (i.e. bipodalic and monopodalic stance), assessed by Libra CDG Test and strongly correlated with ankle stability index, displayed a statistically significant improvement (Table 2). Besides, outcomes regarding postural control, evaluated by Libra SDG Test, also showed a statistically significant improvement in all the prevised stability constraints post-APT compared to baseline (Table 2).

Figure 3 displays the key significant results related to sensorimotor control.

The PWB-18 scale and SF-12 questionnaire score comparison at baseline and post-APT highlighted no statistically significant difference as shown in Table 3.

Of note, a trend toward a mild improvement in PWB-18 environmental mastery subscale and mental component of SF-12 questionnaire was observed (Table 3).

As far as the assessment of training experience satisfaction is concerned, post-APT data showed that 100% of the enrolled sample was satisfied with the protocol practice and the competence of the adapted physical activity kinesiologist. Although 65% of participants considered the APT as strenuous, 100% of them reported that they would willingly continue performing on a regular basis the proposed adapted training. The same percentage of subjects also reported that the practice of this specific protocol provided psychophysical benefits in their daily life. Finally, the experience fully satisfied the expectations of the whole sample.

DISCUSSION

As far as available in literature, the present study was the first to investigate the use of a biofeedback-based sensorized proprioceptive board, specifically Libra Easytech, for high-frequency proprioceptive training in blind adults. Specifically, it was intentionally used both as testing and

Table 2. Mean scores of anatomo-functional and sensorimotor control assessments at baseline and post-adapted proprioceptive training.

Variables	Baseline Mean ± SD (SEM)	Post-APT Mean ± SD (SEM)	p^*
Ankle AROM, degrees			
Right dorsal flexion	14.30 ± 2.65 (0.59)	17.20 ± 1.70 (0.38)	< 0.001
Leftt dorsal flexion	14.20 ± 2.94 (0.65)	17.55 ± 1.87 (0.41)	< 0.001
Right plantar flexion	43.45 ± 5.85 (1.33)	47.85 ± 3.78 (0.84)	< 0.001
Left plantar flexion	43.15 ± 6.53 (1.46)	48.55 ± 3.77 (0.84)	< 0.001
Right inversion	20.65 ± 5.66 (1.26)	18.00 ± 2.55 (0.57)	0.005
Left inversion	19.90 ± 6.47 (1.44)	17.65 ± 2.34 (0.52)	0.046
Right eversion	10.25 ± 1.97 (0.44)	10.00 ± 1.21 (0.27)	NS
Left eversion	10.10 ± 2.26 (0.50)	9.85 ± 1.08 (0.24)	NS
Knee to wall Test, cm			
Right	10.65 ± 2.32 (0.51)	12.65 ± 1.66 (0.37)	< 0.001
Left	9.95 ± 2.16 (0.48)	12.35 ± 1.56 (0.35)	< 0.001
Brief BESTest, score			
Total score	16.10 ± 2.75 (0.61)	20.75 ± 1.83 (0.40)	< 0.001
Libra			
CDG, recovery ratio			
Bipodalic stance	106.60 ± 18.62 (3.22)	89.75 ± 14.84 (3.18)	< 0.001
Right monopodalic stance	79.31 ± 9.63 (2.97)	71.38 ± 10.10 (2.55)	0.002
Left monopodalic stance	84.06 ± 4.90 (1.93)	76.48 ± 4.51 (1,91)	0.004
SDG, performance index			
No constraint	13.20 ± 0.96 (0.21)	11.93 ± 0.90 (0.20)	< 0.001
Straight head	13.64 ± 1.08 (0.24)	12.36 ± 0.80 (0.17)	< 0.001
Closed eyes	14.97 ± 0.54 (0.12)	14.03 ± 0.52 (0.11)	< 0.001

APT, adapted proprioceptive training; SD, standard deviation; SEM, standard error of the mean; AROM, active range of motion; CDG, Cauquil De Gunsch; SDG, Spielman-De Gunsch; NS, not significant. * Paired Student's *t*-test.

training tool since it has been demonstrated that a high-frequency input flow is needed to re-educate and reliably evaluate sensorimotor control in a real frame perspective (Riva et al., 2013, 2016). Of note, Libra settings applied during the training sessions did not recall the ones provided by SDG and CDG test, therefore such dual-purpose use simply reinforced methodological consistency without risking any task-specific adaptation. By designing a circuit training workout that integrates both traditional tools and such an innovative device and using auditory feedback provided by the digital interface, we obtained encouraging results to apply in future studies addressing this poorly investigated target population. Given the key role of the tibio-tarsal joint in orthostatic postural control, the proposed motor protocol evaluated this district in both unloading and loading, as well as on stable and unstable surfaces. This multimodal approach allowed us to detect district deficits/potentialities, both structural and functional, in several settings recalling the multimodal complex nature of reality. The statistically significant bilateral improvement of AROM in unloading dorsal/plantar flexion and in loading dorsal flexion, detectable by comparing baseline and post-APT evaluation, endorsed the benefits of high-frequency proprioceptive training on structure and function of this district (Riva et al., 2016). Contemporarily, the post-intervention bilateral AROM decrease in ankle inversion/eversion indicated an increased joint stability thus reducing ankle sprain risk. This positive correlation has also been confirmed by the outcomes obtained through the validated Libra CDG Test. The use of Libra proved to be effective in improving tibio-tarsal stability, both in mono and bipodalic perturbed supports, a condition frequently experienced in everyday life strongly correlated with traumatic distortion events (Riva et al., 2016; Ha, Han & Sung, 2018). The administration of exercises predominantly performed in orthostatic position on unstable surfaces, widely varied in material, shape, and progressive degree of instability, allowed to train foot proprioceptive sensitivity and responsiveness to perturbations in a wide range of environmental contexts always in interaction with gravity (Riva et al., 2019). Specifically referring to the target group investigated, the

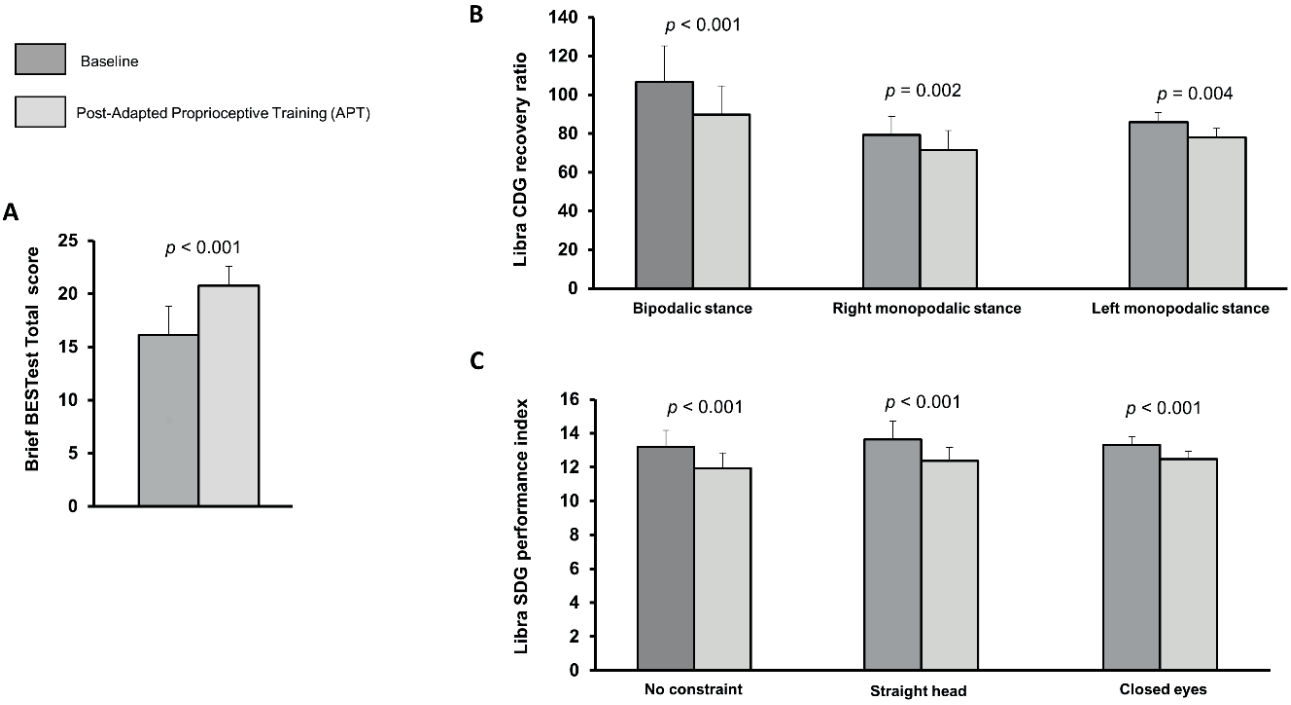

Figure 3. Baseline and post-APT data comparison of Brief BESTest total score (A), Libra CDG recovery ratio in bipodalic and monopodalic orthostatic positions (B), and SDG performance index in relation to three different conditions of visual anchorage (i.e. no constraint, straight head, and closed eyes) (C). Data are mean ± standard deviation. Values of *p* calculated by Student's *t*-test for paired data. APT, adapted proprioceptive training; CDG, Cauquil De Gunsch; SDG, Spielman-De Gunsch.

Table 3. Mean scores of psychological well-being scale and quality of life questionnaire in visually impaired subjects al baseline and post-adapted proprioceptive training.

Variables	Baseline Mean ± SD (SEM)	Post-APT Mean ± SD (SEM)	*p**
Psychological well-being (PWB-18)			
Self-acceptance	11.40 ± 1.66 (0.37)	11.60 ± 1.46 (0.32)	NS
Autonomy	12.00 ± 1.91 (0.42)	11,65 ± 2.23 (0.49)	NS
Environmental mastery	10.70 ± 2.10 (0.47)	11.50 ± 1.96 (0.43)	NS
Personal growth	12.30 ± 2.17 (0.48)	12.65 ± 1.87 (0.41)	NS
Purpose in life	9.15 ± 1.69 (0.37)	8.85 ± 2.64 (0.59)	NS
Positive relations with others	8.65 ± 2.43 (0.54)	8.35 ± 1.66 (0.37)	NS
Total score	64.20 ± 5.74 (1.28)	64.60 ± 4.27 (0.95)	NS
Quality of life (SF-12)			
Physical component	51.26 ± 7.65 (1.71)	52.76 ± 5.24 (1.17)	NS
Mental component	49.47 ± 9.42 (2.10)	52.77 ± 6.81 (1.52)	NS

APT, adapted proprioceptive training; PWB-18, 18-item Psychological Well-Being; SF-12, 12-item Short Form; SD, standard deviation; SEM, standard error of the mean; NS, not significant. * Paired Student's *t*-test.

risk of lower limb injuries is much higher than in sighted peers, both during motor/sports practice and in daily life activities (Alghadir, Alotaibi & Iqbal, 2019; Magno e Silva et al., 2013). Therefore, the results obtained at the end of the APT have not only a training but also a preventive value. Such a result can be traced back to the inclusion in the APT of progressive exercises on Libra board and Slackrack which were specifically designed to stimulate the anatomo-functional components of sensorimotor control under unstable conditions (Dordevic et al., 2020;

Donath et al., 2016). Of note, slacklining, although still poorly applied in research settings, has also been shown to be effective in increasing vestibular-dependent spatial orientation skills (Dordevic et al., 2017). The present intervention has been the first to use Slackrack in blind adults, a target population particularly relying on vestibular channel for dynamic postural control (Tomomitsu et al., 2013). Introducing this tool in the final phase of the APT, according to a didactic progression culminated in the performance of dual-task assignments while moving on the line, generated an improvement in vestibular-related orientation skills. This finding was also corroborated by post-training improvements shown in the SDG Test in all the prevised constraints. These statistically significant results also suggest a reduction in disability-related deficits affecting head-trunk coordination/isolation and auditory-dependent orientation. Such improvements can be attributed to the progressive administration of specific exercises, on traditional unstable surfaces, on Libra, and on Slackrack, purposely involving cross coordinative patterns which are crucial but not naturally acquired during sensorimotor development in visually impaired subjects (Rogge et al., 2021; Haibach, Wagner & Lieberman, 2014). Considering the metamodal and mutable nature of reality, the adapted protocol was peculiarly designed to stimulate postural control in both its anticipatory and reactive functions, in static and dynamic, in stable and unstable conditions, with and without global or segmental coordinative constraints. The benefits achievable through such a methodological-didactic approach are also evidenced by the statistically significant results obtained in the Brief BESTest, recording a post-intervention average score close to the maximum predicted by the validated cut-off. Given the specific sensory disability investigated, it is noteworthy the statistically significant bilateral improvement in the items related to monopodalic stability and postural responsiveness to external perturbations (Riva et al., 2013; Padgett, Jacobs & Kasser, 2012). Since re-educating proprioceptive sensorimotor control initially involves prevalent cortical management of high-frequency inputs, considerable attentional skills were required to participants. This might have triggered central fatigue processes able to explain why 65% of subjects referred to the APT as physically strenuous. Nevertheless, the entire sample stated that they would willingly continue to regularly perform this kind of adapted training and that they perceived psychophysical benefits in everyday life as a direct result of participating in this study. Although slight trends toward an improvement have been detected in some of the qualitative parameters investigated, they were not supported by statistically significant results in the post-intervention scores obtained in the SF-12 questionnaire and the PWB-18 scale. Interestingly, the increased outcome in the PWB-18 subscale was related to environmental mastery, thus proving that targeted sensorimotor training recalling dynamic reality conditions can positively affect the interaction with the surrounding environment. Regarding the lack of post-APT improvement in the psychological parameters assessed through qualitative instruments, it should be mentioned that the entire intervention took place in a pandemic context characterized by heavy restrictions on motor activity and social interactions. Indeed, the recent scientific literature has widely demonstrated that such anti-contagion measures have heavily impacted the psychological well-being and quality of life of the general population and, to a greater extent, of the most vulnerable social groups such as visually impaired individuals (Bubbico et al., 2021). On this evidence, the trend toward an improvement registered in the SF-12 questionnaire mental index, following participation in the protocol, is worthy of mention.

The main limitations of the present research mostly concern the shortness of the proposed APT protocol, peculiarly due to the pandemic frame in which it was conducted, the lack of a control group, and the small sample size investigated. Nevertheless, we should consider that it is recommendable to lead tailored training interventions addressing visually impaired people in small classes in order to properly manage the disability-related needs while granting individual and collective safety (Carretti et al., 2024). Indeed, if examined in a target-specific perspective, this potential limitation simply reflects the demographic peculiarities and the complex safety needs of blind individuals thus remarking the necessity of real-frame research. In line with such research perspective, a control group was not provided since it has been widely demonstrated that motor efficiency is strongly linked to regular physical activity practice in visually impaired individuals, even more than in sighted peers (Alghadir, Alotaibi & Iqbal, 2019; Rogge et al., 2021). In fact, it is well-known that visual disability deeply affects sensorimotor control, especially if combined with a sedentary lifestyle (Carty et al., 2021; Carretti, Manetti & Marini, 2023). Therefore, studies comparing physically active and sedentary individuals within this target population have been progressively relegated only to clinical contexts or elderly individuals. Given that the present study is the first applying the high-frequency biofeedback-based technology to test and train sensorimotor control in blind adults, and there are almost no validated guidelines or experimental research specifically focusing on this topic, our encouraging short-term results may represent a promising methodological and research approach to effectively investigate

and improve such skills in this target population. For such a reason, from a methodological perspective, it can be considered a preliminary research approach that needs to be deepened, hence making available further kinesiological hints and tailored protocols to be compared in future studies. In fact, our findings, though encouraging, highlight the necessity of further research involving larger samples and longer adapted training protocols, also monitoring over time the obtained benefits to detect and evaluate detraining timing. In addition, given the crucial role of movement in the overall harmonious development of the individual, which is deeply jeopardized by a sight lack, large-scale sensorimotor interventions addressing visually impaired children and adolescents should be planned globally (Rogge et al., 2021; Greguol, Gobbi & Carraro, 2015). This kind of initiative could provide them concrete opportunities of being regularly involved in ludic and sport activities designed, managed, leaded, and monitored by highly specialized kinesiologists, thus promptly preventing and counteracting disability-related deficits (Houwen, Hartman & Visscher, 2009; Columna et al., 2019).

CONCLUSIONS

In conclusion, given the multimodal complex nature of sensorimotor control, targeted high frequency proprioceptive interventions are needed to effectively counteract eventual disuse- or disability-related deficits and re-educate/improve the primary postural stabilizer recruitment. A biofeedback-based proprioceptive device such as Libra Easytech may allow to provide multimodal stimuli tailored to the peculiar needs of blind subjects, thus safely and effectively promoting sensorimotor efficiency. The present study is the first to investigate sensorimotor control in blind adults using both validated and innovative evaluation and training tools to improve daily life functionality and motor efficiency, hence offering pioneering methodological hints to be applied in future research in this field. Finally, our tailored proprioceptive training conceived, led, and monitored by an adapted physical activity kinesiologist highlights the crucial role of such a professional figure in the global management of this vulnerable and still under investigated target population.

ACKNOWLEDGMENTS

The authors are most grateful to all the visually impaired participants who took part in the study. The authors also wish to thank the sport associations which contributed to the logistical and communication aspects of this research.

AUTHOR CONTRIBUTIONS

GC: Conceptualization, Methodology, Formal analysis, Data curation, Investigation, Visualization, Writing – original draft, Writing – review & editing. MM (Mirko Manetti): Writing – original draft, Writing – review & editing. MM (Mirca Marini): Conceptualization, Methodology, Formal analysis, Data curation, Investigation, Supervision, Visualization, Writing – original draft, Writing – review & editing.

REFERENCES

Adamo, D.E., Pociask, F.D. & Goldberg, A. (2013) The contribution of head position, standing surface and vision to postural control in young adults. *Journal of Vestibular Research: Equilibrium & Orientation*. 23 (1), 33–40. https://doi.org/10.3233/VES-130473.

Alghadir, A.H., Alotaibi, A.Z. & Iqbal, Z.A. (2019) Postural stability in people with visual impairment. *Brain and Behavior*. 9 (11), e01436. https://doi.org/10.1002/brb3.1436.

Alotaibi, A.Z., Alghadir, A., Iqbal, Z.A. & Anwer, S. (2016) Effect of absence of vision on posture. *Journal of Physical Therapy Science*. 28 (4), 1374–1377. https://doi.org/10.1589/jpts.28.1374.

Apolone, G., Mosconi, P., Quattrociocchi, L., Gianicolo, E., Groth, N. & Ware, J. (2001) *Questionario sullo stato di salute SF-12. Versione italiana.*

Aspell, J.E., Lenggenhager, B. & Blanke, O. (2012) Multisensory Perception and Bodily Self-Consciousness: From Out-of-Body to Inside-Body Experience. In: M.M. Murray & M.T. Wallace (eds). *The Neural Bases of Multisensory Processes*. Frontiers in Neuroscience. Boca Raton (FL), CRC Press/Taylor & Francis. p. http://www.ncbi.nlm.nih.gov/books/NBK92870/.

Bell, L., Wagels, L., Neuschaefer-Rube, C., Fels, J., Gur, R.E. & Konrad, K. (2019) The Cross-Modal Effects of Sensory Deprivation on Spatial and Temporal Processes in Vision and Audition: A Systematic Review on Behavioral and Neuroimaging Research since 2000. *Neural Plasticity*. 2019, 9603469. https://doi.org/10.1155/2019/9603469.

Block, H.J. & Liu, Y. (2023) Visuo-proprioceptive recalibration and the sensorimotor map. *Journal of Neurophysiology*. 129 (5), 1249–1258. https://doi.org/10.1152/jn.00493.2022.

Bronstein, A.M. (2016) Chapter 4 - Multisensory integration in balance control. In: J.M. Furman & T. Lempert (eds). *Handbook of Clinical Neurology*. Neuro-Otology. Elsevier. pp. 57–66. https://doi.org/10.1016/B978-0-444-63437-5.00004-2.

Bubbico, L., Bellizzi, S., Ferlito, S., Maniaci, A., Leone Guglielmotti, R., Antonelli, G., Mastrangelo, G. & Cegolon, L. (2021) The Impact of COVID-19 on Individuals with Hearing and Visual Disabilities during the First Pandemic Wave in Italy. *International Journal of Environmental Research and Public Health*. 18 (19), 10208. https://doi.org/10.3390/ijerph181910208.

Canu, M.-H., Fourneau, J., Coq, J.-O., Dannhoffer, L., Cieniewski-Bernard, C., Stevens, L., Bastide, B. & Dupont, E. (2019) Interplay between hypoactivity, muscle properties and motor command: How to escape the vicious deconditioning circle? *Annals of Physical and Rehabilitation Medicine*. 62 (2), 122–127. https://doi.org/10.1016/j.rehab.2018.09.009.

Carretti, G., Bianco, R., Sgambati, E., Manetti, M. & Marini, M. (2023) Reactive Agility and Pitching Performance Improvement in Visually Impaired Competitive Italian Baseball Players: An Innovative Training and Evaluation Proposal. *International Journal of Environmental Research and Public Health*. 20 (12), 6166. https://doi.org/10.3390/ijerph20126166.

Carretti, G., Manetti, M. & Marini, M. (2023) Physical activity and sport practice to improve balance control of visually impaired individuals: a narrative review with future perspectives. *Frontiers in Sports and Active Living*. 5, 1260942. https://doi.org/10.3389/fspor.2023.1260942.

Carretti, G., Mirandola, D., Sgambati, E., Manetti, M. & Marini, M. (2022) Survey on Psychological Well-Being and Quality of Life in Visually Impaired Individuals: Dancesport vs. Other Sound Input-Based Sports. *International Journal of Environmental Research and Public Health*. 19 (8), 4438. https://doi.org/10.3390/ijerph19084438.

Carretti, G., Spano, F., Sgambati, E., Manetti, M. & Marini, M. (2024) Adapted Training to Boost Upper Body Sensorimotor Control and Daily Living Functionality in Visually Impaired Baseball Players. *Medicina (Kaunas, Lithuania)*. 60 (7), 1136. https://doi.org/10.3390/medicina60071136.

Carty, C., Ploeg, H.P. van der, Biddle, S.J.H., Bull, F., Willumsen, J., Lee, L., Kamenov, K. & Milton, K. (2021) The First Global Physical Activity and Sedentary Behavior Guidelines for People Living With Disability. *Journal of Physical Activity and Health*. 18 (1), 86–93. https://doi.org/10.1123/jpah.2020-0629.

Chagdes, J.R., Rietdyk, S., Jeffrey, M.H., Howard, N.Z. & Raman, A. (2013) Dynamic stability of a human standing on a balance board. *Journal of Biomechanics*. 46 (15), 2593–2602. https://doi.org/10.1016/j.jbiomech.2013.08.012.

Cheung, T.C.K. & Schmuckler, M.A. (2021) Multisensory postural control in adults: Variation in visual, haptic, and proprioceptive inputs. *Human Movement Science*. 79, 102845. https://doi.org/10.1016/j.humov.2021.102845.

Clanton, T.O., Matheny, L.M., Jarvis, H.C. & Jeronimus, A.B. (2012) Return to Play in Athletes Following Ankle Injuries. *Sports Health*. 4 (6), 471–474. https://doi.org/10.1177/1941738112463347.

Clarkson, H.M. (2023) *Valutazione cinesiologica. Articolarità, test muscolari e valutazione funzionale*. Piccin-Nuova Libraria.

Columna, L., Dillon, S.R., Dolphin, M., Streete, D.A., Hodge, S.R., Myers, B., Norris, M.L., McCabe, L., Barreira, T.V. & Heffernan, K.S. (2019) Physical activity participation among families of children with visual impairments and blindness. *Disability and Rehabilitation*. 41 (3), 357–365. https://doi.org/10.1080/09638288.2017.1390698.

Donath, L., Roth, R., Zahner, L. & Faude, O. (2016) Slackline training and neuromuscular performance in seniors: A randomized controlled trial. *Scandinavian Journal of Medicine & Science in Sports*. 26 (3), 275–283. https://doi.org/10.1111/sms.12423.

Dordevic, M., Hökelmann, A., Müller, P., Rehfeld, K. & Müller, N.G. (2017) Improvements in Orientation and Balancing Abilities in Response to One Month of Intensive Slackline-Training. A Randomized Controlled Feasibility Study. *Frontiers in Human Neuroscience*. 11, 55. https://doi.org/10.3389/fnhum.2017.00055.

Dordevic, M., Taubert, M., Müller, P., Riemer, M., Kaufmann, J., Hökelmann, A. & Müller, N.G. (2020) Which Effects on Neuroanatomy and Path-Integration Survive? Results of a Randomized Controlled Study on Intensive Balance Training. *Brain Sciences*. 10 (4), 210. https://doi.org/10.3390/brainsci10040210.

Forbes, P.A., Chen, A. & Blouin, J.-S. (2018) Sensorimotor control of standing balance. *Handbook of Clinical Neurology*. 159, 61–83. https://doi.org/10.1016/B978-0-444-63916-5.00004-5.

Francesconi, K. & Gandini, G. (2015) *L'intelligenza nel movimento. Percezione, propriocezione, controllo posturale*. Edi. Ermes.

Greguol, M., Gobbi, E. & Carraro, A. (2015) Physical activity practice among children and adolescents

with visual impairment--influence of parental support and perceived barriers. *Disability and Rehabilitation*. 37 (4), 327–330. https://doi.org/10.3109/09638288.2014.918194.

Ha, S.-Y., Han, J.-H. & Sung, Y.-H. (2018) Effects of ankle strengthening exercise program on an unstable supporting surface on proprioception and balance in adults with functional ankle instability. *Journal of Exercise Rehabilitation*. 14 (2), 301–305. https://doi.org/10.12965/jer.1836082.041.

Haibach, P.S., Wagner, M.O. & Lieberman, L.J. (2014) Determinants of gross motor skill performance in children with visual impairments. *Research in Developmental Disabilities*. 35 (10), 2577–2584. https://doi.org/10.1016/j.ridd.2014.05.030.

Harvey, R.H., Peper, E., Mason, L. & Joy, M. (2020) Effect of Posture Feedback Training on Health. *Applied Psychophysiology and Biofeedback*. 45 (2), 59–65. https://doi.org/10.1007/s10484-020-09457-0.

Houwen, S., Hartman, E. & Visscher, C. (2009) Physical activity and motor skills in children with and without visual impairments. *Medicine and Science in Sports and Exercise*. 41 (1), 103–109. https://doi.org/10.1249/MSS.0b013e318183389d.

Magno e Silva, M.P., Morato, M.P., Bilzon, J.L.J. & Duarte, E. (2013) Sports injuries in Brazilian blind footballers. *International Journal of Sports Medicine*. 34 (3), 239–243. https://doi.org/10.1055/s-0032-1316358.

Padgett, P.K., Jacobs, J.V. & Kasser, S.L. (2012) Is the BESTest at Its Best? A Suggested Brief Version Based on Interrater Reliability, Validity, Internal Consistency, and Theoretical Construct. *Physical Therapy*. 92 (9), 1197–1207. https://doi.org/10.2522/ptj.20120056.

Riva, D., Bianchi, R., Rocca, F. & Mamo, C. (2016) Proprioceptive Training and Injury Prevention in a Professional Men's Basketball Team: A Six-Year Prospective Study. *Journal of Strength and Conditioning Research*. 30 (2), 461–475. https://doi.org/10.1519/JSC.0000000000001097.

Riva, D., Fani, M., Benedetti, M.G., Scarsini, A., Rocca, F. & Mamo, C. (2019) Effects of High-Frequency Proprioceptive Training on Single Stance Stability in Older Adults: Implications for Fall Prevention. *BioMed Research International*. 2019, 2382747. https://doi.org/10.1155/2019/2382747.

Riva, D., Mamo, C., Fanì, M., Saccavino, P., Rocca, F., Momenté, M. & Fratta, M. (2013) Single stance stability and proprioceptive control in older adults living at home: gender and age differences. *Journal of Aging Research*. 2013, 561695. https://doi.org/10.1155/2013/561695.

Rogge, A.-K., Hamacher, D., Cappagli, G., Kuhne, L., Hötting, K., Zech, A., Gori, M. & Röder, B. (2021) Balance, gait, and navigation performance are related to physical exercise in blind and visually impaired children and adolescents. *Experimental Brain Research*. 239 (4), 1111–1123. https://doi.org/10.1007/s00221-021-06038-3.

Ruini, C., Ottolini, F., Rafanelli, C., Ryff, C. & Fava, G. (2003) Italian validation of Psychological Well-Being Scales (PWB). *Rivista di Psichiatria*. 38, 117–130.

Stamatakis, E., Gale, J., Bauman, A., Ekelund, U., Hamer, M. & Ding, D. (2019) Sitting Time, Physical Activity, and Risk of Mortality in Adults. *Journal of the American College of Cardiology*. 73 (16), 2062–2072. https://doi.org/10.1016/j.jacc.2019.02.031.

Tchórzewski, D., Jaworski, J. & Bujas, P. (2010) Influence of Long-Lasting Balancing on Unstable Surface on Changes in Balance. *Human Movement*. 11. https://doi.org/10.2478/v10038-010-0022-2.

Tomomitsu, M.S.V., Alonso, A.C., Morimoto, E., Bobbio, T.G. & Greve, J.M.D. (2013) Static and dynamic postural control in low-vision and normal-vision adults. *Clinics (Sao Paulo, Brazil)*. 68 (4), 517–521. https://doi.org/10.6061/clinics/2013(04)13.

West, S.K., Rubin, G.S., Broman, A.T., Muñoz, B., Bandeen-Roche, K. & Turano, K. (2002) How does visual impairment affect performance on tasks of everyday life? The SEE Project. Salisbury Eye Evaluation. *Archives of Ophthalmology (Chicago, Ill.: 1960)*. 120 (6), 774–780. https://doi.org/10.1001/archopht.120.6.774.

Winter, L., Huang, Q., Sertic, J.V.L. & Konczak, J. (2022) The Effectiveness of Proprioceptive Training for Improving Motor Performance and Motor Dysfunction: A Systematic Review. *Frontiers in Rehabilitation Sciences*. 3, 830166. https://doi.org/10.3389/fresc.2022.830166.

IJAE
ITALIAN JOURNAL OF ANATOMY AND EMBRYOLOGY

Firenze University Press
www.fupress.com/ijae

Citation: Hartman, P. C., & Xhakaza, N. K. (2025). A population study of variations in the brachial artery and its terminal branches: Clinical correlates. *Italian Journal of Anatomy and Embryology* 129(2): 75-86. doi: 10.36253/ijae-16609

Data Availability Statement: All relevant data are within the paper and its Supporting Information files.

Competing Interests: The Author(s) declare(s) no conflict of interest.

A population study of variations in the brachial artery and its terminal branches: Clinical correlates

PC Hartman*, NK Xhakaza

Department of Anatomy, School of Medicine, Sefako Makgatho Health Sciences University, Ga-Rankuwa, Pretoria, South Africa
*Corresponding author. Email: patriacoetzee@gmail.com

Abstract. Reports in the literature suggest that the variations in branching patterns of the upper limb arteries and their prevalence may be influenced by sex and population affinity. A comprehensive investigation of branching patterns of the brachial artery and its branches is lacking in South Africans, with many reports focusing on the axillary artery. Therefore the current study aimed to record the incidence of the variations of the brachial, radial and ulnar arteries in a sample of the South African population. One hundred and eighty (180) upper limbs of 90 South African cadavers from the Department of Anatomy at Sefako Makgatho Health Sciences University were dissected. Normal anatomy according to standard anatomy textbooks and variant branching patterns of the brachial, radial and ulnar arteries were identified and recorded. SPSS software was used to establish the differences in variant branching patterns between side and sex. Upper limb arterial variations appeared in all the dissected cadavers. The recorded variations ranged from abnormal origin of the deep brachial artery, high division of the brachial artery into the ulnar and radial arteries, tortuous brachial and radial arteries, and superficial course of radial and ulnar arteries. The prevalence of brachial, ulnar and radial artery variations in the current study is comparable to that of previous studies. However, the superficial radial artery is more prevalent in males than in females in South Africans. The results of the current study provide crucial information for planning surgical procedures and interpretation of angiograms.

Keywords: brachial artery, ulnar artery, radial artery, median artery.

INTRODUCTION

The branching pattern of the upper limb arteries are highly variable, with an average incidence of 25% [1]. Literature reports describing the prevalence of the variant branching patterns of upper limb vessels usually focus on the axillary artery due to frequent incident reports on its variations [2–6]. Consequently, there is a lack of population studies on variations of brachial, radial and ulnar arteries as much focus on arterial variations is put on incident reports encountered during routine dissections in the university setting [7–10]. A study performed on a sample of African Americans and non-

African-Americans showed a higher incidence of a high brachial artery bifurcation in African-Americans than in non-African-Americans suggesting that population affinity may influence this branching pattern [11]. The available reports on upper limb arterial variations are mostly based on European and Asian population groups with not many reports on the African populations [4,5,7,12,13]. Studies conducted in African populations specifically focused on the axillary artery, whereby some unique branching patterns were recorded in contrast to standard anatomy textbook descriptions [6,14,15].

Arterial variations have significant clinical implications during surgical procedures [6]. The most common variation noted in the brachial artery, is a superficial brachial artery, which could be easily mistaken for a vein during drug administration [16]. The high origin of the radial and ulnar arteries from axillary or brachial artery has also been reported [17–20]. Knowledge of variant origins of these vessels can be clinically relevant as the radial artery is commonly harvested for coronary artery bypass procedures, in which case, the ulnar artery becomes the principal arterial supply to the hand [21]. The high origin of the ulnar artery is often associated with nerve entrapment as well as trauma during intravenous cannulation [22]. Another upper limb arterial variation reported in the literature is a tortuous radial artery [23–25]. Change in the direction of the flow of blood in a tortuous vessel is often noted and could affect the histological structure of the vessel and cause atherosclerotic plaques [24]. In addition, the tortuous course of the radial artery can cause difficulty to access the radial artery during trans-radial catheterisation, as the tortuosity could hinder the passage of the catheter causing complications or influence the success of the procedure [25].

Another upper limb arterial variation in the forearm arteries is a persistent median artery which has been reported to have a prevalence of 2,8% [26]. When present, the median artery can cause symptoms consistent with median nerve disturbances, either by compression when accompanying the median nerve through the carpal tunnel, or by iatrogenic ischemia [27].

VARIATIONS OF THE BRACHIAL ARTERY

Common variations of the brachial artery include the superficial brachial artery, high origin of radial and ulnar arteries, accessory brachial artery, and trifurcation of the brachial artery to common interosseous, radial and ulnar arteries [28]. The superficial brachial artery is defined as a brachial artery coursing anterior to the median nerve, instead of posterior to it [29]. A superficial brachial artery is often more susceptible to trauma and can easily be confused with superficial veins [16]. Additionally, the superficial course and variations in the brachial artery or its derivatives are clinically relevant as the brachial artery is often used as the passage during coronary artery procedures making it prone to injuries leading to bleeding or ischemia [30]. The bifurcation of the brachial artery proximal to the cubital fossa is considered a high division of the brachial artery [31]. The high origin of the radial artery has a prevalence of 3,0-18,0% [13,19,29,32]. Knowledge of the above variations is also crucial for the evaluation of angiographic images, and for vascular and reconstructive surgeries of the arm and forearm [30].

VARIATIONS OF THE RADIAL ARTERY

The radial artery usually originates from the brachial artery in the cubital fossa at the level of the neck of the radius [19]. The radial artery runs along the lateral aspect of the anterior compartment of the forearm deep to the brachioradialis muscle, lateral to the flexor carpi radialis tendon. It winds around the lateral aspect of the radius and passes through the floor of the anatomical snuffbox to pierce the first dorsal interosseous muscle [28].

The high origin of the radial artery is described as the origin from the axillary artery or from the brachial artery proximal to the cubital fossa [29]. The radial artery is commonly used in vascular, plastic and reconstructive surgery and is routinely used for arterial puncture and cannulation [19]. Radial artery anomalies may prolong and diminish the success of coronary angiography and percutaneous coronary intervention [20]. In addition, trans-radial access may be hindered by the presence of an unusual origin or course of the radial artery [33]. The superficial course of the radial artery may be more vulnerable to trauma, and thus haemorrhage [34]. It may also lead to puncture of the radial artery during venipuncture, misinterpretation of angiographic images, or severe disturbance of hand irrigation during surgical procedures on the arm [35]. Furthermore, it has been recorded that the presence of a high origin of the radial artery contributes to the development of tortuosity, which can increase the risk of failure of trans-radial catheterisation [19].

VARIATIONS OF THE ULNAR ARTERY

The ulnar artery passes medially, deep to the pronator teres muscle and intermediate to the flexor digitorum superficialis muscle, to reach the medial aspect of the

forearm after its origin from the brachial artery in the cubital fossa. It passes superficial to the flexor retinaculum at the wrist in Guyon's canal to enter the hand [28, 36]. The ulnar artery courses through the forearm with the ulnar nerve [37].

The superficial artery is described as an ulnar artery with a high origin in the arm that descends over the superficial muscles of the forearm [8]. Knowledge of the superficial ulnar artery has clinical significance as this variant vessel can be easily mistaken for a vein during intravenous drug administration [38]. The tortuosity of the ulnar artery can lead to ulnar nerve compression if tortuosity coincides with the passage of these two structures through the pisohammate hiatus, which may result in paresthesia and numbness of the skin in the dorsum of the hand where the ulnar nerve is distributed [39].

THE MEDIAN ARTERY

During early embryonic life, the arterial axis of the forearm is represented by a transitory vessel known as the median artery. It normally regresses after the second embryonic month [27]. However, if the persistent median artery does not regress, it forms a median artery that accompanies the median nerve, which in some cases may perforate the median nerve [32]. The persistent median artery has also been associated with compressive pathology of the median nerve, which is secondary to arterial calcification, thrombosis and atherosclerosis [12]. In addition, if there is no anastomosis between the persistent median artery and the ulnar artery, it becomes of great importance to plastic surgeons and neurosurgeons as inadvertent damage to the persistent median artery may cause hand ischemia [40]. The prevalence of the variations of the median artery has shown populations difference ranging from 0,5-59,7% in Europeans, and Africans respectively, with the Europeans recording the lowest incidence [13,14,20,41].

TORTUOSITY OF THE UPPER LIMB ARTERIES AND THEIR CLINICAL IMPLICATIONS

Tortuous arteries and veins are increasingly becoming a common observation throughout the human body [25]. Changes in the arterial walls due to mechanical injury, hypertension, diabetes, ageing and atherosclerosis may lead to thrombic events, embolic events, restriction of blood flow, occlusion of blood flow and ultimately change in the gross anatomical structure of the artery leading to tortuosity [24].

The mechanical stability of arteries depends on the wall stiffness [24]. Elastin is an important extracellular matrix component for arterial elasticity and stiffness and elastin degradation weakens the arterial wall [42]. Degradation of elastin in the arterial walls is said to cause weakening of the arteries leading to tortuosity, due to increased blood flow, but the underlying mechanisms are unclear [24]. The fragmentation of elastin has been reported in the walls of tortuous arteries and has been considered the cause of vessel lengthening leading to tortuosity [43].

Clinical observations have linked ageing, atherosclerosis, hypertension, genetic defects, diabetes mellitus and reduced axial tension or elongation of the arteries to some of the factors thought to cause tortuosity [24]. Certain levels of axial tension are essential in maintaining the stability of arteries and preventing tortuosity, decreasing with age as the artery lengthens [44].

Tortuosity of arteries increases the resistance in blood flow and in severe cases, obstruction or even occlusion of blood flow [45]. Han (2012) [24] classified tortuosity into four different types: curving/curling, kinking, looping and spiral twisting vessels. A previous study described three types of tortuous radial arteries [46]. The first type was the tortuous radial artery without stenosis. In this type, trans-radial catheterization was recorded to have a 98,8% success rate. The second type was the stenotic tortuous radial artery where the tortuous segment of the artery was calcified. In this type, difficulty in inserting the guide wire was reported. The third type was the hypoplastic tortuous radial artery, an additional brachioradial artery, which may influence the flow of blood and may require a different approach to gain access to the artery [46]. The aforementioned types of the tortuous radial artery suggest that tortuosity complicates radial catheterisation. Chronic pressure on the vessel wall is considered one of the important predisposing factors of tortuosity, resulting in the vessel wall thickening and also an increase in the length of the artery [24]. In case of an anomaly in the radial artery, like tortuosity, the ulnar artery is used as an alternative in coronary and cerebral angiography and ulnar-cephalic arteriovenous fistula when access to the radial artery fails [8].

MATERIALS AND METHODS

Study design

The current study is a descriptive quantitative study where the types and frequency distribution of the upper limb arterial variations were analysed and recorded in a

select sample of the South African population (black and white) (Ethics Reference Number: SMUREC/M/193/2022: PG). The sampling method used in the current study was convenient sampling. Gross anatomical dissection was used to expose the upper limb arteries by using the methods described by Tank and Grant (2013)[47].

Sample size

One-hundred and eighty (180) upper limb arteries of 90 cadavers were dissected in the Department of Human Anatomy and Histology at Sefako Makgatho Health Sciences University (Table 1). Of the 90 cadavers, 14 were neonatal cadavers, 3 were fresh unembalmed adult cadavers and the remaining 73 cadavers were adult embalmed cadavers. The axillary, brachial, ulnar and radial arteries were exposed via gross anatomical dissection using a method described by Tank and Grant (2013) [47]. The dissection was completed by making use of a standard dissection kit.

Data analysis

The data was analysed using SPSS v.24. Frequency distribution of the variant branching patterns of the tortuosity of the radial, high origin of the radial artery, common trunk for circumflex humeral arteries and the superficial subscapular artery were recorded in the studied population from the left and right upper limbs, Black and White population as well as female and male were compared using the Chi-square statistical test. A p-value ≤ 0,05 was considered statistically significant.

RESULTS

Variations of the brachial artery and its terminal branches

The standard anatomical branching pattern of the brachial artery was recorded in $\frac{101}{180}$ 56,11% cases (Figure 1). In the above-mentioned cases, 73 cases were recorded in males, while 28 cases were recorded in females. Additionally, 15 of the above cases were recorded in the White cadavers while 86 cases were recorded in the Black cadavers. This pattern was observed bilaterally in 96 cadavers and unilaterally in five cadavers.

Table 1. Distribution of the cadaveric material used in the current study.

Sex	Race distribution		Sample size
	Black	White	
Female	18/90 = 20,00%	9/90=10,00%	27
Male	50/90 = 55,56%	13/90 = 14,44%	63
Total	68	22	90

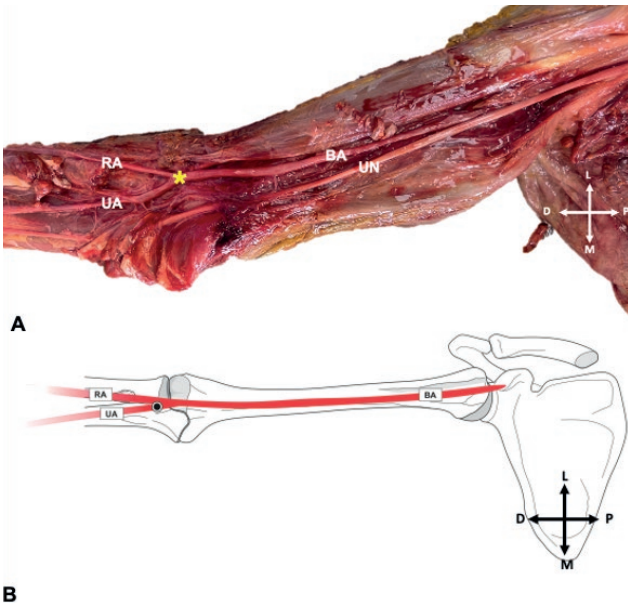

Figure 1. A) The anterior view of the arm showing a textbook branching of the brachial, radial and ulnar arteries. B) A schematic diagram of the anterior view of the arm showing a textbook branching of the brachial, radial and ulnar arteries. Key: BA: Brachial artery; UA: Ulnar artery; UN: Ulnar nerve; RA: Radial artery; *: Point of bifurcation; L: Lateral; M: Medial; P: Proximal; D: Distal.

The radial artery had a high origin in $\frac{10}{180}$ 5,56% cases (Figure 2A and B). The high origin of the radial artery was found bilaterally in $\frac{8}{180}$ 4,44% and unilaterally in $\frac{2}{180}$ 1,11%. In addition, $\frac{9}{180}$ 5,00% were observed in males and $\frac{1}{180}$ 0,56% were observed in females. Considering the race distribution, $\frac{3}{180}$ 1,67% cases of high origins of the radial artery were recorded in the White cadavers and $\frac{7}{180}$ 3,89% were recorded in the Black cadavers.

The Chi-square test comparing the frequency of the high origin of the radial artery in all 180 dissected upper limbs (136 Black, 44 White, 126 males and 54 females) showed no significant differences in the frequency of the high origin of the radial artery in the sides (p = 0,861), sex (p = 0,094) and race (p = 0,732).

In one of the above 10 cases of high origin of radial artery, the radial artery took a superficial course over the forearm muscles.

The ulnar artery had a high origin in $\frac{4}{180}$ 2,22% cases (Figure 3A and B). In one of the above four cases, the ulnar artery took a superficial course (Figure 3 C). The

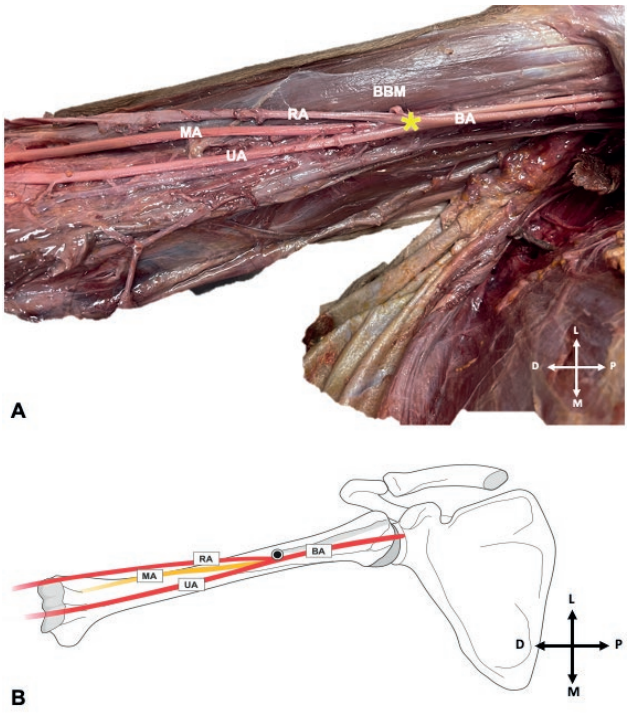

Figure 2. A) The anterior view of the arm showing the high division of the brachial artery. B) A schematic diagram of the anterior view of the arm showing the high division of the brachial artery. Key: BBM: Biceps Brachii muscle; BA: Brachial artery; UA: Ulnar artery; RA: Radial artery; MN: Median nerve; *: Point of bifurcation; L: Lateral; M: Medial; P: Proximal; D: Distal.

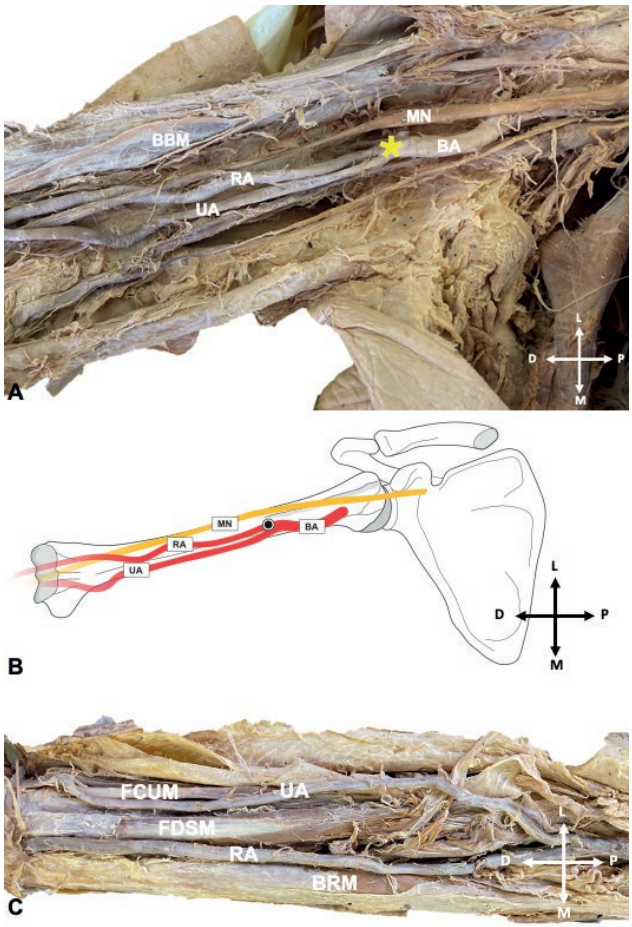

Figure 3. A) Anterior view of the arm showing the high division of the brachial artery with the ulnar artery taking a superficial course in the forearm. B) A schematic diagram of the anterior view of the arm showing the high division of the brachial artery with the ulnar artery taking a superficial course in the forearm. C) Superficial course of the ulnar artery over the flexor muscles in the forearm. Key: BA: Brachial artery; MN: Median nerve; RA: Radial artery; UA: Ulnar artery; BBM: Biceps Brachii muscle; BRM: Brachioradialis muscle; FDSM: Flexor digitorum superficialis muscle; FCUM: Flexor carpi ulnaris muscle; *: Point of bifurcation; L: Lateral; M: Medial; P: Proximal; D: Distal.

above cases were recorded bilaterally in two White male cadavers.

In $\frac{1}{180}$ 0,56% cases the deep brachial artery originated from the posterior circumflex humeral artery on the right of a male cadaver (Figure 4).

The median artery was recorded in $\frac{8}{180}$ 4,44% cases (Figure 5). It was unilateral in $\frac{4}{180}$ 2,22% cases and bilateral in $\frac{4}{180}$ 2,22% cases. In the above cases, $\frac{6}{180}$ 3,33% were observed in males, while $\frac{2}{180}$ 1,11% cases were observed in females. Considering the race distribution, $\frac{3}{180}$ 1,67% cases of the median artery were recorded in the White cadavers and $\frac{5}{180}$ 2,78% cases were recorded in the Black cadavers.

Superficial course of the radial artery

In one cadaver the radial artery ran superficial to the extensor pollicis longus and extensor pollicis brevis tendons instead of passing through the anatomical snuffbox on both sides (Figure 6 A-B). On the right side, the radial artery continued on the dorsum of the first web lying superficial to the first dorsal interosseous muscle and joining the superficial palmar arch (Figure 6 A). On the left side, before passing superficial to the extensor pollicis longus and extensor pollicis brevis tendons, the radial artery gave rise to a branch that passed through the anatomical snuff box and makes no entry into the deep palmar aspect. The radial artery then continues to loop around the first web to anastomose with the junction of the princeps pollicis artery and the radialis indicis artery (Figure 6 B). Even though the course of this branch was not followed further, it is believed to

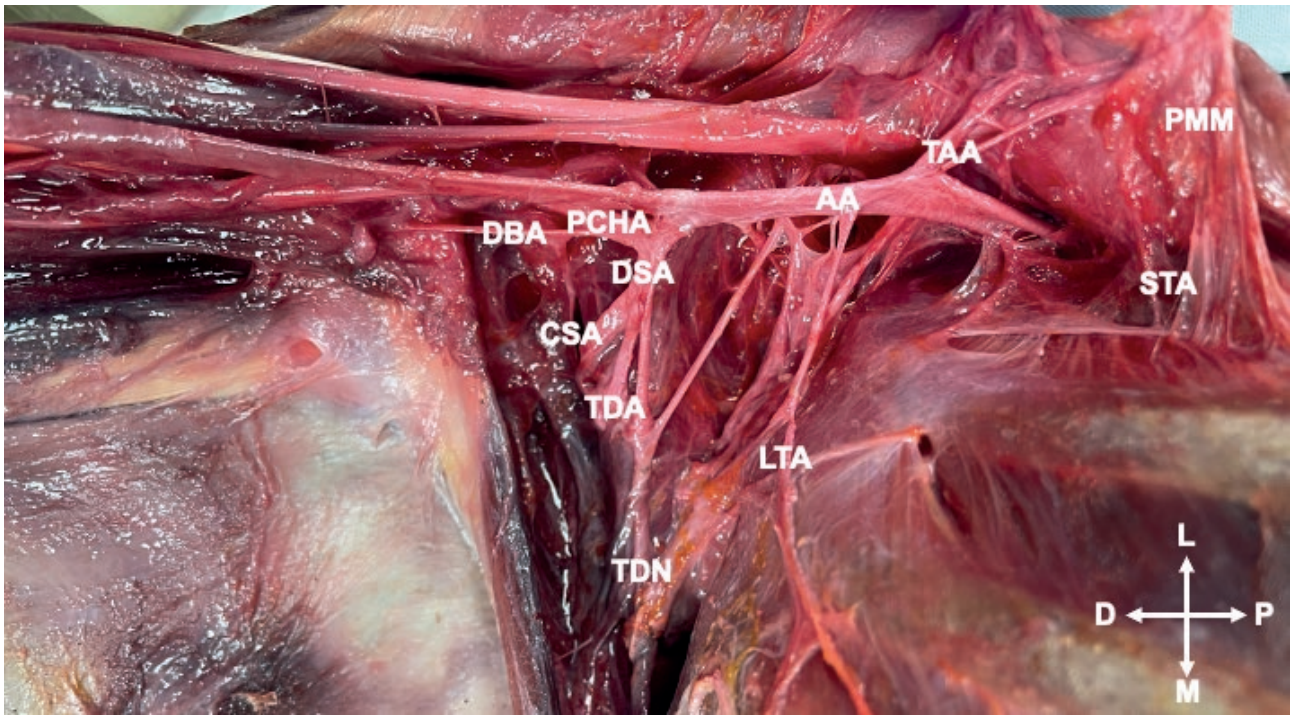

Figure 4. The anterior view of the axilla showing the deep brachial artery arising from the posterior circumflex humeral artery. Key: AA: Axillary artery; STA: Superior Thoracic artery; TAA: Thoraco-acromial artery; LTA: Lateral Thoracic artery; DSA: Deep Subscapular artery; CSA: Circumflex Scapular artery; TDA: Thoracodorsal artery; TDN: Thoracodorsal nerve; PCHA: Posterior Circumflex Humeral Artery; DBA: Deep brachial artery; PMM: Pectoralis minor muscle; L: Lateral; M: Medial; P: Proximal; D: Distal.

Figure 5. Anterior view of the forearm showing the median artery entrapped by the median nerve. Key: BA: Brachial artery; RA: Radial artery; UA: Ulnar artery; CT: Common Trunk; MN: Median nerve; MA: Median artery; L: Lateral; M: Medial; P: Proximal; D: Distal.

have continued to the deep palmar arch. After giving off the above branch, unlike on the right side, the radial artery did not continue superficial to the first dorsal interosseous muscle but rather penetrated and went deep to this muscle. Our literature search could not find this variation in the previous studies.

Tortuosity of the brachial artery and its branches

The brachial artery was tortuous in $\frac{20}{180}$ 11,11% cases (Figure 7A). Of these 20 cases, the tortuous brachial artery presented bilaterally in $\frac{18}{180}$ 10,00% cases and unilaterally in $\frac{2}{180}$ 1,11% cases. It was observed in males $\frac{15}{180}$ 8,33% cases and females in $\frac{5}{180}$ 2,78% cases.

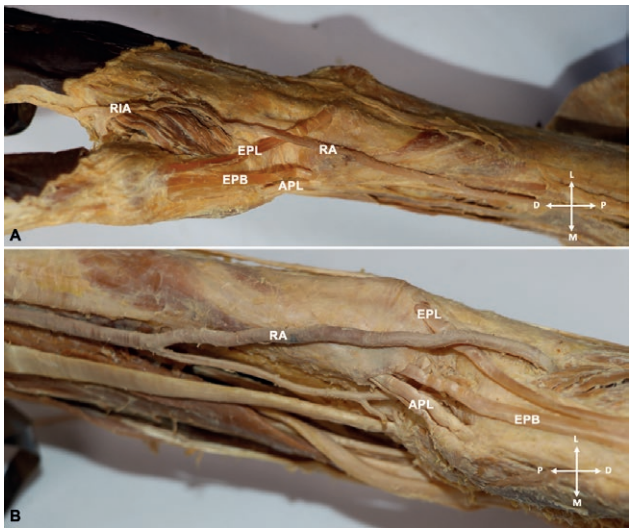

Figure 6. A) The posterior view of the right forearm showing the radial artery superficial to the extensor pollicis longus and extensor pollicis brevis tendons, and not passing through the anatomical snuffbox. B) The superior view of the left forearm showing the radial artery superficial to the extensor pollicis longus and extensor pollicis brevis tendons, giving off a branch to the anatomical snuffbox. Key: RA: Radial artery; EPL: Extensor Pollicis Longus; EPB: Extensor Pollicis Brevis; APL: Abductor Pollicis longus; RIA, Radialis indicis artery. B: RA, Radial artery; EPL, Extensor Pollicis Longus; EPB: Extensor Pollicis Brevis; APL: Abductor Pollicis longus; L: Lateral; M: Medial; P: Proximal; D: Distal.

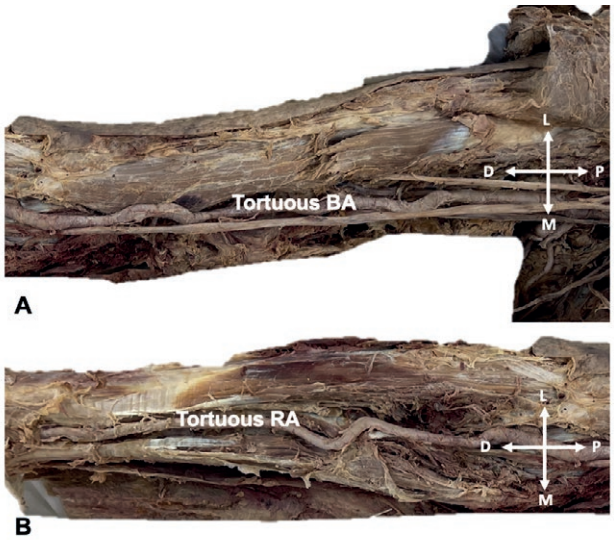

Figure 7. Anterior view of the upper limb showing tortuosity of its arteries. A) Brachial artery showing tortuosity. B) Tortuous radial artery with kinking and curving tortuosity. Key: BA: Brachial artery; RA: Radial artery; L: Lateral; M: Medial; P: Proximal; D: Distal.

The radial artery was tortuous in $\frac{31}{180}$ 17,22% cases (Figure 7 B). The tortuosity of the radial artery was unilateral in $\frac{7}{180}$ 3,89% cases and bilateral in $\frac{24}{180}$ 13,33% cases. In addition, $\frac{17}{180}$ 9,44% were observed in male cadavers, while $\frac{14}{180}$ 7,78% were observed in female cadavers. Considering the race distribution, the tortuous radial artery was observed in $\frac{23}{180}$ 12,78% cases of White cadavers, while $\frac{8}{180}$ 4,44% cases were recorded in Black cadavers.

The Chi-square test comparing the frequency of tortuous arteries in all 180 dissected upper limbs (136 Black, 44 White, of which 126 were males and 54 were of females) showed a significantly high frequency of tortuosity of arteries in the White cadavers compared to Black cadavers ($p<0,001$), while side ($p=0,230$) and sex ($p=0,230$) comparisons were not statistically significant.

The frequency of the upper limb arterial variations recorded in the sections above are summarised in Figure 8 and Table 2 below.

DISCUSSION

Introduction

The current study evaluated the variations in the brachial artery and its terminal branches to record the incidence of these variations in the studied population and the possible clinical implications that these variations may have during surgical and treatment interventions involving the upper limb vessels studied. The study records the information with limited availability in the current literature, more specifically pertaining to the African population, as much focus has been given to the axillary artery which is known to be a highly variable artery of the upper limb. Even though the above is true regarding the axillary artery, the knowledge of the variations of the brachial artery and its branches is of crucial importance as these vessels are sometimes used to perform arterial bypass and are also vulnerable to venipuncture during drug administration.

While the current study has done extensive comparisons of the variations in different sex and race groups of the studied population, care should be taken when using the results of the current study to project the possible variations of the brachial artery and its branches for surgical planning and drug administration. This is due to the fact that the limited availability of human cadaveric material did not allow a balance between sex and race

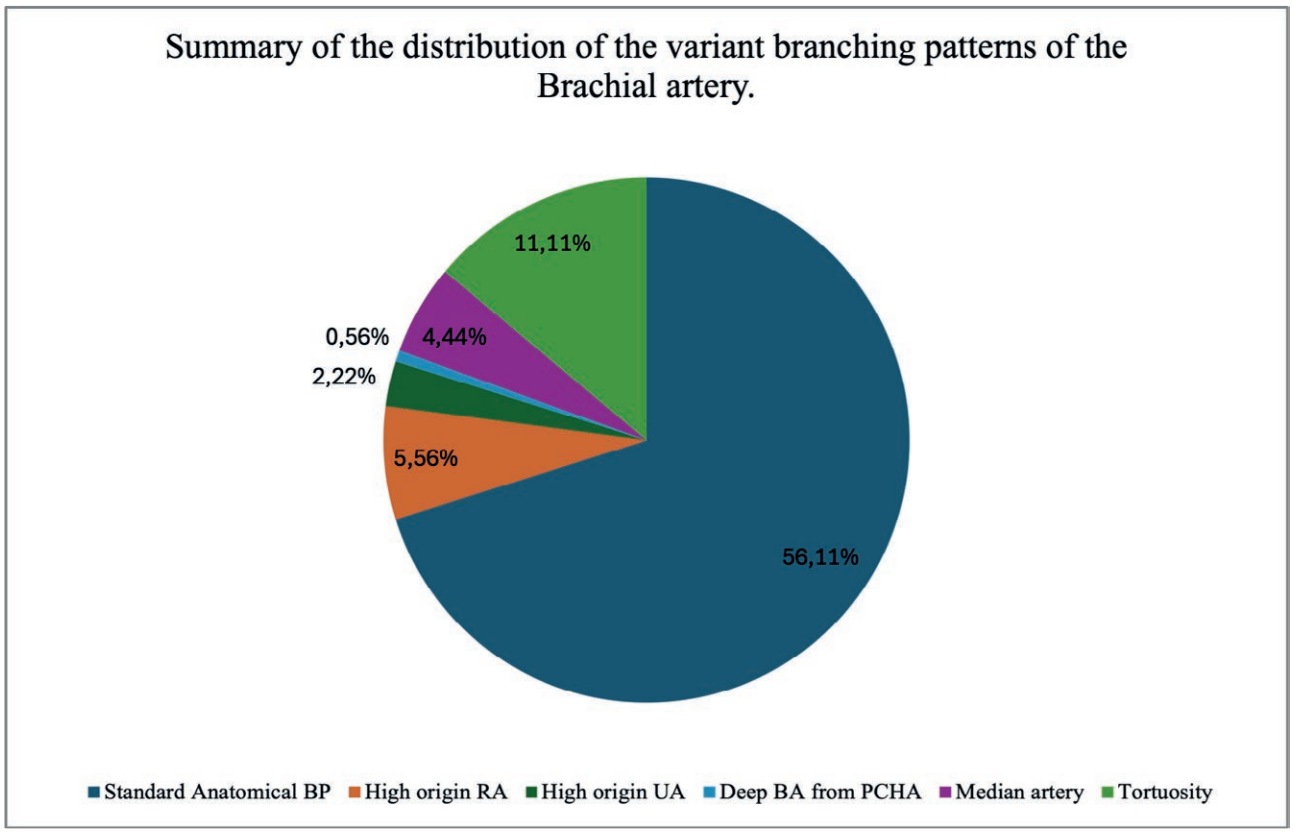

Figure 8. Summary of the distribution of the variant branching patterns of the Brachial artery.

groups, and therefore some statistical analysis shown in comparing the groupings might have lost statistical power. Authors nevertheless believe that the data presented in this article carriers significant scientific value that may inform the decisions for surgical procedures and treatment interventions to prevent iatrogenic injuries.

Variations of the brachial artery and its terminal branches

The current study reported 5,56% of cases of the high origin of the radial artery, in agreement with previous studies which recorded 2,84% in the European Population [13] and 14,27% in the Spanish population [48]. The presence of a high origin of the radial artery may lead to failure during trans-radial catheterisation as the catheter may be hindered, partly due to the fact that the presence of a high origin of the radial artery is associated with its tortuosity [19]. In some cases, the radial artery with high origin takes a superficial course, making it vulnerable to be mistaken as a vein during drug administration, a situation that could lead to gangrene of the forearm and hand [49].

The high origin of the ulnar artery was recorded in 2,22% of cases in the current study. Its reported frequency ranges from 0,17% to 2,00% in previous studies [27,29,50]. The presence of an ulnar artery of high origin is considered a rare anatomical variation with clinical significance [8]. The high origin of the ulnar artery is often related to ulnar nerve compression and entrapment [51]. Its clinical importance should not be underestimated as several cases of intra-arterial injection of drugs and subsequent amputations have been reported in patients with this type of variation [51]. Additionally, the ulnar artery of high origin is extremely vulnerable to iatrogenic injury during surgery [52].

A rare case of a common trunk of PCHA and deep brachial artery was recorded in 0,56% of cases in the current study. Our literature search found one study that recorded a similar variation in 2% of cases [53]. This variation is important for arteriovenous bypass, especially where the axillary artery is used [54]. It should also be considered for shoulder and axillary tissue flaps used for the reconstruction of cervical and axillary scar contractures and reconstruction [55].

The rare superficial course of the radial artery that ran on the roof of the anatomical snuff box was found in 1,11% of cases in the current study. According to our

Table 2. Summary of the prevalence of arterial variations.

Variations	Prevalence of variation (%) (n/180)	Male (n/126)		Female (n/54)	
		Bilateral	Unilateral	Bilateral	Unilateral
Brachial artery					
Median artery	4.44%	4	2	0	2
Tortuous brachial artery	11.11%	14	1	4	1
Tortuous radial artery	17.22%	14	3	10	4
High origin of radial artery	5.56%	4	6	0	0
High origin of ulnar artery	2.22%	4	0	0	0
Superficial RA	1.11%	2	0	0	0
Normal brachial artery	56.11%	70	3	26	2

Table 3. Summary of population differences in the brachial artery variations reported by different authors.

Brachial artery	Henneberg & George, 1991 & 1992	Rodríguez-Niedenführ et al., 2001	Li et al., 2013	Konarik et al., 2020	Shetty et al., 2022	Current study
	SA	European	Chinese	European	Indian	SA
Median artery	54%	0%	-	0%	-	4,44%
Tortuous brachial artery	-	-	0,4%	-	10,00%	11,11%
Tortuous radial artery	-	-	3,6%	-	-	17,22%
High origin of radial artery	-	14,2%	-	2,84%	15,00%	5,56%
Superficial RA	-	-	-	-	-	1,11%

literature review, this variation has only been reported recently in a case study reported on a Korean male cadaver [56]. Clinical classifications of variants in the radial artery are important as they are the main reasons for technical failures during trans-radial catheterisations [56]. The looping of the radial artery around the first web in the current study resulted in it taking a superficial unexpected course where it could be vulnerable to injuries with potential profuse bleeding.

Median artery

The median artery was present in 4,44% of cases in the current study, in agreement with a previous study conducted in a sample of Indian population which recorded 6,6% of cases of the median artery [12]. The presence of the median artery is often coupled with idiopathic median nerve pain due to nerve entrapment [26]. A few cases of median nerve neuropathies encountered in the clinical setting are reported to be idiopathic probably due to compression by arteries that take the abnormal course or the presence of the median artery [10]. This could have been a possibility in the case observed in the current study as the median artery pierced through the median nerve.

Tortuosity of the main upper limb arteries

The tortuous brachial artery was reported in 11,11% of cases in the current study. Tortuosity of the brachial artery is a rare occurrence and is mostly reported in case reports [23,25,39]. The presence of tortuous arteries can lead to difficulty during catheterization and may result in iatrogenic injury [57]. The tortuosity of the upper limb arteries was high (28,33%) in the current study compared to previous studies (1,25%) [23,25].

The tortuous radial artery was reported in 17,22% of cases in the current study. Tortuosity of the radial artery has been reported to range from 3,6% to 23% of cases [23,25,39] which is in agreement with the results of the current study. Considering the race distribution, the tortuous radial artery was observed in 12,78% of the White South African cadavers and 4,44% recorded in the Black South African cadavers. These results suggest a higher prevalence of tortuosity of the radial artery in

the White South Africans compared to the Black South Africans. It has previously been suggested that tortuosity of the arteries may be related to diabetes and hypertension [24]. Medical records were not available to relate the tortuosity to the disease in the current study.

CONCLUSION

All dissected cadavers showed variations in either brachial, ulnar or radial artery, confirming the high incidence of upper limb arterial variations. The incidence of variations in branching patterns of the brachial artery and its terminal branches in the South African population compares to that of the previous studies, suggesting that these variations are not race or population dependent. This study also noted that the high origin of the radial artery is more prevalent in males than in females, a point noted for the first time in the current study. Tortuosity of the brachial and radial arteries are much higher in the South African population compared to other populations.

The results of the current study provides crucial information for planning surgical procedures and interpretation of angiograms more specifically in the South African population. Such data is currently not available except the current study.

LIMITATIONS

Due to the limited availability of cadaveric material, a proper balance between race and sex was not possible and hence the current study may not sufficiently elucidate the distinct racial disparities and variations with regards to sex. In addition the variations in smaller branches might have been missed due to poor visibility after the embalming process.

RECOMMENDATIONS

We recommend an increase in sample size to accurately determine statistical variations between sexes and race groups to enhance the knowledge of the upper limb arterial variations. The effects of age and BMI should also be investigated. Future studies should consider including radiographic imaging to increase the sample size.

ACKNOWLEDGEMENTS

We acknowledge Professor Anna Oettle, a full Professor of the Department of Anatomy and histology of Sefako Makgatho health Sciences University for her advise in analysisng the statistics, more especially with regards possibilities of regression analyses as she specialisies in Athropology research.

REFERENCES

1. Tsoucalas G, Eleftheriou A, Panagouli E. High Bifurcation of the Brachial Artery: An Embryological Overview. Cureus. 2020 Feb 25.
2. De Garis CF, Swartley WB. The axillary artery in white and negro stocks. Am J Anat. 1928 May;41(2):353–97.
3. Huelke DF. Variation in the origins of the branches of the axillary artery. Anat Rec. 1959 Sep;135(1):33–41.
4. Astik R, Dave U. Variations in branching pattern of the axillary artery: a study in 40 human cadavers. J Vasc Bras. 2012 Mar;11(1):12–7.
5. Majumdar S, Bhattacharya S, Chatterjee A, Dasgupta H. A Study on Axillary Artery and its Branching Pattern among the Population of West Bengal, India. 2013;
6. Xhakaza NK, Satyapal KS. Origin of the subscapular artery in the South African Black population. Folia Morphol. 2014 Nov 28;73(4):486–91.
7. Bhat KM, Gowda S, Potu BK, Rao MS. A unique branching pattern of the axillary artery in a South Indian male cadaver. 2008;
8. Casal D, Pais D, Toscano T, Bilhim T, Rodrigues L, Figueiredo I, et al. A rare variant of the ulnar artery with important clinical implications: a case report. BMC Res Notes. 2012 Dec;5(1):660.
9. Piagkou M, Totlis T, Panagiotopoulos NA, Natsis K. An arterial island pattern of the axillary and brachial arteries: a case report with clinical implications. Surg Radiol Anat. 2016 Oct;38(8):975–8.
10. Nkomozepi P, Xhakaza N, Swanepoel E. Superficial brachial artery: a possible cause for idiopathic median nerve entrapment neuropathy. Folia Morphol. 2017 Sep 7;76(3):527–31.
11. Pham XBD, Kim JJ, Parrish AB, Tom C, Ihenachor EJ, Mina D, et al. Racial and Gender Differences in Arterial Anatomy of the Arm. Am Surg. 2016 Oct ;82(10):973–6.
12. Kumar Singla R. Prevalence of the Persistant Median Artery. J Clin Diagn Res. 2012;
13. Konarik M, Musil V, Baca V, Kachlik D. Upper limb principal arteries variations: A cadaveric study with terminological implication. Bosn J Basic Med Sci. 2020 Apr 6.

14. Henneberg M, George BJ. High incidence of the median artery of the forearm in a sample of recent Southern African cadavers. 1991;
15. Cheruiyot I, Bundi B, Munguti J, Olabu B, Ngure B, Ogeng'o J. Prevalence and anatomical pattern of the median artery among adult black Kenyans. Anat J Afr. 2017 Nov 30;6(3):1015–23.
16. Claassen H, Schmitt O, Wree A. Large patent median arteries and their relation to the superficial palmar arch with respect to history, size consideration and clinic consequences. Surg Radiol Anat. 2008 Feb;30(1):57–63.
17. Aharinejad S, Nourani F, Hollensteiner H. Rare case of high origin of the ulnar artery from the brachial artery. Clin Anat. 1997;10(4):253–8. A
18. Natsis K, Papadopoulou AL, Paraskevas G, Totlis T, Tsikaras P. High origin of a superficial ulnar artery arising from the axillary artery: anatomy, embryology, clinical significance and a review of the literature. Folia Morphol. 2006;65(4).
19. Haładaj R, Wysiadecki G, Dudkiewicz Z, Polguj M, Topol M. The High Origin of the Radial Artery (Brachioradial Artery): Its Anatomical Variations, Clinical Significance, and Contribution to the Blood Supply of the Hand. BioMed Res Int. 2018 Jun 11;2018:1–11.
20. Lufukuja G. High Bifurcation of Brachial Artery and its Clinical Significance. 2018;
21. Habib J, Baetz L, Satiani B. Assessment of collateral circulation to the hand prior to radial artery harvest. Vasc Med. 2012 Oct;17(5):352–61.
22. Bozer C, Ulucam E, Kutoglu T. A case of originated high superficial ulnar artery. Trakia J Sci. 2004;2(3).
23. Carter Y, Bennett DJ, Molla V, Wink AE, Collins AJ, Giannaris EL. A case of distal limb arterial tortuosity and dilation: observations and potential clinical significance. Folia Morphol. 2022 Aug 24;81(3):791–7.
24. Han HC. Twisted Blood Vessels: Symptoms, Etiology and Biomechanical Mechanisms. J Vasc Res. 2012 ; 49(3):185–97.
25. Mishra AK, Mishra A. Tortuous forearm arteries and its clinical implications: A Case Report. 2017;
26. Osiak K, Elnazir P, Mazurek A, Pasternak A. Prevalence of the persistent median artery in patients undergoing surgical open carpal tunnel release: A case series. Transl Res Anat. 2021 Jun;23:100113.
27. Natsis K, Iordache G, Gigis I, Kyriazidou A, Lazaridis N, Noussios G, et al. Persistent median artery in the carpal tunnel: anatomy, embryology, clinical significance, and review of the literature. Folia Morphol. 2009;68(4).
28. Standring S, editor. Gray's anatomy: the anatomical basis of clinical practice. Forty-first edition. New York: Elsevier Limited; 2016. 1562 p.
29. Rodríguez-Niedenführ M, Vázquez T, Nearn L, Ferreira B, Parkin I, Sañudo JR. Variations of the arterial pattern in the upper limb revisited: a morphological and statistical study, with a review of the literature. J Anat. 2001 Nov; 199(5):547–66.
30. Chakravarthi KK. Anatomical Variations of Brachial Artery - Its Morphology, Embryogenesis and Clinical Implications. J Clin Diagn Res. 2014.
31. Shetty H, Patil V, Mobin N, Gowda MHN, Puttamallappa VS, Vamadevaiah RM, et al. Study of course and termination of brachial artery by dissection and computed tomography angiography methods with clinical importance. Anat Cell Biol. 2022 Sep 30;55(3):284–93.
32. Keen JA. A study of the arterial variations in the limbs, with special reference to symmetry of vascular patterns. Am J Anat . 1961 May;108(3):245–61.
33. Zheng Y, Shao L, Mao J yuan. Bilaterally symmetrical congenital absence of radial artery: a case report. BMC Surg. 2014 Dec;14(1):15.
34. Singh R. Abnormal origin of posterior circumflex humeral artery and subscapular artery: case report and review of the literature. J Vasc Bras. 2017 Aug 21;16(3):248–51.
35. Deligonul U, Gabliani G, Kern MJ, Vandormael M. Percutaneous brachial catheterization: The hidden hazard of high brachial artery bifurcation. Cathet Cardiovasc Diagn. 1988; 14(1):44–5.
36. Moore KL, Dalley IAF, Agur AMR. Clinically Oriented Anatomy. 2018;
37. Singh D, Malhotra M, Agarwal S. Variations in the Axillary Artery Branching Pattern. J Clin Diagn Res. 2020.
38. Yazar F, Kirici Y, Ozan H, Aldur MM. An unusual variation of the superficial ulnar artery. Surg Radiol Anat. 1999 May;21(2):155–7.
39. Mahajan R, Raheja S, Tuli A, Singh S, Agarwal S. Tortuous ulnar artery and Gantzer's muscle: A rare presentation with clinical implications. 2015;
40. Eid N, Ito Y, Shibata MA, Otsuki Y. Persistent median artery: Cadaveric study and review of the literature. Clin Anat. 2011 Jul;24(5):627–33.
41. Henneberg M, George BJ. A further study of the high incidence of the median artery of the forearm in Southern Africa. 1992;
42. Dobrin PB, Canfield TR. Elastase, collagenase, and the biaxial elastic properties of dog carotid artery. Am J Physiol-Heart Circ Physiol. 1984 Jul 1;247(1):H124–31. A
43. Leeson CR, Leeson TS. Histology. 4th ed. Philadelphia: W.B. Saunders; 1981. 600 p.
44. Nichols WW, O'Rourke M, Vlachopoulos C, Edelman ER. McDonald's Blood Flow in Arteries: Theo-

retical, Experimental and Clinical Principles. 7th ed. Boca Raton: CRC Press; 2022.
45. Hutchins GM, Miner MM, Bulkley BH. Tortuosity as an index of the age and diameter increase of coronary collateral vessels in patients after acute myocardial infarction. Am J Cardiol. 1978 Feb;41(2):210–5.
46. Wysiadecki G, Polguj M, Haładaj R, Topol M. Low origin of the radial artery: a case study including a review of literature and proposal of an embryological explanation. Anat Sci Int. 2017 Mar;92(2):293–8. A
47. Tank PW, Grant JCB. Grant's dissector: Patrick W. Tank. 15th ed. Philadelphia: Lippincott Williams & Wilkins; 2013. 285 p.
48. Gonzalez-Compta X. Origin of the radial artery from the axillary artery and associated hand vascular anomalies. J Hand Surg. 1991 Mar;16(2):293–6.
49. Singh R, Malhotra R, Wadhawan M. Anomalies of radial and ulnar arteries. J Vasc Bras. 2017 Mar;16(1):56–9.
50. Jacquemin G, Lemaire V, Medot M, Fissette J. Bilateral case of superficial ulnar artery originating from axillary artery. Surg Radiol Anat. 2001 Jun;23(2):139–43.
51. Vollala VR, Jetti R, Soni S. High Origin of An Ulnar Artery – Development and Surgical Significance. 2011;34(6).
52. Senanayake KJ, Salgado S, Rathnayake MJ, Fernando R, Somarathne K. A rare variant of the superficial ulnar artery, and its clinical implications: a case report. J Med Case Reports. 2007 Dec;1(1):128. A
53. Paula RCD, Erthal R, Fernandes RMP, Babinski MA, Silva JG, Chagas CAA. Anomalous origin of the deep brachial artery (profunda brachii) observed in bilateral arms: case report. J Vasc Bras. 2013 Mar;12(1):53–6.
54. Morsy MA, Khan A, Chemla ES. Prosthetic axillary-axillary arteriovenous straight access (necklace graft) for difficult hemodialysis patients: A prospective single-center experience. J Vasc Surg. 2008 Nov;48(5):1251-1254.e1.
55. Olinger A, Benninger B. Branching patterns of the lateral thoracic, subscapular, and posterior circumflex humeral arteries and their relationship to the posterior cord of the brachial plexus. Clin Anat. 2010 May;23(4):407–12.
56. Park HJ, Kim S, Kim S, Song WC, Kim HJ. The radial artery running over the anatomical snuffbox: a case report. Surg Radiol Anat. 2022 May;44(5):659–63.
57. Ariyo O. A High Origin Subscapular Trunk and its Clinical Implications. Anat Physiol. 2018;08(02).

IJAE
ITALIAN JOURNAL OF ANATOMY AND EMBRYOLOGY

Firenze University Press
www.fupress.com/ijae

OPEN ACCESS

Citation: Grabarek, P., Masełko, J., Radecka, W., & Simka, M. (2025). 3-dimensional scanning of the fresh cadaver brains for anatomy education. *Italian Journal of Anatomy and Embryology* 129(2):87-95. doi:10.36253/ijae-16839

Data Availability Statement: All relevant data are within the paper and its Supporting Information files.

Competing Interests: The Author(s) declare(s) no conflict of interest.

3-dimensional scanning of the fresh cadaver brains for anatomy education

Paweł Grabarek[1], Jacek Masełko[2], Weronika Radecka[1], Marian Simka[1,*]

[1] *Department of Anatomy, Institute of Medical Sciences, University of Opole, 45-040 Opole, Poland*
[2] *Department of Forensic Medicine, Institute of Medical Sciences, University of Opole, 45-040 Opole, Poland*
*Corresponding author. E-mail: msimka@uni.opole.pl

Abstract. Background. Nowadays, anatomy education use 3D digital models, which are particularly helpful when a cadaveric material is scarce or absent. Such models can be created using the photogrammetry, which consists of multiple digital photographs taken from various angles and then are used for constructing a virtual anatomical model. With the advance of novel smartphones and applications, a high-quality and easy-to-perform photogrammetry became user-friendly. Methods. In this study we assessed the feasibility and technique of creating 3D digital models of the fresh cadaver brains. For this purpose we applied the KIRI Engine application installed on the iPhone smartphone. With this method, five brains of recently deceased patients were scanned and 3D virtual models of these organs were created. Results. We did not encounter major problems with scanning of the brain with the above-described method. After completion of the scanning, models of the brain could be downloaded and either displayed as the virtual reality objects, or as isolated 3D objects. These virtual brains could be moved or rotated or enlarged in order to see details. Also, it was possible to transfer the file containing virtual model the scanned organ to another phone or computer, in order to be handled by another user. Conclusions. We found 3D scanning of the brains with the use of a smartphone application feasible and highly valuable from the educational perspective, especially considering visual appearance of 3D virtual models of the brains, which were very similar to the alive organs.

Keywords: anatomy, brain, medical education, photogrammetry.

INTRODUCTION

Although anatomy based on cadaveric dissections is regarded the backbone of undergraduate medical education, nowadays such dissections are increasingly augmentted or even displaced by other educational tools. This shift in the approach to teaching anatomy was not exclusively associated with the limited access to cadaver bodies. It has rather been associated with the shift toward clinically oriented undergraduate medical education, which is not easy to achieve when teaching is solely based on cadaver dissections. Besides, new attractive educational tools, such as virtual immersive reality or

"living anatomy" with the use of ultrasonography, were introduced to the anatomical education, which made the traditional approach to teaching anatomy debatable.

There is also another problem with the education based on cadaver dissections. For the purpose of such a teaching, the bodies should be embalmed with chemicals. Traditionally, formaldehyde had been used. Nowadays, since this chemical substance is highly toxic and carcinogenic, it is displaced by novel chemical preservatives, for example Thiel fluid [1-10]. However, chemical embalming of the cadaver bodies, irrespective of the chemical compound used, is associated with good preservation of some tissues, while other tissues and organs easily disintegrate. Moreover, embalmed cadaver bodies, especially when formaldehyde is used, poorly resemble living tissues and organs. Consequently, the undergraduate anatomical education quiet often focuses at these structures that are well preserved and are easily recognizible on embalmed bodies, such as bones, muscles and ligaments. By contrast, organs and structures poorly preserved during embalming, are often neglected during anatomical courses, if other educational methods are not used. Besides, quite often in embalmed organs details of negligible clinical relevance are well preserved, while those of clinical importance are not well visible in these speciments.

All these problems concern teaching of neuroanatomy. Although the brain can be quite well preserved if formaldehyde embalming is used, such an embalmed organ changes its color from whitish to grey, blood vessels are no longer visible and only superficial macroscopic structures are recognizible [11-13]. Besides, a free use of formaldehyde is no longer possible in the European Union. Due to toxic and carcinegenic activity of this chemical compound, its use during anatomical education is strictly limited and requires a costly equipment in the lab to minimize side effects related to its toxicity [14,15]. Unfortunatelly, the brain is poorly preserved following less toxic methods of the embalming, such as the Thiel fluid. In addition, handling with the nervous tissue is associated with potential risk of prion infection [16,17].

Although contemporary clinical imaging, particularly magnetic resonance, offers a valuable alternative for the brain dissection speciemens, especially regarding the subcortical structures, still such a teaching, which is exclusively based on radiological images cannot replace traditional methods completely. Importantly, magnetic resonance or computed tomography scans are 2-dimensional (2D). Unlike graduated doctors, students during their first years at the medical university are usually incapable of mental transformation of the 2D scans into 3-dimensional (3D) structures. This skill is steadily developed during subsequent medical education but is typically undeveloped when the anatomy courses are performed [18]. Hence, need of a good quality brain specimens at anatomical classes.

This conudrum could be partially solved if 3D digital brains were used, instead of the real embalmed organs. Until recently, it was not easy to do and was not economically affordable. Still, with the advance of novel smartphones and applications, a high-quality and easy-to-perform photogrammetry became assessible and cheap. In this study, we assessed the feasibility and technical challenges associated with the creation of 3D digital models of the fresh cadaver brains.

DESCRIPTION

For the purpose of this study, we applied the KIRI Engine application (KIRI Innovations, Shenzhen, China) installed on the iPhone 13Pro Max (Apple Inc., Cupertino, CA, USA) smartphone. With this method, five brains of recently deceased patients were scanned. The brains were scanned using the Light Detection and Ranging (LiDAR) Object Capture tool of the KIRI Engine application. This particular tool utilizes the algorithm that captures and processes high-quality 3D models, using a combination of the LiDAR's light-detection technology and the photogrammetry. After switching on the Object Capture tool of the application, the phone was moved around the brain, following the instructions given by the application. The pictures of the target object were taken automatically, finally creating highly detailed 3D virtual models of the brain.

We did not encounter major problems with scanning of the brain with the above-described method. There were, however, some technical issues that should be solved in the future, and these will be further discussed. After completion of the scanning, models of the brain could be downloaded from the phone and either displayed as virtual reality objects (Figure 1), or as isolated 3D objects (Figure 2). These virtual brains could be moved or rotated or enlarged in order to see details (Supplementary File). Also, it was possible to transfer the file containing virtual model the scanned organ to another phone or computer, in order to be handled by another user.

We found this method feasible and highly valuable from the educational perspective, especially considering visual appearance of these virtual organs, which were very similar to the alive brains (Figure 3). Since these virtual objects were created using the high-resolution photographs, after augmentation of a model, the details were clearly visible (Figures 4-6). Still, at this stage of research,

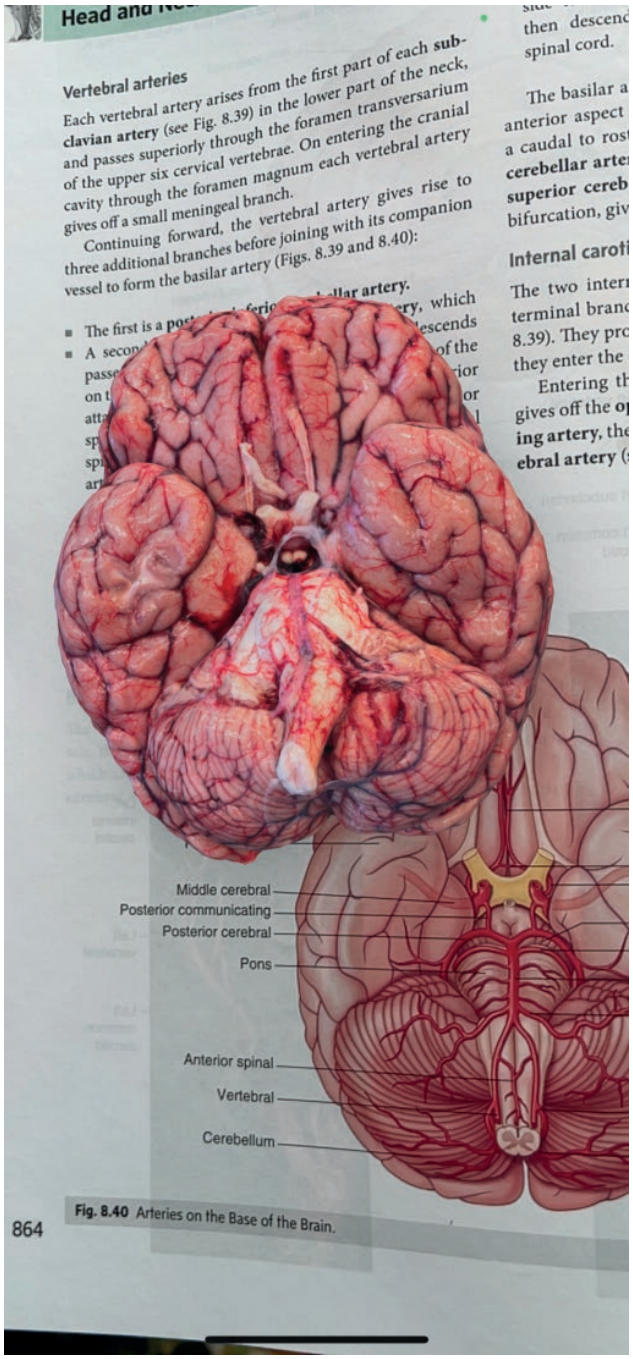

Figure 1. Scanned brain displayed on the screen of a smartphone seen as virtual reality object; here, the page from the student's anatomy textbook is visible in the background.

Figure 2. Scanned brain displayed on the screen of a smartphone seen as the 3D object.

we encountered some problems with creation of the 3D models. Unlike embalmed brains, fresh brains are quite soft and prone to gravitational distortions. Consequently, some parts of this organ that topographically are close together, after removal from the cranial cavity moved aside (Figure 7). However, although the virtual brain was somewhat distorted, on the other hand this distortion enabled the view of the medial surface of the brain with its important anatomical structures (Figure 8).

Until now, we were unable to build a virtual model of the whole brain. It was possible to scan this organ

Figure 3. Virtual model of the fresh cadaver brain seen from below; all superficial details are clearly visible, while the brain's color and its blood vessels are similar to those of an alive organ.

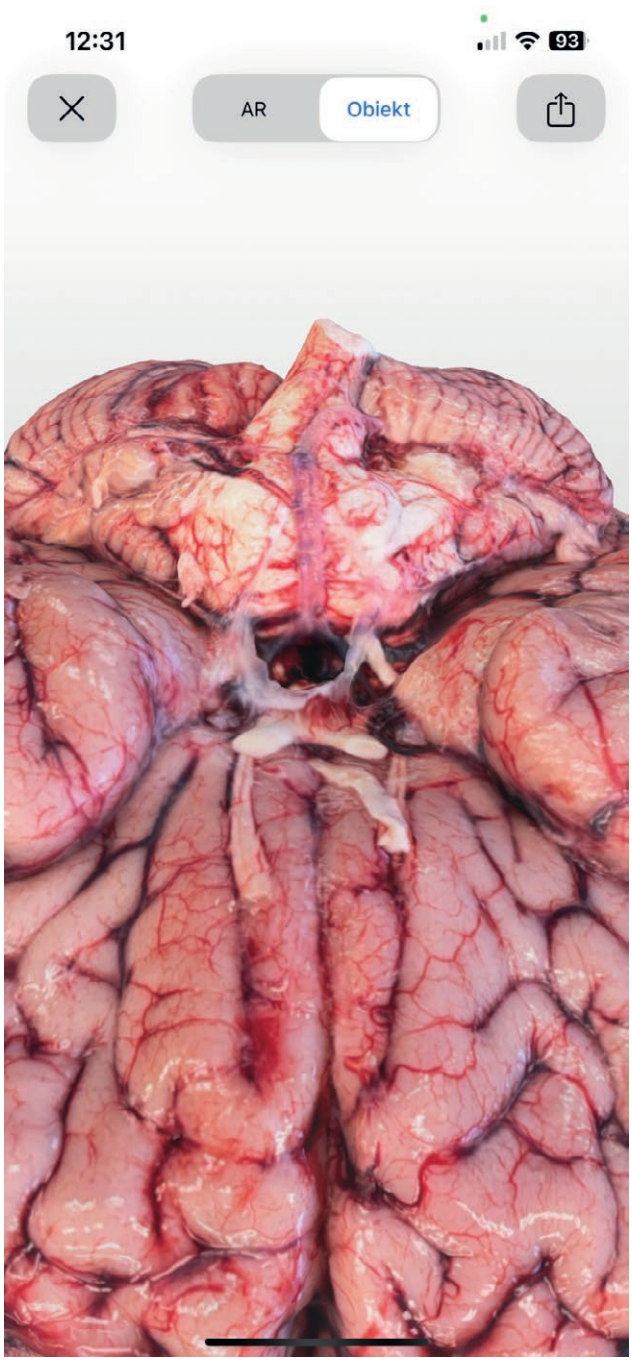

Figure 4. Augmented virtual model of the fresh cadaver brain; small blood vessels of the pia are well visible, with their color and appearance similar to those of an alive brain.

from above, with the brain lying either on its lower or upper surface. Unfortunately, unlike other more rigid anatomical specimens that could either be suspended in the air or steadily rotated during scanning, a fresh brain was too soft and prone to distortion. Consequently, it was possible to get good quality 3D virtual brains (Figure 9), either seen from below or above (Figure 8), but actually these models lacked the other surface (Figure 10) when rotated. Still, even considering these shortcomings, which probably can be solved in the future with

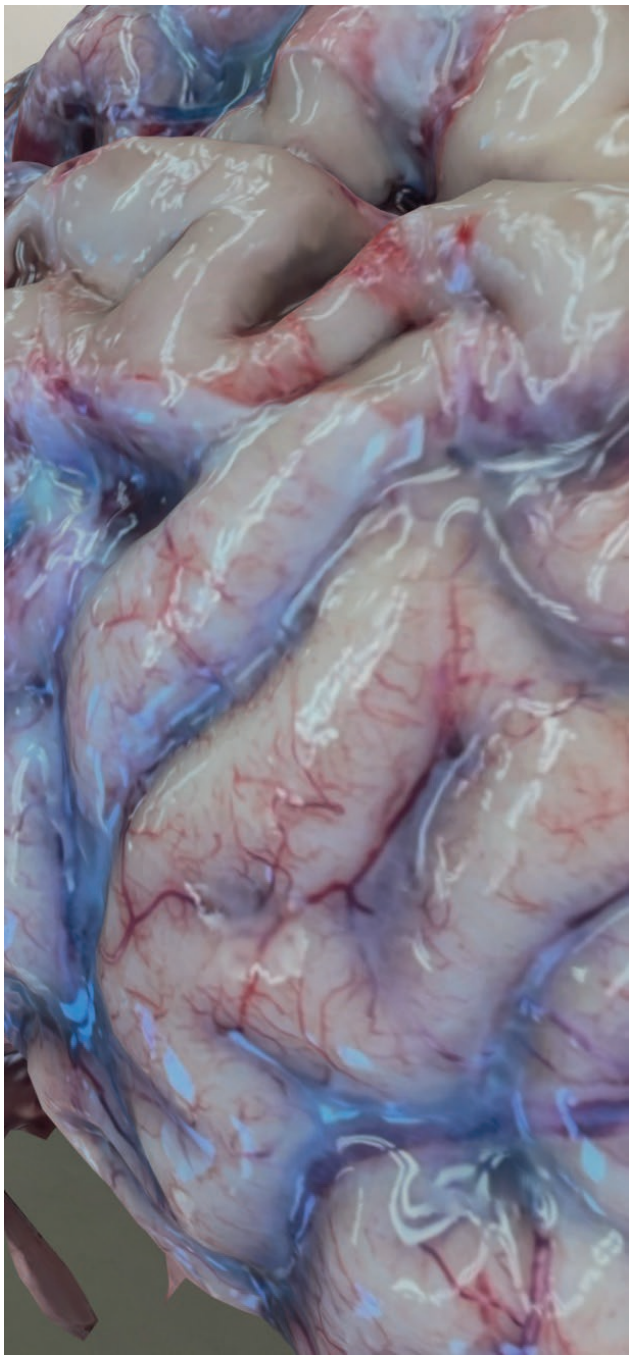

Figure 5. Augmented virtual model of another fresh cadaver brain, in which the arachnoid mater was not removed; a translucent arachnoid is well visible, and below it there is the pia with its small blood vessels.

more experience in the scanning, 3D virtual models of the fresh brains seem to be a promising educational tool for undergraduate medical students.

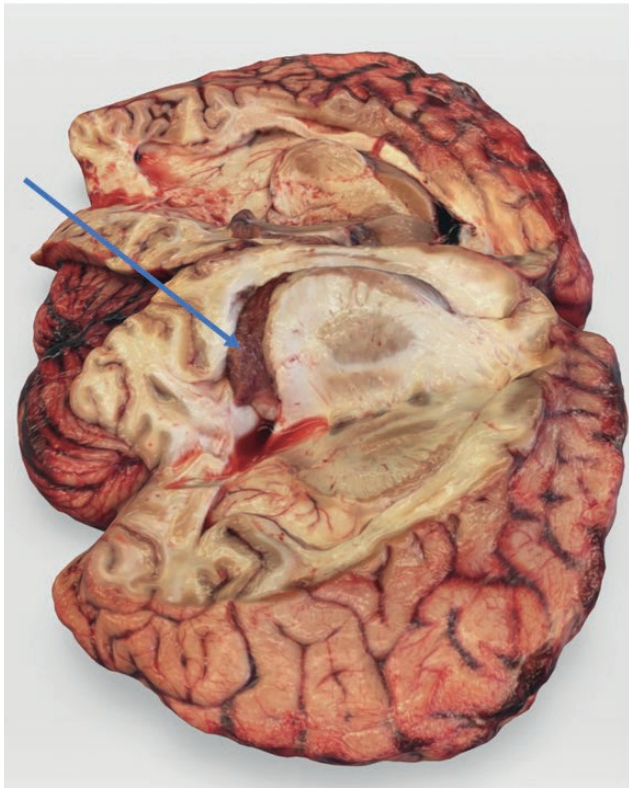

Figure 6. Brain transected alongside the lateral ventricle – the choroid plexus (arrow) with its vivid reddish color is clearly visible.

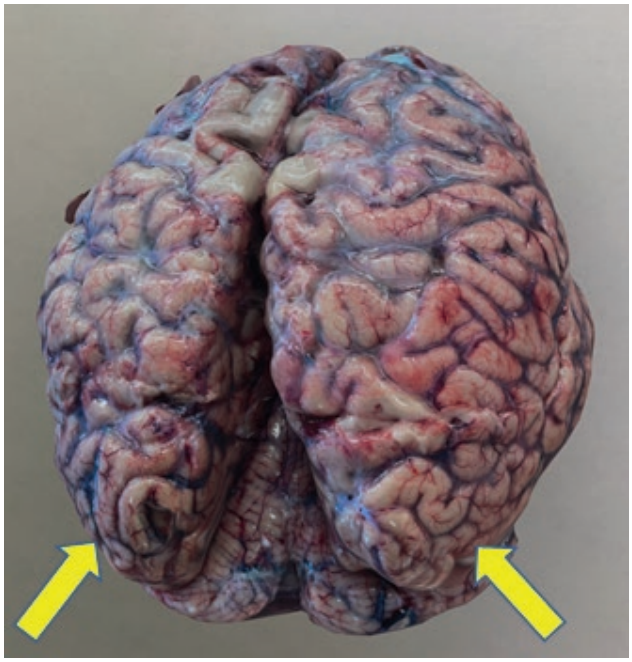

Figure 7. Distortion of the brain after its removal from the cranial cavity; the occipital lobes (yellow arrows) that normally are close to each other, moved aside due to the gravitation.

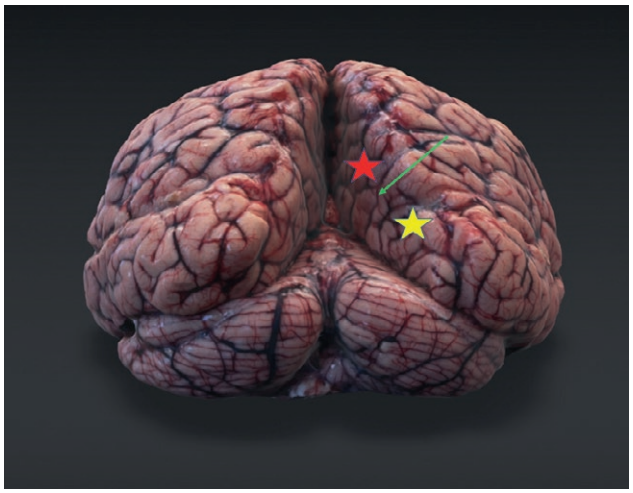

Figure 8. Gravitational distortion of the occipital lobes enables inspection of anatomical details located at the medial surface of the digital brain; green arrow: the parieto-occipital sulcus, red asterisk: the precuneus, yellow asterisk: the cuneus.

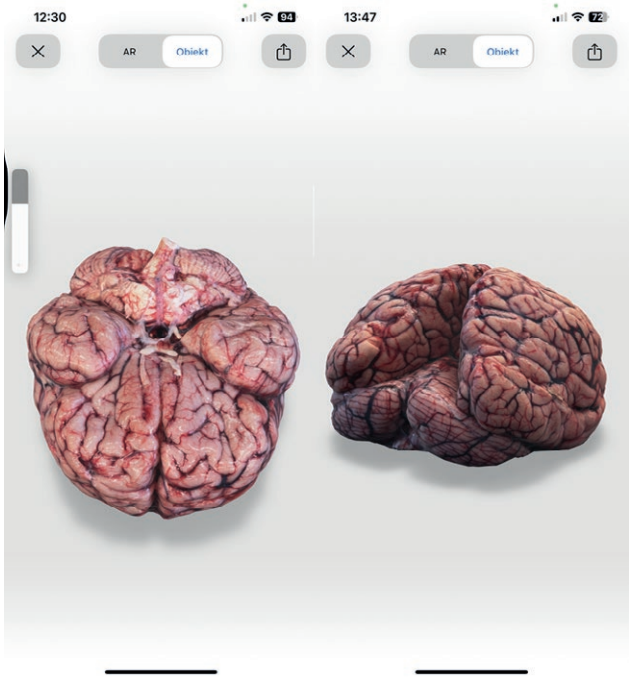

Figure 9. On the left: virtual brain seen from below; on the right: virtual brain seen from above.

Figure 10. Virtual brain scanned from its basal surface; after rotating the model the other surface is missing.

DISCUSSION

Our preliminary observations demonstrate that scanning of the fresh cadaver brains with the KIRI Engine application is easy, feasible and of potentially high educational value, especially considering the visual appearance of these models, which were very similar to alive brains. Several anatomical features, such as the tiny blood vessels of the pia mater, a translucent arachnoid mater, or the choroid plexus, unlike brains preserved by chemical solutions, are quite similar to those structures of the alive organ, seen for example

during the neurosurgical procedures. Although we have encountered several technical problems during scanning (discussed in the Results section of this paper), they seem to be of minor educational importance and most likely can be solved in the future. Besides, during this feasibility study we scanned only superficial aspects of the whole brains. In the future, we plan to scan also the internal structures of brain. Of note, since the brains are scanned during the autopsies, such a scanning should not interfere with this examination and, in general, with the work of a hospital morgue or forensic pathology center. Alternatively, more detailed and focused scanning of a brain of recently deceased donor could be performed, still it should be remembered that an opening of the skull may disturb the process of embalming of the rest of cadaver's body.

Over the last decade, the photogrammetry (the term refers to a technology that measures something using the recording of light) has been steadily introduced to the medical education, including anatomy [19-23]. However, until recently, its use has been limited by high costs of the scanners and an IT-expertise needed to operate the models acquired after the scanning. Recent advance in technology, especially development of the operator-friendly applications, and the fact that some modern smartphones are equipped with the LiDAR device (LiDAR is a remote sensing technology that uses the laser light to measure distances) made possible a creation of highly accurate, 3D representations of the target object. Consequently, it became possible to scan anatomical specimens and create their 3D virtual representations. In the recent publications, a shift from expensive commercial scanners to the free smartphone applications is notable. Several different smartphone applications were used [24,25]. Currently, it remains unclear which of them is of the best educational value, especially because they are being constantly updated and improved. In addition to the KIRI Engine, applications that may be potentially used for anatomical scanning comprise: the Qlone, the Polycam, the Scandy Pro, the Trnio 3D Scanner, the SCANN3D, and the RealityScan. Probably, those basing on the LiDAR technology should be chosen, since this method provides better quality pictures.

In this feasibility study we have chosen the KIRI Engine application, since for the purpose of this research it was possible to use the non-commercial version of this application, with no associated costs for our university. Besides, in the not yet published study (*Wawer, J.; et al. Evaluation of the commercial applications for mobile devices for the scanning of 3D anatomical model. Presented at the 3rd Conference on Anatomical Didactics; 08-09.05.2024, Łódź, Poland*), it was reported that for anatomical scanning, this particular application is of the best usefulness. Another advantage of the KIRI Engine is the fact that photogrammetry requires a high computing power. The KIRI Engine effectively utilizes cloud-processing and storage to combat this limitation.

Importantly, until now, 3D anatomical virtual models were created from the embalmed prosection specimens [25,26-30]. By contrast, in our study we used fresh brains of the recently deceased individuals. The scanning was performed during the post-mortem, not during dissecting the body of a cadaver. It seems that the use of fresh organs can overcome limitations associated with the use of embalmed brains for anatomy education. Although embalmed brains can be used for a longer period of time, yet after the embalming they change their color and structure, while some important anatomical structures, particularly blood vessels, are no longer well visible. Some authors tried to solve the problems of poorly visible cerebral vessels in brain specimens by injecting the cerebral vessels with a colored silicone or another filling material [31-33]. Still, such injected specimens, even if valuable from educational point of view, lack the appearance of an alive brain. Besides, a wider use of virtual models instead of embalmed cadaver specimens would reduce the risk associated with exposure of the students and academic teachers to formaldehyde and other toxic and carcinogenic chemicals, as well as to a potential exposure to the brain-residing prions.

We found 3D scanning of the brains with the use of a smartphone application feasible and highly valuable from the educational perspective, especially considering visual appearance of 3D virtual models of the brains, which were very similar to the alive organs. Such a 3D scanning of the organs of fresh cadavers seems to be a new and promising educational tool for undergraduate medical students.

ETHICS STATEMENT

This study was conducted in accordance with the Declaration of Helsinki and has been approved by the Bioethical Committee of the University of Opole; approval No UO/0015/KB/2024.

This research received no external funding. The authors declare no conflicts of interest.

There are no conflicts of interest associated with this submission**.** No AI tools were used in the preparation of this manuscript.

AUTHOR CONTRIBUTIONS

Conceptualization, M.S.; methodology, P.G.; validation, P.G. and M.S.; investigation, P.G.,J.M. and W.R.; data curation, P.G.; writing – original draft preparation, M.S.; writing – review and editing, P.G.,J.M. and W.R.; visualization, P.G.; supervision, M.S.; project administration, M.S. All authors have read and agreed to the published version of the manuscript.

REFERENCES

1. Benet, A.; Rincon-Torroella, J.; Lawton, M.T.; González Sánchez, J.J. Novel embalming solution for neurosurgical simulation in cadavers. *J Neurosurg* **2014**, *120*, 1229-37.
2. Hammer, N.; Löffler, S.; Bechmann, I.; Steinke, H.; Hädrich, C.; Feja, C. Comparison of modified Thiel embalming and ethanol-glycerin fixation in an anatomy environment: Potentials and limitations of two complementary techniques. *Anat Sci Educ* **2015,** *8*, 74-85.
3. Hammer, N. Thirty years of Thiel embalming-A systematic review on its utility in medical research. *Clin Anat* **2022**, *35*, 987-997.
4. Antipova, V.; Niedermair, J.F.; Siwetz, M.; Fellner, F.A.; Löffler, S.; Manhal, S.; Ondruschka, B.; Pietras, S.M.; Poilliot, A.J.; Pretterklieber, M.L.; Wree, A.; Hammer, N. Undergraduate medical student perceptions and learning outcomes related to anatomy training using Thiel- and ethanol-glycerin-embalmed tissues. *Anat Sci Educ* **2023**, *16*, 1144-1157.
5. Thompson, B.; Green, E.; Scotcher, K.; Keenan, I.D. A Novel cadaveric embalming technique for enhancing visualisation of human anatomy. *Adv Exp Med Biol* **2022**, *1356*, 299-317.
6. Haizuka, Y.; Nagase, M.; Takashino, S.; Kobayashi, Y.; Fujikura, Y.; Matsumura, G. A new substitute for formalin: Application to embalming cadavers. *Clin Anat* **2018**, *31*, 90-98.
7. Nagase, M.; Nagase, T.; Tokumine, J.; Saito, K.; Sunami, E.; Shiokawa, Y.; Matsumura, G. Formalin-free soft embalming of human cadavers using N-vinyl-2-pyrrolidone: perspectives for cadaver surgical training and medical device development. *Anat Sci Int* **2022,** *97*, 273-282.
8. Waerlop, F.; Rashidian, N.; Marrannes, S.; D'Herde, K.; Willaert, W. Thiel embalmed human cadavers in surgical education: Optimizing realism and long-term application. *Am J Surg* **2021,** *221*,1300-1302.
9. Balta, J.Y.; Cronin, M.; Cryan, J.F.; O'Mahony, S.M. Human preservation techniques in anatomy: A 21st century medical education perspective. *Clin Anat* **2015**, *28*, 725-34.
10. Hachabizwa, C.; Banda, M.; Hainza, J.; Mutemwa, S.; Erzingastian, K.; Kafumukache, E. Cadaveric embalming using a modified Thiel method as an alternative to the formalin method. *Anat J Africa* **2020,** *9*, 1797-1806.
11. Miyake, S.; Suenaga, J.; Miyazaki, R.; Sasame, J.; Akimot,o T.; Tanaka, T.; Ohtake, M.; Takase, H.; Tateishi, K.; Shimizu, N.; Murata, H.; Funakoshi, K.; Yamamoto, T. Thiel's embalming method with additional intra-cerebral ventricular formalin injection (TEIF) for cadaver training of head and brain surgery. *Anat Sci Int* **2020**, *95*, 564-570.
12. Tomalty, D.; Pang, S.C.; Ellis, R.E. Preservation of neural tissue with a formaldehyde-free phenol-based embalming protocol. *Clin Anat* **2019**, *32*, 224-230.
13. Nardi, L.; Schmeisser, M.J.; Schumann, S. Fixation and staining methods for macroscopical investigation of the brain. *Front Neuroanat* **2023**, *17*, 1200196.
14. Hauptmann, M.; Stewart, P.A.; Lubin, J.H.; Beane Freeman, L.E.; Hornung, R.W.; Herrick, R.F.; Hoover, R.N.;, Fraumeni, J.F. Jr.; Blair, A.; Hayes, R.B. Mortality from lymphohematopoietic malignancies and brain cancer among embalmers exposed to formaldehyde. *J Natl Cancer Inst* **2009,** *101*, 1696-708.
15. Soonklang, N.; Saowakon, N. Evaluation of formaldehyde exposure among gross dissection after modified embalming solution and health assessment. *Environ Sci Pollut Res Int* **2022**, *29*, 65642-65654.
16. Ogami-Takamura, K.; Saiki, K.; Endo, D.; Murai, K.; Tsurumoto, T. The risk of Creutzfeldt-Jakob disease infection in cadaveric surgical training. *Anat Sci Int* **2022**, *97*, 297-302.
17. Koyama, S.; Yagita, K.; Hamasaki, H.; Noguchi, H.; Shijo, M.; Matsuzono, K.; Takase, K.I.; Kai, K.; Aishima, S.I.; Itoh, K.; Ninomiya, T.; Sasagasako, N.; Honda, H. Novel method for classification of prion diseases by detecting PrP^{res} signal patterns from formalin-fixed paraffin-embedded samples. *Prion* **2024**, *18*, 40-53.
18. Simka, M. Teaching anatomy of the lower extremity veins: Educational challenges.*Vasc Invest Ther* **2025**, *8*, 1-6.
19. Chytas, D.; Paraskevas, G.; Noussios, G.; Demesticha, T.; Salmas, M.; Vlachou, C.; Vasiliadis, A.V.; Troupis, T. Use of photogrammetry-based digital models in anatomy education: An overview. *Morphologie* **2024,** *108*, 100792.
20. de Oliveira, A.S.; Leonel, L.C.; LaHood, E.R.; Nguyen, B.T.; Ehtemami, A.; Graepel, S.P.; Link, M.J.; Pinheiro-Neto, C.D.; Lachman, N.; Morris, J.M.; Peris-

Celda, M. Projection of realistic three-dimensional photogrammetry models using stereoscopic display: A technical note. *Anat Sci Educ* **2024** , *17*, 39-46.
21. Struck, R.; Cordoni, S.; Aliotta, S.; Pérez-Pachón, L.; Gröning, F. Application of photogrammetry in biomedical science. *Adv Exp Med Biol* **2019**, *1120*, 121-130.
22. Krause, K.J.; Mullins, D.D.; Kist, M.N.; Goldman, E.M. Developing 3D models using photogrammetry for virtual reality training in anatomy. *Anat Sci Educ* **2023,** *16*, 1033-1040.
23. Tóth, D.; Petrus, K.; Heckmann, V.; Simon, G.; Poór, V.S. Application of photogrammetry in forensic pathology education of medical students in response to COVID-19. *J Forensic Sci* **2021,** *66*, 1533-1537.
24. Piazza, A.; Corvino, S.; Ballesteros, D.; Campeggi, A.; Agosti, E.; Serioli, S.; Corrivetti, F.; Bortolotti, C.; De Notaris, M. Neuroanatomical photogrammetric models using smartphones: a comparison of apps. *Acta Neurochir (Wien)* **2024,** *166*, 378.
25. de Oliveira Manduca Palmiero, H.; Ribas, E.C.; Carlotti, C.G. Jr.; Figueiredo, E.G. Anatomical assessment of cerebral sulci and gyri for neuroanatomy education using photogrammetry technique to generate 3D-tridimensional models. *Neurosurg Rev* **2025**, *48*, 172.
26. Petriceks, A.H.; Peterson, A.S.; Angeles, M.; Brown, W.P.; Srivastava, S. Photogrammetry of human specimens: An innovation in anatomy education. *J Med Educ Curric Dev* **2018**, *5*, 2382120518799356.
27. Van Vlasselaer, N.; Keelson, B.; Scafoglieri, A.; Cattrysse, E. Exploring reliable photogrammetry techniques for 3D modeling in anatomical research and education. *Anat Sci Educ* **2024,** *17*, 674-682.
28. Morichon, A.; Dannhoff, G.; Barantin, L.; Destrieux, C.; Maldonado, I.L. Doing more with less: Realistic stereoscopic three-dimensional anatomical modeling from smartphone photogrammetry. *Anat Sci Educ* **2024**,*17*, 864-877.
29. de Oliveira, A.S.; Leonel, L.C.; LaHood, E.R.; Hallak, H.; Link, M.J.; Maleszewski, J.J.; Pinheiro-Neto, C.D.; Morris, J.M.; Peris-Celda, M. Foundations and guidelines for high-quality three-dimensional models using photogrammetry: A technical note on the future of neuroanatomy education. *Anat Sci Educ* **2023,** *16*, 870-883.
30. de Oliveira, A.S.; Leonel, L.C.; Bauman, M.M.; De Bonis, A.; LaHood, E.R.; Graepel, S.; Link, M.J.; Pinheiro-Neto, C.D.; Lachman, N.; Morris, J.M.; Peris-Celda, M. Photogrammetry scans for neuroanatomy education - a new multi-camera system: technical note. *Neuroinformatics* **2024,** *22*, 317-327.
31. Smith, K.; Ventre, G.J.; Palmisciano, P.; Hussein, A.E.; Hoz, S.S.; Forbes, J.A.; Lowrie, D.J. Jr.; Zuccarello, M.; Andaluz, N.; Prestigiacomo, C.J. Brain vasculature color-labeling using the triple-injection method in cadaveric heads: A technical note for improved teaching and research in neurovascular anatomy. *Oper Neurosurg (Hagerstown)* **2023,** *24*, 291-300.
32. Çırak, M.; Yağmurlu, K.; Soldozy, S.; Norat, P.; Shaffrey, M.E.; Kalani, M.Y.S. Common challenges and solutions associated with the preparation of silicone-injected human head and neck vessels for anatomical study. *Brain Sci* **2020**, *11*, 32.
33. Sanan, A.; Abdel Aziz, K.M.; Janjua, R.M.; van Loveren, H.R.; Keller, J.T. Colored silicone injection for use in neurosurgical dissections: anatomic technical note. *Neurosurgery* **1999,** *45*, 1267-71; discussion 1271-4.

SUPPLEMENTARY MATERIALS

File S2: Handling of 3D model on the smartphone screen.

IJAE
ITALIAN JOURNAL OF ANATOMY AND EMBRYOLOGY

Firenze University Press
www.fupress.com/ijae

Book

An Illustrated Guide to Anatomical Eponyms

Hans J. ten Donkelaar[1], Marina Quartu[2], David Kachlìk[3]

[1] *Department of Neurology Radboud University Medical Centre Nijmegen, The Netherlands*
[2] *Department of Biomedical Sciences, University of Cagliari, Cagliari, Italy*
[3] *Department of Anatomy Charles University Prague, Czech Republic*

OPEN ACCESS

Citation: ten Donkelaar, H. J., Quartu, M., & Kachlìk, D. (2025). An Illustrated Guide to Anatomical Eponyms. *Italian Journal of Anatomy and Embryology* 129(2): 97-97. doi: 10.36253/ijae-17058

Data Availability Statement: All relevant data are within the paper and its Supporting Information files.

Competing Interests: The Author(s) declare(s) no conflict of interest.

This book provides a comprehensive overview of the anatomical eponyms in use in anatomy and in clinical disciplines. It includes brief descriptions of those to whom eponyms were given with personal data, their relevant publications and illustrations. For the illustrations, engravings, portraits or photographs are included as well as examples of the original illustrations or newer ones showing what is meant by a certain eponym. The book contains three Sections: Section I The Classical Anatomical Eponyms, in which the major classical eponyms on arteries, bands, bodies, bundles, canals, corpuscles, ducts, fasciae, fibres, folds, foramina, fossae, ganglia, glands, ligaments, membranes, muscles, nerves, nodes, nuclei, plexuses, spaces, triangles, tubercles, valves and veins are summarized. This Section clearly shows that in various countries, different eponyms are given for the same structure. Section II lists the anatomical eponyms together with some relevant histological, embryological and anthropological eponyms, from A-Z. In Section III, anatomical eponyms in use in Abdominal Surgery, Dentistry, Neurology, Obstetrics and Gynaecology, Oncology, Ophthalmology, Orthopaedics, Otology, Phlebology, and Radiology of the Digestive System are discussed. Sections II and III are both abundantly illustrated.

The book is intended for advanced medical students, anatomists, and clinicians using anatomical eponyms in their daily practice. Unique to the book is the combination of descriptions of the anatomical eponyms with illustrations.

https://link.springer.com/book/10.1007/978-3-031-91664-9

IJAE
Italian Journal of Anatomy and Embryology
Vol. 129, N. 2 – 2025

€ 26,00 (for Italy)